UNIVERSITÀ DELLA CALABRIA

UNIVERSITÀ DELLA CALABRIA

Dipartimento di Fisica

Scuola di Dottorato

Scienza e Tecnica "Bernardino Telesio"

Indirizzo

Fisica dei Sistemi Complessi

XXVI CICLO

AIR QUALITY AND POLLUTANT MODELLING IN THE MEDITERRANEAN REGION

Settore Scientifico Disciplinare FIS/06

Direttore: Prof. Roberto Bartolino

Supervisori: Prof. Nicola Pirrone

Dr. Ian Michael Hedgecock

Prof. Vincenzo Carbone

Dottorando: Dr. Christian Natale Gencarelli

Abstract

L'inquinamento atmosferico viene definito come la presenza di sostanze che possono avere effetti dannosi sulla salute umana o sull'intero sistema ambientale (EC, 2008), causando effetti misurabili sugli animali, sulla vegetazione e sui diversi materiali. Queste sostanze, dette inquinanti, usualmente non sono presenti nella normale composizione atmosferica o lo sono ma a concentrazioni estremamente basse.

Tra i più pericolosi inquinanti presenti in atmosfera c'è il mercurio (Hg), un inquinante globale sotto controllo soprattutto negli ultimi anni (UNEP, 2013b; Mason *et al.*, 2012; Driscoll *et al.*, 2013) in quanto provoca gravi effetti nocivi sulla salute umana.

Elevate concentrazioni di mercurio negli ecosistemi sono causate dalle emissioni dirette, ma anche da reazioni chimiche che avvengono in atmosfera e dalle condizioni meteorologiche che, governate dalla fisica dell'atmosfera, regolano la distribuzione, il trasporto e la deposizione del mercurio. Per individuare le cause delle elevate concentrazioni di inquinanti in atmosfera è necessaria un adeguata rete di monitoraggio, ma è molto complicato coprire vaste aree geografiche con stazioni di misura. Diviene dunque necessario ricorrere a modelli matematici che simulano le condizioni atmosferiche dal punto di vista sia meteorologico che chimico, in modo da ottenere i fattori sui quali è possibile intervenire per migliorare la qualità dell'aria.

Questo lavoro di tesi mostra lo sviluppo di un modello regionale online che simula il ciclo atmosferico del mercurio, in modo da valutare ed identificare le relazioni tra sorgenti e recettori a scala regionale e gli andamenti temporali degli scenari di emissione di mercurio attuali e futuri. Il risultato è una versione ampliata del modello numerico per la chimica ed il trasporto atmosferico WRF/Chem (modello Weather Research and Forecasting per la meteorologia integrato con la chimica atmosferica, Grell *et al.* (2005)), che può simulare il ciclo atmosferico del mercurio online. Questa versione del modello è in grado di riprodurre i campi di concentrazione ed i flussi di deposizione del mercurio a scala regionale, includendo le emissioni da sorgenti sia antropogeniche che naturali e simulando le interazioni e le reazioni chimiche

che avvengono in atmosfera, nonché i processi di deposizione. Per lo sviluppo di questo modello è stato necessario indagare i diversi aspetti della chimica del mercurio, analizzando ed implementando le interazioni con gli altri gas presenti in atmosfera, con la radiazione solare, con il vapore acqueo e con la pioggia; queste interazioni regolano i processi di ossidazione, riduzione e deposizione del mercurio. Inoltre sono stati implementati nel modello i processi di emissione da parte di sorgenti antropiche e naturali, parametrizzando le emissioni di mercurio dovute agli incendi boschivi e l'evasione di mercurio nell'interfaccia atmosfera - superfice del mare. Oltre alle deposizioni di mercurio da parte delle piogge (deposizione wet) sono stati implementati i meccanismi per deposizione al suolo dovuta alla forza gravitazionale ed ai moti atmosferici (deposizione dry).

Il modello è in grado di riprodurre la variazione stagionale delle concentrazioni di mercurio, rappresentando adeguatamente anche gli andamenti di Hg^{II} e Hg^{P} nello strato atmosferico al limite con la superfice del Mar Mediterraneo (Mediterranean MBL). La medie annuali delle deposizioni di mercurio wet e dry modellate sono simili, ma con differente distribuzione spaziale: la deposizione wet domina nelle zone umide mentre la deposizione dry è maggiore vicino alle sorgenti di emissione. Comparando le deposizioni con l'evasione di mercurio dalla superfice del mare risulta che il Mar Mediterraneo è una sorgente di mercurio per tutta l'area, con circa 70 Mg di mercurio emessi in un anno. I risultati suggeriscono inoltre che nel MBL Mediterraneo il Bromo è un importante ossidante del mercurio.

Il modello WRF/Chem è stato inizialmente usato per investigare la produzione fotochimica di un importante costituente atmosferico che influenza il ciclo del mercurio nell'area del Mar Mediterraneo, l'ozono troposferico (O_3). Oltre ad influenzare il ciclo del mercurio, l'ozono è anche un pericoloso inquinante: elevate concentrazioni di ozono in prossimità del suolo sono infatti dannose sia per la salute umana che per la produzione agricola. L'analisi modellistica dell'inquinamento da ozono troposferico mostra una forte influenza delle emissioni prodotte dalle navi che transitano nel Mar Mediterraneo, stimando il loro contributo in circa il 10–20 % delle concentrazioni di ozono nelle aree continentali.

Introduction

Air pollution is defined as the presence of a substance that may have harmful effects on human health and/or on the whole environment (EC, 2008), causing a measurable effect on humans, animals, vegetation and on different materials. These substances, called pollutants, usually are not present in normal ambient air, or are present in the atmosphere but at extremely low concentration.

Among the most dangerous pollutants in the atmosphere is Mercury (Hg), a global pollutant which has come under increasing scrutiny over recent years (UNEP, 2013b; Mason *et al.*, 2012; Driscoll *et al.*, 2013), because it can cause severe effects on human health.

Elevated concentrations of mercury in ecosystem are caused by high emissions, but also by the chemical reactions that occur in the atmosphere and meteorological conditions. Meteorological conditions, governed by the physics of the atmosphere, regulate the distribution, transport and deposition of mercury. To identify the causes of high concentrations of pollutants an adequate monitoring network is needed, but it is very difficult to cover the whole large areas with measurement stations. Thus it is necessary to use mathematical models that simulate the atmosphere in terms of meteorological and chemical conditions, in order to have an idea of the factors on which it is possible to intervene to improve air quality.

This thesis shows the development of a regional online model for the simulation of the atmospheric Hg cycle, to evaluate and identify source-receptor relationships at local scales and their temporal trends for current and future scenarios of mercury emissions. The result is a modified version of the numerical Chemistry Transport Model WRF/Chem (Weather Research and Forecasting model integrated with chemistry, Grell *et al.* (2005)), which can simulate atmospheric Hg chemistry online. This model can estimate the concentration fields and deposition fluxes of mercury on a regional scale, simulating the emissions from anthropogenic and natural sources, chemical interactions and reactions in the atmosphere and the deposition processes. A detailed description of this modified model version is given in chapter 3, while

a general description of the Hg atmospheric cycle can be found in chapter 1.

Initially the standard WRF/Chem model (described in section 2.3) was used to investigate the photochemical production of an important atmospheric constituent that influences the Hg cycle in Mediterranean region, tropospheric ozone (O_3). In addition to influencing the Hg cycle, O_3 is also a dangerous pollutant. In fact elevated concentrations of ground level ozone are both hazardous to human health and detrimental to agricultural production. In this study, as described in chapter 2, ozone pollution in Mediterranean basin area has been studied. The model meteorological and O_3 concentrations output was compared to measurement data. The model was also used to investigate the influence of ship emissions on air quality in the Mediterranean region.

Mercury has a long (6 - 18 months) atmospheric residence time allowing it to be transported long distances in the atmosphere. For this reason it is necessary to develop global models for the study of the Hg cycle, from which the necessary boundary conditions for regional models can be obtained. Mercury atmospheric concentrations are strongly influenced by long range transport, and a description of the global model ECHMERIT (De Simone *et al.*, 2013; Jung *et al.*, 2009), used for the boundary and initial conditions for the WRF/Chem with Hg model, is given in the Appendix A.

Model application for the investigation of the processes that occur in the Mediterranean Marine Boundary Layer, mercury air-water fluxes and recent developments on the impact that Bromine-containing compounds have on the atmospheric Hg cycle are described in chapter 4.

List of Figures

1.1 Soil Hg emissions simulated for preindustrial (upper panel) and present day (lower panel) conditions. Concentrations are in μg m^{-2} y^{-1}. Adapted from Smith-Downey *et al.* (2010). . . 13
1.2 Ice core record of deposition Upper Fremont Glacier. Image from UNEP (2013a). 14
1.3 Global Hg budgets illustrate the main environmental compartments and pathways that are of importance in the global mercury cycle, and the ways in which natural and anthropogenic releases to air land and water move between these compartments. Emissions to air arise from natural sources and anthropogenic sources, as well as reemissions of mercury previously deposited from air onto soils, surface waters, and vegetation. Image adapted from UNEP (2013a). 15
1.4 Region to the table 1.2 (UNEP, 2013a). 20
1.5 Global distribution of anthropogenic mercury emissions to air in 2010 (UNEP, 2013a). 21

2.1 The Med-Oceanor campaign routes over the years. Also shown are the sites of the EMEP stations used in the model validation. 32
2.2 The largest modelling domain (black), and examples of the nested grids, for 2003 in red, and for 2005 in yellow. The two horizontal white lines in the smallest 2003 domain are the cross-sections at roughly 34 and 39°N described in section 2.4.3. 34
2.3 Measured and modelled O_3 concentration in ppb during the 2000 oceanographic campaign. Mean bias -3.7 ppb 42
2.4 Measured and modelled O_3 concentration in ppb during the 2005 oceanographic campaign. Mean bias 3.0 ppb 43
2.5 Measured and modelled O_3 concentration in ppb during the 2010 oceanographic campaign. Mean bias -0.7 ppb 44

2.6 The influence of ship emission height on the modelled O_3 concentration in ppb, in the lowest model layer at midday on 16 June 2009. Left, Em_low scenario right, Em_hi scenario. . . 45
2.7 The average O_3 concentration and concentration difference in the first model layer for 2005 (left) and 2006 (right). Row one shows the difference Tot_Emiss − No_ships in ppb, row 2 the actual value in ppb and row 3 the difference in %. 46
2.8 The difference (ppb) in the maximum O_3 concentrations between the Tot_emiss and No_ships simulations for the 2003 measurement campaign. 47
2.9 The vertical profile of O_3 concentration along ≈39° N (top row),and ≈34° N, bottom row. Column 1 shows the difference Tot_Emiss − No_ships in ppb, column 2 the actual value in ppb and column 3 the difference in %. The values are the average for the whole simulation period, 5 to 27 August 2003. 48
2.10 Examples of the difference in O_3 concentration with and without ship emissions along the route of the R.V. Urania. 49

3.1 Model domains, location of the EMEP measurement stations (yellow points for wet deposition flux, red for TGM, blue for Hg^P, white for ozone concentrations) and Med-Oceanor 2009 route (red line). The numbers over the route represent the June data. 58
3.2 Total anthropogenic AMAP Hg emission to air (g km^{-2}). Image adapted from http://amap.no/. 61
3.3 Box and whisker plots of hourly ozone concentration metrics for the 111 EMEP sites. Points represent the mean value. The correlation for just the 11 EMEP coastal sites is also shown. . 65
3.4 Ozone concentrations measured (black) and modelled (blue) during the Med-Oceanor measurement campaign and values of metrics (bias is in ppb). Grey boxes contain the model-measurements pairs near the coastal area. 66
3.5 Monthly distribution of measured and modelled TGM concentrations at EMEP measurement stations. 67
3.6 Monthly RGM concentrations measured (black) and modelled (blue) at Waldhof station. The metrics (bias is in pg m^{-3}) of the comparison and the standard deviation of the data (dashed line) are also shown. 68
3.7 Monthly distribution of measured and modelled PBM concentrations at EMEP stations. 68

3.8 Hourly TGM concentrations measured (black) and modelled (blue) at Waldhof station. 69
3.9 Mercury concentrations measured (black) during the MedOceanor campaign and modelled values (blue). The time axis indicates the day in June while the bias is in ng m^{-3} for GEM and in pg m^{-3} for RGM and PBM. Dashed line represents the standard deviations to the data. 70
3.10 Monthly mean of the mercury wet deposition flux at EMEP sites and in the correspondenting model cells. 71
3.11 Monthly rainfall at EMEP stations and and in the correspondenting model cells. 72
3.12 Monthly mean to the mercury wet deposition concentrations in EMEP sites and in correspondents model cells. 73
3.13 Mercury deposition in model domain. Note that the colour scale is not linear. 74
3.14 Mediterranean Sea evasions. The upper colour scale is for the "All 2009" image, while the lower is for evasion to May and December. Note that the colour scale is not linear. 75
3.15 Mediterranean sea Hg mass balance. For every month the Hg sea evasion is shown on the right and the deposition on the left. Deposition is divided into gas and particulate wet deposition (WD) and dry deposition (DD). 76

4.1 Mercury concentrations measured (black) during the MedOceanor campaign and modelled values (blue for O_3/OH oxidation and red for Br/BrO oxidation). The time axis indicates the day in June while the bias is in ng m^{-3} for GEM and in pg m^{-3} for RGM. 84
4.2 Model Hg deposition (μg m^{-2}) for June 2009. On the left for oxidation by O_3 and OH and on the right for oxidation by Br and BrO. 84

List of Tables

1.1 Global natural and anthropogenic emissions (Mg yr^{-1}) from various estimates. 17
1.2 Emissions from various regions (Mg yr^{-1}) and as a percentage of total global anthropogenic emissions. See figure 1.4 for the regions specification. Table adapted from UNEP (2013a). . . . 20

2.1 The oceanographic campaign periods 31
2.2 The metrics used to assess the model performance. 38
2.3 Comparison between the model output and meteorological parameters measured aboard the R. V. Urania. There was no relative humidity data available for 2010 39
2.4 Comparison of the model results and the ozone concentrations measured aboard the R. V. Urania, see section 2.3.2 for the definition of the Em_low amd Em_hi emission scenarios. UF refers to the unsystematic fraction of the RMSE. The results for 2003 consider only the first half of the campaign, see section 2.4.1 41
2.5 Comparison of the model results and the ozone concentrations measured at the EMEP stations within the highest resolution modelling domain, see section 2.3.2 for the description of the Em_low and Em_hi emission scenarios. The stations are ES07 Vznar, ES10 Cabo de Creus, ES12 Zarra, ES14 Els Torms, FR13 Peyrusse Vieille, FR16 Le Casset, FR17 Montfranc, GR02 Finokalia, GR03 Livadi, IT01 Montelibretti, IT04 Ispra,MT01 Giordan Lighthouse. The locations of the EMEP stations are shown in figure 2.1. UF refers to the unsystematic fraction of the RMSE 52
2.6 Concentration differences between the Em_low and Em_hi scenarios, over the marine part of the 9 km modelling domain (Em_low - Em_hi). (Percentage differences calculated as (Em_low - Em_hi)/Em_low × 100 %) 53

2.7 The influence (%) of shipping emissions on the average concentrations of O_3, NO and NO_2 in the lowest model layer and on the first six layers (over the marine parts of the modelling domain). Calculated as (Tot_Emiss - No_Ships) / Tot_Emiss × 100 % 54

3.1 Hg emissions ($Mg\,year^{-1}$) in the middle model domain. The proportions of Hg^0, Hg^{II} and Hg^P are from the anthropogenic emission database (Pacyna *et al.*, 2005). 63
3.2 TGM concentration statistical analysis in the EMEP stations. Mean (M), Standard Deviation (SD) and bias are in $ng\,m^{-3}$. . 67
3.3 Mercury Mediterranean Sea evasion and deposition ($Mg\,year^{-1}$). 73

4.1 Hg deposition and evasion obtained by atmospheric and hydrological models in the Mediterranean area. All values are in Mg $year^{-1}$. Table from Žagar *et al.* (2013). 81

Contents

1 Introduction to the Mercury cycle **12**
- 1.1 Emissions . . . 17
  - 1.1.1 Natural sources . . . 18
  - 1.1.2 Anthropogenic sources . . . 19
  - 1.1.3 Speciation of anthropogenic Hg emissions . . . 21
- 1.2 Atmospheric transport and transformations . . . 22
  - 1.2.1 O_3/OH oxidation . . . 22
  - 1.2.2 Br/BrO oxidation . . . 23
  - 1.2.3 Hg reduction . . . 23
- 1.3 Atmospheric Hg modelling . . . 24
  - 1.3.1 Regional Hg modelling . . . 25
  - 1.3.2 Global Hg modelling . . . 25
  - 1.3.3 Offline and Online model . . . 26
  - 1.3.4 Measurements and model development . . . 27

2 Tropospheric Ozone Modelling **28**
- 2.1 Measurements . . . 30
  - 2.1.1 Measurements aboard the R. V. Urania . . . 30
  - 2.1.2 The Med-Oceanor Series of Oceanographic Campaigns 31
  - 2.1.3 Observations from the EMEP Network . . . 31
- 2.2 Modelling . . . 32
- 2.3 The WRF/Chem model . . . 32
  - 2.3.1 The model setup . . . 33
  - 2.3.2 Emissions . . . 35
  - 2.3.3 The simulations performed . . . 36
- 2.4 Results and discussion . . . 37
  - 2.4.1 Model validation . . . 37
  - 2.4.2 The influence of ship emission height in the model . . . 43
  - 2.4.3 The influence of ship emissions . . . 45
- 2.5 Conclusions . . . 50

3 WRF/Chem with Mercury model 55
3.1 Model Description 57
3.1.1 Modelling domains 57
3.1.2 The chemical mechanism 59
3.1.3 Dry and wet deposition 60
3.1.4 Emissions 60
3.2 Measurements 62
3.3 Results 64
3.3.1 Ozone concentrations 64
3.3.2 Atmospheric Hg concentrations over Europe 66
3.3.3 Marine Boundary Layer air concentrations 69
3.3.4 Mercury deposition 71
3.3.5 Mediterranean flux 72
3.4 Discussion 74
3.5 Conclusions 77
3.6 Appendix A: ECHMERIT global atmospheric model 78

4 Mediterranean mass balance 79
4.1 Processes in Marine Boundary Layer 80
4.2 Model intercomparison of the air-water fluxes 81
4.3 Conclusion regarding the Mediterranean mass balance 82
4.4 Bromine oxidation in WRF/Chem with Hg 83
4.4.1 Result using Bromine-compounds oxidation 83

5 Summary and conclusions 86

Bibliography 88

Chapter 1

Introduction to the Mercury cycle

Mercury (Hg), also known as quicksilver, is a heavy metal which is liquid at room temperature and evaporates easily (UNEP, 2013b). It is a natural element that cannot be created or destroyed, and the same amount has existed on the planet since the Earth was formed (Pirrone *et al.*, 2001). Many research studies indicates that natural and anthropogenic activities can redistribute this element in the atmospheric, soil and water ecosystems through a complex combination of transport and transformations. Once it has entered the environment, mercury cycles between air, land, and water until it is eventually removed from the system through burial in deep ocean sediments or lake sediments and through entrapment in stable mineral compounds.

During industrial times, due to its unique physical-chemical properties (high specific gravity, low electrical resistance, constant volume of expansion), it has been employed in a wide array of applications (manufacturing, dentistry, metallurgy, etc.) and as result of its use the amount of mercury mobilised and released into the atmosphere has increased compared to pre-industrial levels. Figure 1.1 shows the Hg emission obtained by model simulations (Smith-Downey *et al.*, 2010) for pre and post-industrial conditions. This model simulation highlights a factor of 3 difference between pre-industrial and present-day conditions in the Hg emissions (around 2900 Mg y^{-1} in present-day conditions respect the 1000 Mg y^{-1} estimated for pre-industrial time). The net difference in global Hg concentrations between pre and post-industrial time is evident also considering the amount of atmospheric Hg deposited at Upper Fremont Glacier (Wyoming, USA). Using the measurements of Hg in ice core over the last 270 years, reported in figure 1.2, it is possible identify a positive trend in Hg concentrations. Considering the oldest measurements as natural background it is possible attribute the

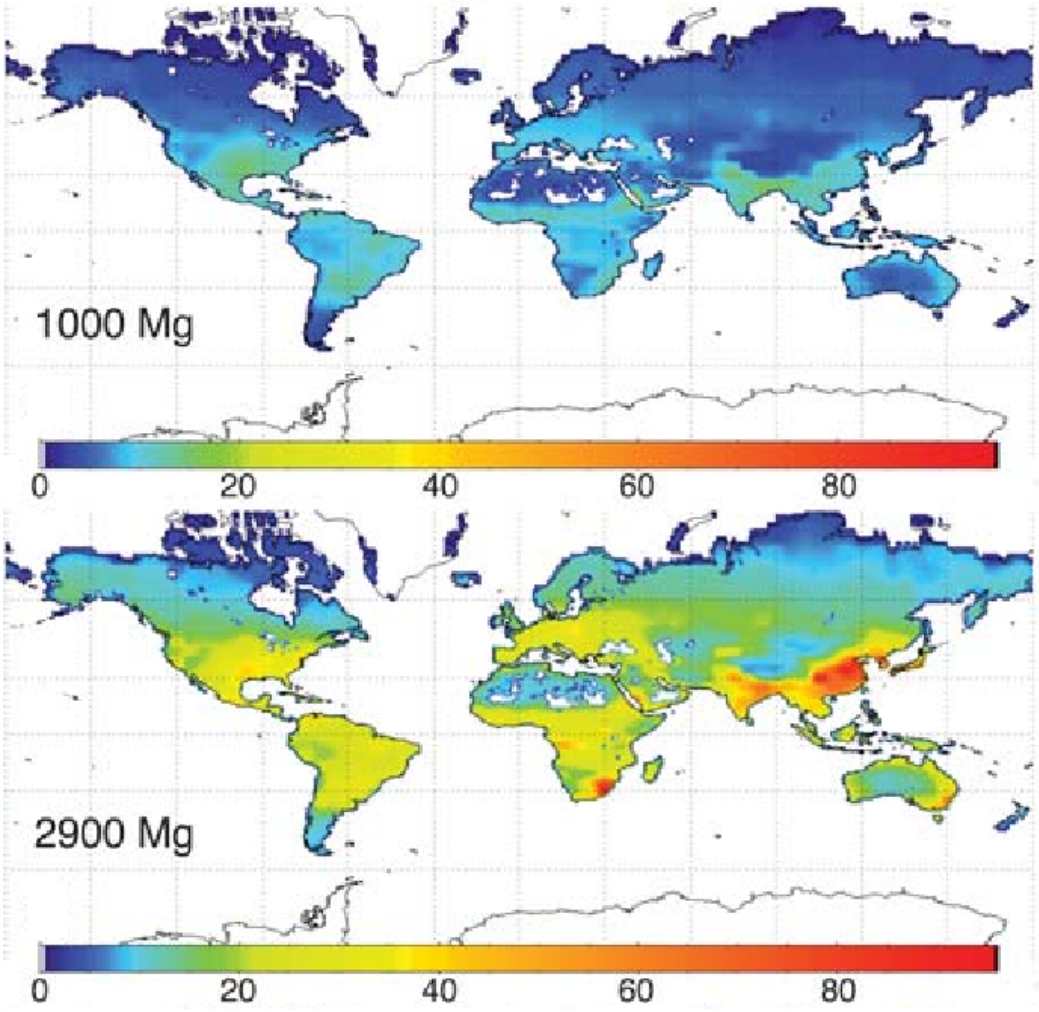

Figure 1.1: Soil Hg emissions simulated for preindustrial (upper panel) and present day (lower panel) conditions. Concentrations are in μg m^{-2} y^{-1}. Adapted from Smith-Downey *et al.* (2010).

elevated concentrations at natural (volcanic eruptions to the 1815, 1883 and 1980) and anthropogenic (global and local) source.

Research on atmospheric emissions and transport, deposition mechanisms to terrestrial and aquatic receptors, chemical transformations of elemental mercury to more toxic species, studies on the bioaccumulation of mercury in the aquatic food web as well as exposure and risk assessments has driven the scientific and political communities to consider this toxic element as a pollutant of global concern (Nriagu and Pacyna, 1988; Mason *et al.*, 1994; Pleijel and Munthe, 1995; Pacyna and Keeler, 1995; Pirrone *et al.*, 1996,

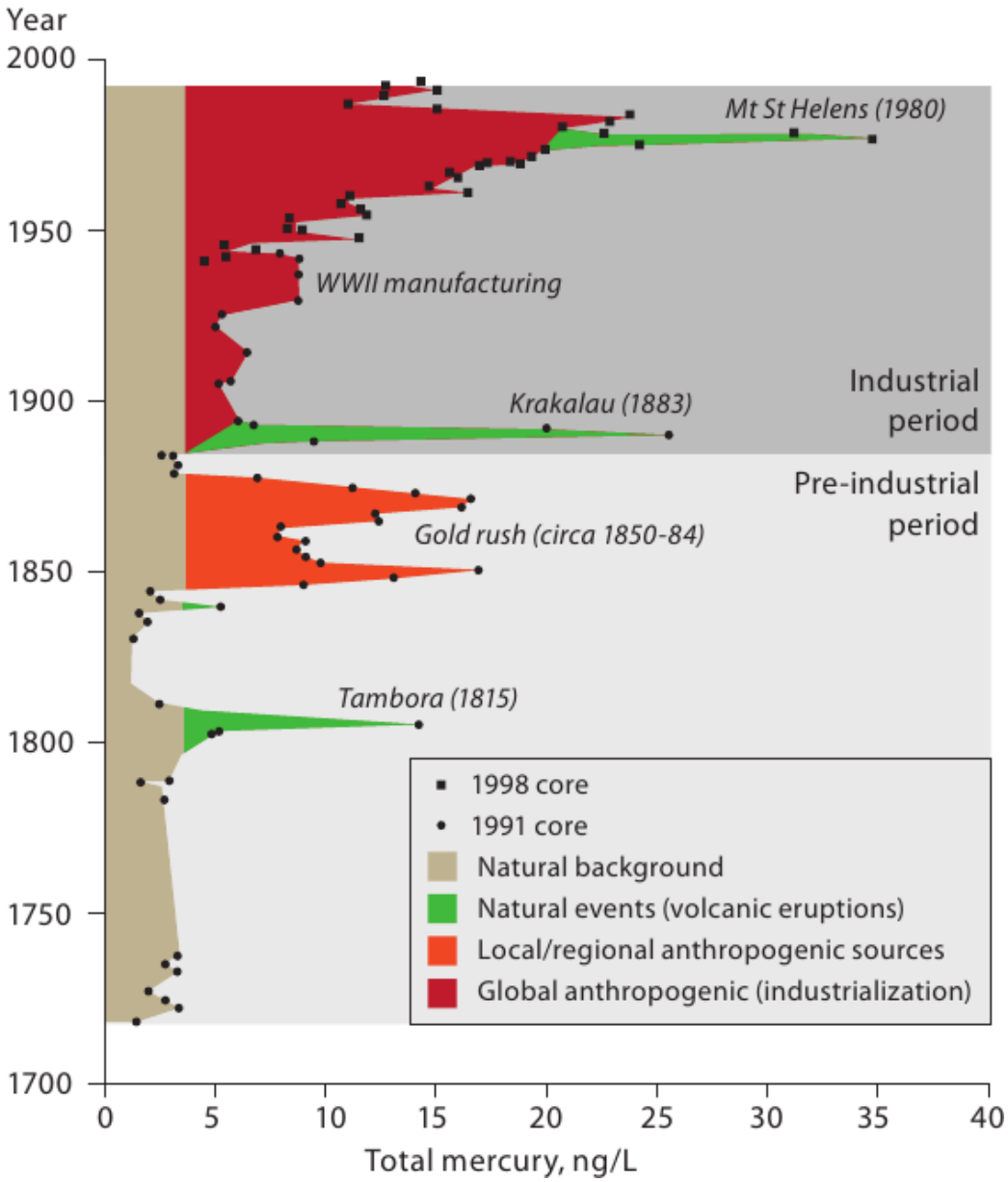

Figure 1.2: Ice core record of deposition Upper Fremont Glacier. Image from UNEP (2013a).

1998; Petersen *et al.*, 1998; Pirrone *et al.*, 2000; Pacyna and Pacyna, 2000; Munthe *et al.*, 2001; Wängberg *et al.*, 2001b).

The global mercury cycle in the biosphere is a very complex system. As indicated in figure 1.3, mercury is emitted in the atmosphere from a variety of sources, is dispersed and transported in the air, deposited to the Earth

and stored in or redistributed between water, soil, sediment and atmospheric compartments. Therefore, mercury cycling and mercury partitioning between different environmental compartments are complex phenomena that depend on numerous environmental parameters.

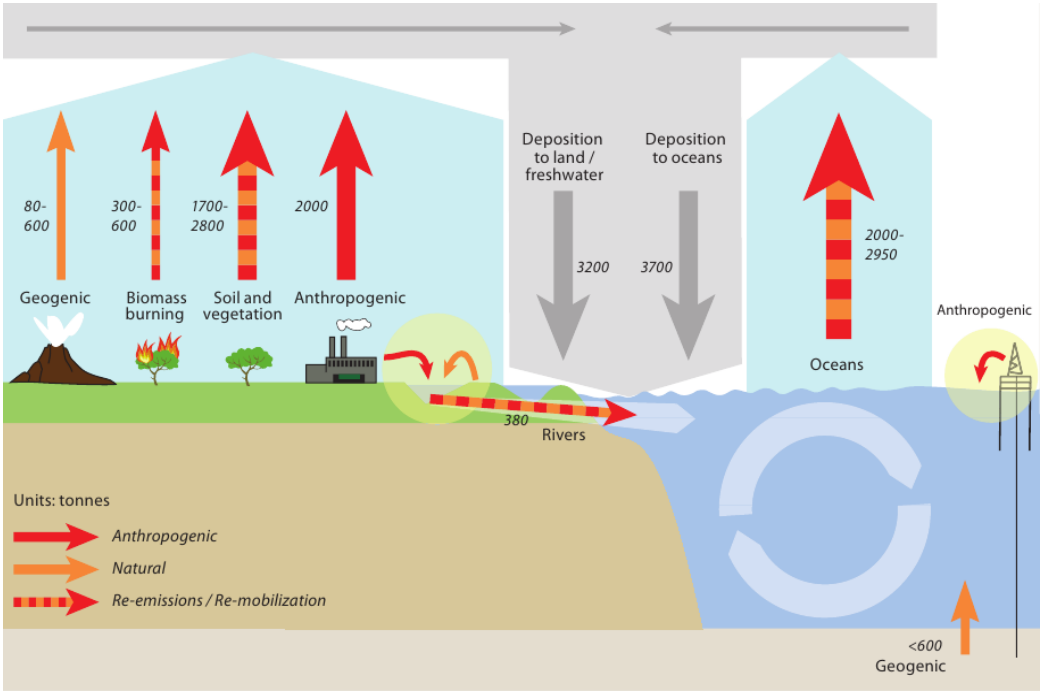

Figure 1.3: Global Hg budgets illustrate the main environmental compartments and pathways that are of importance in the global mercury cycle, and the ways in which natural and anthropogenic releases to air land and water move between these compartments. Emissions to air arise from natural sources and anthropogenic sources, as well as reemissions of mercury previously deposited from air onto soils, surface waters, and vegetation. Image adapted from UNEP (2013a).

Mercury is a global threat to human and environmental health (UNEP, 2013a), and an increase in ambient air levels of mercury will result in an increase of direct human exposure and in an increase of the mercury flux entering terrestrial and aquatic ecosystems, leading to elevated concentrations of organic mercury in freshwater fish and marine biota. Methylmercury (MeHg) is the most toxic and bioaccumulative form of organic mercury that accumulates in aquatic food web. It represents the greatest health risk to humans and wildlife and is mainly formed in aquatic environments through natural microbial processes. Humans are predominately exposed to MeHg

by consuming fish (Pirrone *et al.*, 2013).

Atmospheric mercury exists in three forms: gaseous elemental mercury (GEM or Hg^0), gaseous oxidised mercury (Hg^{II} or GOM) compounds, and Hg associated with particulate matter (Hg^P). Oxidised mercury compounds are emitted from anthropogenic sources and readily transferred to aquatic and terrestrial receptors by dry deposition processes and wet scavenging by precipitations. Oxidised mercury compounds are much less volatile, and are mostly more water soluble than GEM. The precise chemical nature of these compounds is still not known and thus the term GOM is used to describe all forms of mercury sampled from the atmosphere using a KCl-coated denuder and analysed by CVAAFS (Cold Vapor Atomic Absorption Fluorescence Spectroscopy, Landis and Keeler (2002)). Mercury associated with particulate matter can be emitted from anthropogenic sources, active volcanoes and evaporation of cloud/aerosol droplets that contained mercury compounds. These particles are generally part of the fine aerosol fraction and their transport and deposition characteristics are defined by the particle's properties. Mercury in this form is thought to be mostly insoluble. Both humans and wildlife are adversely affected by exposure to multiple chemical forms of mercury (Pirrone and Keating, 2010a) and the severity of health impacts varies with the intensity and duration of exposure. Adverse human health effects range from those detectable only with specialized testing protocols at those clinically evident, as well as death (Clarkson and Magos, 2006). High levels of MeHg exposure cause a variety of negative health effects in humans and wildlife, including kidney and liver failure, endocrine disruption, reproductive abnormalities, neurodevelopmental delays, long-term IQ deficits and compromised cardiovascular health in adults (Clarkson and Magos, 2006; Mergler *et al.*, 2007; Scheuhammer *et al.*, 2007; Tan and Mahaffey, 2009; Pirrone *et al.*, 2013)

Neurological damage produced by concurrent exposure to multiple forms of mercury may produce additive or cumulative neurological damage (Mergler *et al.*, 2007). People living in artisanal gold mining areas with long-term environmental contamination in mining wastes are exposed concurrently to inorganic mercury vapor and MeHg. Within these regions, elevated MeHg exposures among fish-consuming workers and their families are attributable to bioaccumulation of MeHg in the aquatic food chain (Pirrone and Keating, 2010a). Thus MeHg is the most dangerous Hg form for human health, and the oxidation processes are very important in the increase of MeHg. Infact GOM is deposited more readily at the ground and in the water, where it turns into MeHg.

1.1 Emissions

Mercury is a naturally occurring element that is contained in many minerals, particularly cinnabar, an ore mined to produce mercury, also is much of the present day demand for mercury is met by supply from mercury recovered from industrial sources and stock rather than from mercury mining. Mercury is also present as an impurity in many other economically valuable minerals (in particular the non-ferrous metals) and in fossil fuels, coal in particular (UNEP, 2013b). Thus processing of mineral resources at high temperatures, such as combustion of fossil fuels, roasting and smelting of ores, kiln operations in the cement industry, as well as incineration of wastes and the production of certain chemicals, result in the release of several volatile trace elements to the environment. Mercury is one of the most important trace elements emitted to the environment due to its toxic effects on the environmental and human health. Our knowledge of mercury emissions on a global and regional scale is still incomplete (Pirrone *et al.*, 2001). The majority anthropogenic emissions and releases have occurred since 1800, associated with the industrial revolution based on coal burning, base-metal ore smelting, and gold rushes in various parts of the world (figure 1.2).

Hg is emitted in the atmosphere from a variety of natural and anthropogenic sources (Nriagu and Pacyna, 1988; Pirrone *et al.*, 1996; Pacyna and Pacyna, 1996; Pirrone *et al.*, 1998; Pacyna and Pacyna, 2000; Pacyna *et al.*, 2001). Thus the Hg emission can be classified in natural and anthropogenic, and the ratio between the relative contributions of these sources category may vary within a region and time of the year (Pirrone and Mason, 2009).

Source	Mason (2009) Pacyna *et al.* (2010)	Pirrone *et al.* (2010)	UNEP (2013a)
Natural (total)	4532	5207	4080-6950
Ocean	2682	2682	2000-2950
Biomass burning		675	300-600
Volcanoes-geogenic	90	90	80-600
Anthropogenic (total)	1926	2320	1960

Table 1.1: Global natural and anthropogenic emissions (Mg yr^{-1}) from various estimates.

Global estimate shown for the year 2008 an amount between 4500 Mg yr^{-1} (Mason, 2009) and 5200 Mg yr^{-1} (Pirrone *et al.*, 2010) of Hg emitted from natural sources, while for anthropogenic sources estimate for year 2005 are between 1900 Mg yr^{-1} (Pacyna *et al.*, 2010) and 2300 Mg yr^{-1} (Pirrone *et al.*, 2010), as shown in table 1.1. More recent estimates (UNEP, 2013a) confirm

these values and shows around 2000 Mg yr^{-1} for anthropogenic source and a range among 4000 and 7000 Mg yr^{-1} for natural emissions.

1.1.1 Natural sources

Natural sources are very important contributors to the total budgets of atmospheric mercury. They include crustal degassing, volcanoes, a component of the reemission of previously deposited Hg from soils and aquatic surfaces, weathering processes of the Earth's crust and some forest fires (Pirrone *et al.*, 2010). In particular the Hg evasion from the oceans is the largest source of mercury in the atmosphere. On a global scale, the dominant component of the mercury released from terrestrial and oceanic systems is previously deposited anthropogenic mercury (legacy) rather then geogenic sources (Streets *et al.*, 2011). Contributions from natural sources and processes vary geographically and over time depending on a number of factors including meteorological conditions, the presence of volcanic or geothermal activities, the presence of Hg bearing minerals such as cinnabar, the magnitude of exchange processes between waters and the atmosphere, the reemission of previously deposited Hg from top soils and plants, and also the occurrence of forest fires (Mason, 2009; Friedli *et al.*, 2009; Pirrone *et al.*, 2010).

Two major source categories would include the sources related to the geological presence of mercury in various minerals and evasion of mercury from aquatic and terrestrial ecosystems. The latter source category is very much related to the historical atmospheric deposition of mercury to these ecosystems, emitted originally also from anthropogenic activities. It is extremely difficult with the current status of our knowledge to differentiate between the reemission of mercury originally from anthropogenic and natural sources (Pirrone *et al.*, 2001).

Mercury from the oceans

Mercury in ocean waters is mostly present as GEM (Mason *et al.*, 2012). Globally, total Hg concentrations in the ocean mixed layer are generally < 1 pM (1 M = 1 moles l^{-1}) (Soerensen *et al.*, 2010). Mercury air-sea exchange is primarily driven by the concentration gradient of GEM between the top-water microlayer and the air above, by solar irradiation (responsible for redox processes) and by wind speed and temperature at the air-water interface (Pirrone and Wichmann-Fiebig, 2003; Soerensen *et al.*, 2010). A detailed description of sea water-air exchange processes is given in section 3.1.4.

Mercury from the volcanoes and geothermal areas

Emissions from volcanoes are one of the major geological sources of Hg globally and in Europe (especially in Southern Europe) together with evasion of the element from lands containing Hg minerals. The volcanic contribution, which may be an important source at the local scale, varies over time depending if they are in degassing or eruption phase (Pirrone and Mason, 2009). Table 1.1 summarises the amount of Hg emissions from this sources. As a consequence of mercury content in vegetation, Hg emission from biomass burning can be significant (Friedli *et al.*, 2003; Pirrone and Mason, 2009). This contribution is often not well constrained in regional emissions estimates, especially in very dry regions such as the Mediterranean and several countries of African, South American and South-East Asian. However it represents an important contribution to the global atmospheric Hg budget (Pirrone and Mason, 2009).

1.1.2 Anthropogenic sources

Mercury is released to the atmosphere from a large number of human sources, linked to large-scale industrial facilities, particularly coal fired electricity generation, cement production and metallurgical industries (Pirrone *et al.*, 2013; Pirrone and Mason, 2009; Pirrone *et al.*, 2010). Information on chemical and physical species of mercury emitted from various anthropogenic sources is needed for the development of models of transport and transformations of the element in the environment. Globally more than half of mercury from anthropogenic sources is emitted as GEM, while only 10% of emissions occur as Hg^P. The rest of the mercury is emitted as GOM (Pirrone *et al.*, 2001).

Recent estimates of global emission (UNEP, 2013a), reported in table 1.2, indicate that Europe and North America contribute less than 8% to the global anthropogenic emissions of the Hg to the atmosphere while the majority of the emissions, originate from combustion of fossil fuels, are in the East and Southeast Asia (see figure 1.5). Combustion of coal in Southeast Asia is and will remain in the near future as the main source of energy (Pirrone *et al.*, 2001).

Most of the anthropogenic Hg emission occurs in the northern hemisphere (Pirrone *et al.*, 2013; Pacyna *et al.*, 2010; Pirrone *et al.*, 2010; Pirrone and Keating, 2010b), and the lifetime of atmospheric mercury (Hedgecock and Pirrone, 2004; Corbitt *et al.*, 2011) is such that this is reflected in the difference in the background concentration of Hg in the northern and southern hemispheres: at the North of the equator observed background Hg concentra-

Region	Emission	%
Australia, New Zealand and Oceania	22.3	1.1
Central America and the Caribbean	47.2	2.4
CIS and other European countries	115	5.9
East and Southeast Asia	777	39.7
European Union	87.5	4.5
Middle Eastern States	37.0	1.9
North Africa	13.6	0.7
North America	60.7	3.1
South America	245	12.5
South Asia	154	7.9
Sub-Saharan Africa	316	16.1
Undefined	82.5	4.2
Total	1960	100

Table 1.2: Emissions from various regions (Mg yr^{-1}) and as a percentage of total global anthropogenic emissions. See figure 1.4 for the regions specification. Table adapted from UNEP (2013a).

Figure 1.4: Region to the table 1.2 (UNEP, 2013a).

tions are around 1.7 ng m^{-3}, while in the southern hemisphere these values are around 1.2 ng m^{-3}.

Generally the Hg emissions estimates are calculated by multiplying the amount of activity (amounts of fuels burned, raw materials consumed, materials produced, etc.) by an Emission Factor (EF), that is an estimate of the

mercury emitted per unit of activity. But emissions control technology and coal types burned at the various industry often vary between nations so it is not always possible to use EF measured at one installation to another in a different area (Pirrone *et al.*, 2001).

One of the most important factors concerning mercury emissions is the speciation of mercury emitted (GEM, GOM and Hg^P), because the proportion of GOM and Hg^P dictates the extent of local deposition. In figure 1.5 are reported the spatial distribution of global anthropogenic Hg emissions estimated for the year 2010.

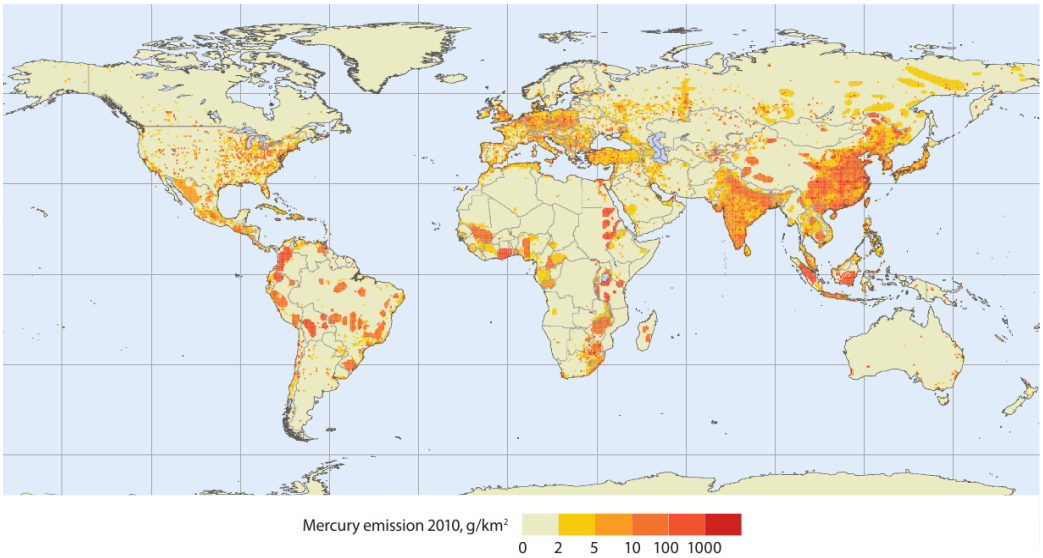

Figure 1.5: Global distribution of anthropogenic mercury emissions to air in 2010 (UNEP, 2013a).

1.1.3 Speciation of anthropogenic Hg emissions

Accurate information on emissions of the various chemical forms of Hg is needed by the modelers simulating long-range transport and atmospheric deposition of the element to the marine and terrestrial surfaces (Pirrone *et al.*, 2001). While the natural emissions are almost 100% GEM (some particles from volcanoes and fires), there are many uncertainties about the speciation of Hg anthropogenic emissions. The major chemical form of mercury emitted from the anthropogenic sources in Europe to the atmosphere is GEM (61% to the total; GOM 32% and Hg on particles around 7%) of the total.

1.2 Atmospheric transport and transformations

In the atmospheric Hg cycle a critical aspects is the oxidation of Hg^0 to Hg^{II}. This reaction controls the distance which Hg is transported, determining deposition patterns and fluxes because the elemental and oxidised Hg have very different chemical and physical characteristics.

GEM is relatively volatile and inert to chemical reactions with other atmospheric constituents and is only slightly soluble in pure water. This gives elemental mercury an atmospheric residence time of approximately one year (Pirrone *et al.*, 2001; Slemr *et al.*, 1985). Once released to the atmosphere Hg can be dispersed and transported for long distances over hemispheric and global scales before being deposited to terrestrial and aquatic ecosystems. Hg^{II} does not remain in the atmosphere for long before it is either dry deposited or scavenged by clouds or rain. Hg^{II} and Hg^{P} are typically present in concentrations less than 1 % of the Hg^0. Especially near the emissions sources it is possible have large variations in the Hg emissions speciation (Pirrone *et al.*, 2001).

There are a number of possible oxidation pathways for Hg in the atmosphere, some have been measured in laboratory kinetics experiments and others have been estimated using theoretical chemistry methods. Some have even been hypothesised from regional/global modelling studies, because the model results failed to a greater or lesser extent to match observations. Actually there are two different Hg oxidation mechanisms which are considered possible: oxidation by Br and BrO and oxidation by O_3 and OH. The level of uncertainty is such that both O_3/OH and Br/BrO oxidation mechanisms are used regularly (but not together) in global and regional models.

1.2.1 O_3/OH oxidation

The most important gas phase oxidation pathways are the reactions with ozone (Hall, 1995) and OH radicals (Hynes *et al.*, 2009; Ariya *et al.*, 2009; Subir *et al.*, 2011, 2012). Oxidation of Hg^0 leads to Hg^{II} species which are notably less volatile than Hg^0 and will tend to condense onto atmospheric particulate matter or be deposited to terrestrial or marine surfaces. In the presence of liquid water in the atmosphere (fog, cloud water or precipitation) small amounts of Hg^0 are dissolved and can be oxidised in the aqueous phase by ozone (Munthe and McElroy, 1992) or OH radicals (Gårdfeldt *et al.*, 2001). The reactions in the aqueous phase occur at a significantly higher rate than in the gas phase. However the rate of oxidation in aqueous and in gas phase

are comparable, because the liquid water content in the atmosphere and the solubility of Hg^0 in water are low.

1.2.2 Br/BrO oxidation

Recent laboratory kinetic studies suggest that the global mean lifetime of Hg^0 under atmospheric conditions considering the oxidation by ozone (120 - 210 days, Hall (1995); Pal and Ariya (2004)) and OH (60 - 1500 days, Sommar *et al.* (2001a); Pal and Ariya (2004)) can not explain the observed residence time of total atmospheric mercury (6 month - 2 years, Schroeder and Munthe (1998)).

Recently Goodsite *et al.* (2012) developed a homogeneous mechanism for Hg-Br chemistry in the troposphere based on theoretical kinetic calculations, and showed that gas-phase oxidation of Hg^0 by Br atoms could explain mercury depletion events in the Arctic springtime boundary layer (Hedgecock *et al.*, 2008), and suggested that this mechanism would be important more generally in the marine boundary layer (Hedgecock *et al.*, 2005; Sprovieri *et al.*, 2010) and on the global scale (Holmes *et al.*, 2006). Subsequently Lin *et al.* (2006) suggested that Hg-Br chemistry is also significant in the upper troposphere. Actually oxidation by Bromine compounds is used in many global model (GEOS-Chem Holmes *et al.* (2010), GRAHM (Durnford *et al.*, 2012) and CTM-Hg (Seigneur *et al.*, 2006)), though there are doubts about the possibility that Br atoms and Br containing compounds can oxidise elemental Hg in the atmosphere.

1.2.3 Hg reduction

Reduction back of Hg^{II} to Hg^0 and subsequent transfer back to the gas phase may also occur via reactions with dissolved sulphite dioxide and HO_2 radicals. The complex chemistry of Hg^{II} in the liquid phase regulate the rate of reduction. There is a range of possible products of more or less importance depending on the pH of the aqueous phase and on the chemical composition of the original aerosol particle. In particular Hg^{II} in fog and raindrops may adsorb to particulate matter scavenged by the droplets, that is particularly likely if the particulate matter is rich in elemental carbon, as in the case of soot that have high adsorption coefficient for Hg (Pirrone *et al.*, 2001).

1.3 Atmospheric Hg modelling

Chemical Transport Models (CTMs) are a useful tools for investigate the mercury pollution. Their role is particularly important for the evaluation of atmospheric mercury dispersion over long distances, taking into account the limited coverage of existing monitoring networks. In particular, model simulations provide estimates of mercury ambient concentration and soil deposition on global and regional scales, forecasts of future pollution changes and evaluation of intercontinental transport. The application of chemical transport models can supplement direct measurements, giving more detailed and comprehensive information on mercury cycle.

Current knowledge on Hg behavior in the atmosphere and its potential to cycle among different environmental media is still incomplete, in spite of the development of modelling approaches and the considerable progress in analytical chemistry of atmospheric mercury during the last decade. Remain significant gaps in the knowledge of chemical processes affecting mercury atmospheric transport and deposition, the characteristics of air-surface exchange and the processes responsible for reemission of mercury to the atmosphere. Therefore, application of global and regional scale mercury models, in combination with extensive monitoring data, could facilitate further understanding of the principle mechanisms governing mercury cycling and dispersion in the environment, as well as improving model parameterizations.

Another important use of atmospheric modelling is the evaluation of global emission inventories. Existing global mercury emissions data contain significant uncertainties, particularly as they relate to estimates of natural emissions from terrestrial and oceanic sources. Using global atmospheric models with different emission estimates and comparing the model results with measurements, it can provide an additional evaluation of the emission inventories. Therefore, development of an integrated approach that include combined consideration of emissions inventories, monitoring data and modelling results, could significantly improve the assessment process. A key element of such an integrated approach is the availability of feedbacks between the assessment elements (emissions, monitoring and modelling).

Currently a number of mathematical models have been developed to simulate the emission, dispersion, transport and deposition of mercury in the atmosphere. The simulation of atmospheric mercury is a challenging task, because it requires extensive treatment of multiple species that exist in different phases in the atmosphere and shows distinct physical and chemical properties. The different interactions between various mercury species and the atmospheric environment are very complex, and require careful consideration of the science processes in atmospheric mercury models. These models

vary extensively in their scope, formulation and specially spatial and temporal scales. In fact a first model classification is based on the spatial scale of model application, with the distinction between regional and global models. Another import distinction is between online and offline models.

1.3.1 Regional Hg modelling

A regional CTM is a type of numerical model which typically simulates atmospheric chemistry, atmospheric dispersion and trans-boundary transport within a continent or particular region, with spatial resolution from 1 to 100 km. These models are usually applied for the simulations of mercury dispersion over areas containing numerous emission source, and where want to get a high details level. The primary strengths of these models are the detailed treatment of Planetary Boundary Layer (PBL) processes and relatively high spatial resolutions. Mercury deposition is mostly determined by regional emissions of short-lived mercury forms (GOM and Hg^P) and by in-situ oxidation of Hg^0 transported regionally and globally. Because the inflow of various mercury species from the domain boundaries can significantly influence the simulation results of regional models, they rely on appropriate boundary concentration fields for simulations, often by assuming background mercury concentrations at domain boundaries but preferably interpolated from global model results.

1.3.2 Global Hg modelling

Global models were developed to study the global mercury atmospheric cycle. Hemispheric models are an intermediate case between regional and global models because they cover mercury dispersion over one of the hemispheres, but still have a lateral boundary along the equator. Global and hemispheric models are commonly applied for long-term simulations (several years). In addition to the detailed treatment of gaseous chemistry and upper air circulations, one important advantage of global models respect regional models is that they are capable of creating global concentration fields constrained to available field measurements. However, they commonly have lower spatial resolution compared to regional models (spatial resolution around 100 - 500 km).

A very useful application of global models is to provide the Boundary and the Initial Conditions (BC/IC) to regional mercury models which perform simulations at higher spatial and temporal resolutions. Regional CTM simulations of atmospheric Hg chemistry and deposition have been shown to be particularly sensitive to the BC which are used (Pongprueksa *et al.*, 2008).

Boundary conditions for regional simulations are generally more important than initial conditions for regional Hg CTMs, and therefore recently most regional models make use of time and space varying BC from global model output. However there can be some variation in the regional modelling results depending on which global model output is used (Bullock *et al.*, 2008; Harris *et al.*, 2012).

1.3.3 Offline and Online model

The offline air quality models have the fundamental assumption that it is possible to make accurate air quality simulations ignoring the coupling between chemical and meteorological processes (Grell *et al.*, 2004). This approach requires an initially running a meteorological model, independently of the CTM. The output from the meteorological model, typically available every 30-60 minutes, is used to drive the transport in the chemistry simulation. This methodology has many computational advantages, but the separation of meteorology and chemistry can also lead to a loss of potentially important information about atmospheric processes that often have a time scale much smaller than the meteorological model output frequency (wind speed and directional changes, cloud formation and rainfall). Furthermore, in an offline model the feedback from chemistry to meteorology cannot be considered, and these deficiencies make the alternative online approach more attractive.

In online model the chemistry is integrated simultaneously with the meteorology, allowing feedback at each model time step both from meteorology to chemistry and from chemistry to meteorology. In this way is possible reproduce the strong coupling of meteorological and chemical processes in the atmosphere. Online models can also be used to study the influence of air quality on regional climate and weather.

Thus the online modeling allow the feedback between chemistry and meteorology, permitting a better characterization of the dispersion of air pollutants. But there are also disadvantages in online approaches. One such disadvantage is seen in operational weather forecasting, where a longer computational time is required to produce the meteorological conditions with an online air quality prediction, while an offline chemical transport simulations require only a single meteorological data set to produce many chemical transport simulations to examine a particular situation. These research issues may only be related to air chemistry, thus it may not be necessary to run the modeling system online.

1.3.4 Measurements and model development

Models for transport and chemistry of atmospheric species are based on input with a significant range of uncertainty (Pirrone and Mason, 2009). This is true especially for Hg models, because essential characteristics of atmospheric cycling and photochemical transformation of Hg concern more uncertainty relative also to other atmospheric species. The principal role of measurements in model development is to provide a basis for evaluating the model accuracy in simulating ambient conditions. Comparisons to the predicted values with the observed ambient measurements are the central test for establishing the accuracy of models (e.g. Selin *et al.* (2007); Strode *et al.* (2008); Hedgecock *et al.* (2006); De Simone *et al.* (2013); Gencarelli *et al.* (2013a)). When model predictions show significant differences from measured values, this is frequently concerned as evidence of errors in the models, and suggest investigation and modification of model input assumptions or spatial resolution. Thus ensembles of measured values provide a basis for constraining the assumptions used by models (Pirrone and Mason, 2009). Ambient meteorological measurements can be also used as input directly in CTMs.

Thus the model evaluation is an essential part of the model development process. Model-measurement comparisons can be used to provide indication on problem that are relevant to policy concerns and provide a basis for constraining the range of assumptions used by models, especially with regard to emission rates and photochemical reaction sequences (Pirrone and Mason, 2009).

Models also represent a key component of a global research framework, as they are able to play many important roles such as:

- helping to determine the optimal locations for long-term observational sites and short-term process studies, in order to maximize the usefulness of the data collected;
- assimilating the observational data acquired from different monitoring systems and helping to place isolated measurements in a larger context;
- providing simulations of future Hg trends, fluxes, and coupling with water quality changes.

Chapter 2

Tropospheric ozone in Mediterranean area modelling

Measurements of ozone at numerous locations in the Mediterranean area have all shown that the region shows significantly higher levels of ozone concentrations than European background sites. The region also shows episodes during which ozone concentrations reach and remain at levels which exceed European Union standard values (considered harmful for human health and which also have a detrimental effect on vegetation and agriculture).

A recent report to the European Environment Agency shows that up to 15% of the European's urban population is exposed to ozone concentrations above 120 μg m^{-3} (EEA, 2013). Elevated concentrations of O_3 have been observed at coastal sites (Nolle *et al.*, 2002; Saliba *et al.*, 2008; Gerasopoulos *et al.*, 2005), inland sites (Cristofanelli and Bonasoni, 2009), during intensive field campaigns (Lelieveld *et al.*, 2002), and also over the sea itself as shown by measurements performed on board a cruise liner (Velchev *et al.*, 2010) and on board the Italian Research Council's R. V. Urania as described in this chapter (section 2.1).

The Mediterranean Basin is contributes to the production of elevated levels of O_3 for both geographical and meteorological reasons. During the summer the Mediterranean is under the descending arm of the Hadley circulation, leading to prolonged periods of stable, warm and sunny weather, which favours both O_3 formation and the natural production of VOC (Millán *et al.*, 2002). In the Western Basin the formation of diurnal recirculation patterns between the land and the sea mean that O_3 rich air produced over land during the day is moves over the sea in the evening, where it is effectively stored over night. In the morning the onshore breeze carries that same air back over land, where it can continue to accumulate precursors and produce more O_3 (Millán *et al.*, 2002; Adame *et al.*, 2009).

The recirculation phenomena seems to be more important in the Western Basin than the Eastern (Velchev *et al.*, 2010), both the Eastern and Western Basins of the Mediterranean are influenced by the outflow of polluted air masses from more central and northern parts of Europe (Lelieveld *et al.*, 2002; Kalabokas *et al.*, 2007, 2008; Cristofanelli and Bonasoni, 2009). The Eastern region of the Mediterranean is also becoming more influenced by increasing urbanization, the growth of Istanbul and Cairo being the most obvious examples (Kanakidou *et al.*, 2011; Im and Kanakidou, 2011). The transport of polluted air form central to Northern Europe has been implicated in air quality high levels in North Africa and the Middle East (Duncan *et al.*, 2008), while trans-Atlantic transport of polluted air from North America appears to influence O_3 concentrations in the free troposphere over the Mediterranean (Lelieveld *et al.*, 2002; Auvray and Bey, 2005; Cristofanelli and Bonasoni, 2009).

Ozone produced in the boundary layer can be advected upwards to the free troposphere, for example polluted air from the Po Valley in Italy has regularly been detected on Monte Cimone in the Apennines (Bonasoni *et al.*, 2000; Cristofanelli *et al.*, 2007; Cristofanelli and Bonasoni, 2009). Increased O_3 in the free troposphere over the Mediterranean is of interest because its impact efficacy as a greenhouse gas is greater in the free troposphere than it is in the boundary layer, generally speaking the capacity of O_3 to trap heat in the atmosphere increases from the ground to the tropopause (Worden *et al.*, 2011). The impact of regional climate change on O_3 concentrations in the Mediterranean region has also been investigated recently, with a particular focus on the Eastern Mediterranean, where the rapid growth of a number of population centers and the envisaged increase in temperature in a future climate (particularly in summertime), has led to some concern over future air quality. Im and Kanakidou (2011) have performed a series of air quality modelling studies in which the effect of temperature perturbations have been investigated. The authors found an increase of approximately 1 ppb in the O_3 concentration with each 1K rise in temperature. The Mediterranean has been identified as a regional hot spot in terms of air quality (Monks *et al.*, 2009), and is a region that has been identified as susceptible to climate change, the probable future summer time temperature increase, will have repercussions for both atmospheric composition and the hydrological cycle (IPCC, 2007).

In addition to the characteristics described above the Mediterranean is one of the busiest shipping routes in the world. Emissions from shipping have been coming under increasing scrutiny over the last several years (Eyring *et al.*, 2005, 2007, 2010; Marmer and Langmann, 2005; Corbett *et al.*, 2007; Matthias *et al.*, 2010; Miola and Ciuffo, 2011). The impact of shipping emissions is expected in to increase in magnitude as global maritime traf-

fic increases, and in relative importance as legislation regulating emissions from terrestrial industry and transportation becomes increasingly strict, and widely applied. The environmental consequences of ship emissions can be numerous; the particulate matter directly emitted has consequences for human health (Corbett *et al.*, 2007), SO_2 emissions can lead to sulphate particle formation, which can have a cooling effect on climate, while the black carbon emitted can have the opposite effect. NO_x emissions can locally titrate O_3, but after being dispersed lead to enhanced O_3 production in coastal areas (Vutukuru and Dabdub, 2008; Song *et al.*, 2010). Ship emissions can also to acidification and eutrophication via nitrate deposition to coastal waters and land (Derwent *et al.*, 2005; Dalsøren *et al.*, 2009). The role ship emissions play in tropospheric photochemistry and the methodologies to include them in Chemical Transport Models (CTMs) is discussed in more detail in section 2.3.2. Oceanographic campaigns with the primary aim of studying the mercury cycle in the Mediterranean have been performed aboard the Italian Research Council's Research Vessel, the R. V. Urania, almost every year since 2000 (section 2.1.2). During these campaigns O_3 measurements were also made. The results from 2005 campaign (in the Adriatic) were used to examine the oxidation of Hg in the Marine Boundary Layer (MBL) (Sprovieri *et al.*, 2010), because of the particularly high average O_3 concentration, slightly over 60 ppb. To investigate the reasons behind the high O_3 concentrations observed, a preliminary study of this campaign using WRF/Chem (Grell *et al.*, 2005) was performed. During this study the influence of shipping emissions on O_3 production over the Adriatic region became evident. This study has now been extended to include the the oceanographic campaigns performed over different routes in the Mediterranean in 2000, 2003, 2004, 2006, 2009 and 2010 as described in this chapter (based on Hedgecock *et al.* (2012)).

2.1 Measurements

2.1.1 Measurements aboard the R. V. Urania

Ozone concentrations were measured using an Teledyne–API model 400A UV ozone analyser. The analyser was calibrated every 24 hours using an internal permeation source, and employing a sampling flow rate of $0.8\,\mathrm{l\,min^{-1}}$, over a five minute period gave a detection limit of 0.6 ppb. The same instrument has been used on all the oceanographic campaigns to date. The R. V. Urania is equipped with an automated weather station which is approximately 30 m above the sea surface. Of most interest to the validation

Year	Start	End	Route
2000	Palermo 14 July	Rome 09 August	Strait of Messina, South of Crete, Sicily, Gulf of Naples, Sardinia
2003	Palermo 05 August	Livorno 28 August	Strait of Sicily, towards Crete, Ionian Sea, Naples, Alboran Sea
2004	Naples 17 March	Naples 05 April	Gulf of Genoa, Corsica, Sicily, Strait of Otranto, Strait of Messina
2005	Naples 17 June	Naples 03 July	Sicily, Ionain Sea, Adriatic Sea
2006	Rome 04 July	Messina 20 July	Sicily, Eastern Med., Ionian Sea
2009	Rome 04 June	Messina 30 June	Corsica, Sardinia, Naples, Strait of Sicily, Ionian Sea
2010	Naples 27 August	Palermo 12 Sept.	Strait of Messina, Ionian sea, Gulf of Taranto, Eastern Med., Strait of Sicily

Table 2.1: The oceanographic campaign periods

were the temperature, humidity, wind speed and direction data which were available at five minute intervals.

2.1.2 The Med-Oceanor Series of Oceanographic Campaigns

The Med–Oceanor oceanographic campaigns are part of a continuing series of almost yearly research cruises aboard the R. V. Urania, which began in 2000. Their primary aim has been to investigate Hg cycling in the Mediterranean boundary layer, surface water, the water column, sediments and the exchange of Hg species between the water and the atmosphere (Sprovieri *et al.*, 2003; Andersson *et al.*, 2007; Kotnik *et al.*, 2007; Ferrara *et al.*, 2003; Gårdfeldt and Jonsson, 2003). However as well as Hg species, a number of gas and aerosol phase atmospheric species have been measured each year. The campaign periods, and their start and end ports are summarised with a brief description of the area covered in table 2.1.2, and the routes are shown in figure 2.1

2.1.3 Observations from the EMEP Network

Data form the EMEP network of monitoring sites have been used for the validation of the both the meteorological and chemistry output from the WRF/Chem model.The EMEP stations chosen were those located in the highest resolution modelling domain, the positioning of which varied with the cruise path of the year in question (section 2.3.1).

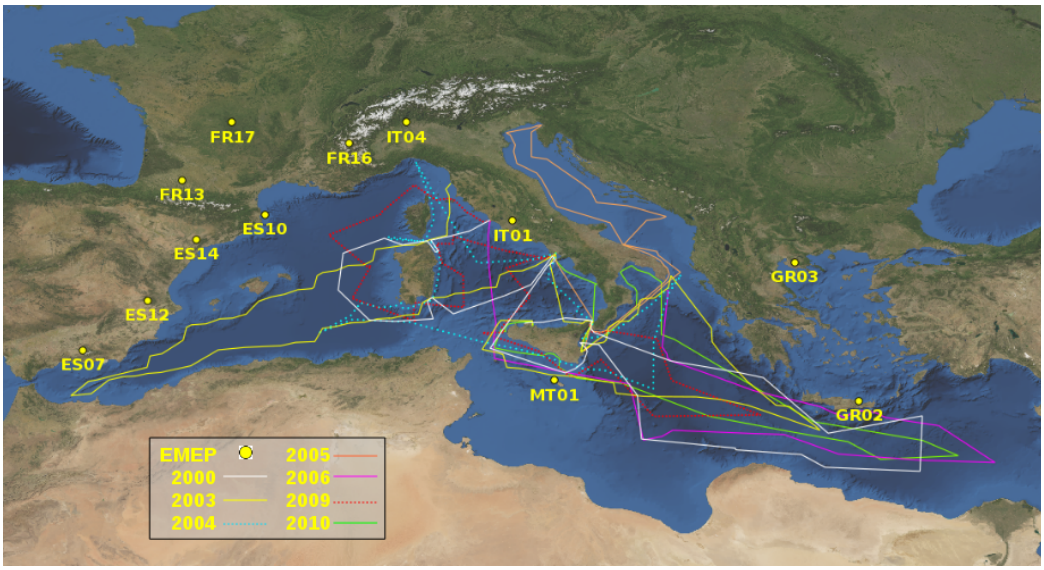

Figure 2.1: The Med-Oceanor campaign routes over the years. Also shown are the sites of the EMEP stations used in the model validation.

2.2 Modelling

2.3 The WRF/Chem model

The WRF/Chem (Grell *et al.*, 2005) is a three-dimensional model for forecasting and meteorological research, where the transport of pollutants is coupled to the dynamics and evolution of meteorological fields. This model incorporates at the model Weather Research and Forecasting (WRF, `http://www.wrf-model.org/`) modules that consider emissions of chemicals into the atmosphere, their chemical interaction and the interaction with the radiation and aqueous vapor, transport, diffusion and deposition phenomena.

WRF/Chem is an "on-line" (both physics and chemistry of the atmosphere are calculated in the same time step, instead of using meteorological data calculated above) and the transport of chemicals is solved using the same vertical and horizontal coordinates (avoiding interpolations both vertically and horizontally). This is very important feature when the spatial resolution of the pattern is high. The model in fact allows you to define different spatial domains of investigation, also with horizontal resolution of the order of 1-3 km that can define geographic areas of interest where simulate atmospheric dynamics. For the boundary conditions the model uses the results from simulations on a global scale or the same model WRF/Chem results, used to simulate larger areas. Only thanks to these high resolutions

can adequately represent atmospheric dynamics and chemical reactions that occur in areas characterized by a complex orography.

The WRF/Chem has a choice of different chemical mechanisms able to reproduce the chemical concentrations of both primary pollutants that of secondary ones. It also provides the ability to define new mechanisms ad-hoc for specific cases or situations, in order to investigate specific chemical reactions.

The model can simulate the chemistry and physics of atmospheric particulate matter, describing the nucleation, growth and deposition of both inorganic and organic secondary particulate.

Anthropogenic emissions can be included by global and regional databases, and they can also be supplemented by measurements.

The biogenic emissions can also be calculated "on-line" from the model. In this case the flows are function of the use of the soil, to the season and to the hour of day, using the system USGS (U.S. Geological Survey) to describe the use of the soil (this system divides land use into 24 different categories).

The model can reproduce the flow of ground dry and wet deposition: the flows of deposition of atmospheric particles and gases are calculated as function of the concentration and deposition rate, calculated from the model, while for the wet deposition are considered the nucleation phenomena and scavenging at ground.

2.3.1 The model setup

Modelling domains

The first modelling domain of 66 by 66 grid cells (81 km by 81 km resolution centred at 51°N and 13°E), covers an area from the edge of Greenland, includes all of Scandinavia, and extends as far south as the northern part of the Red Sea and to the East beyond the Black Sea, see figure 2.2. The intermediate domain has a resolution of 27 km by 27 km and was chosen according to the cruise route in such a way that to provide an adequate number of grid cells between its boundaries and the inner (9 km by 9 km) domain, which was chosen to cover the area taken in by the campaign as shown in figure 2.2. Twenty-eight vertical levels up to 5000 Pa were used for all three domains in all the simulations.

Physics

The non-hydrostatic mesoscale chemical transport model WRF/Chem offers a number of parametrisation options to represent the physical processes

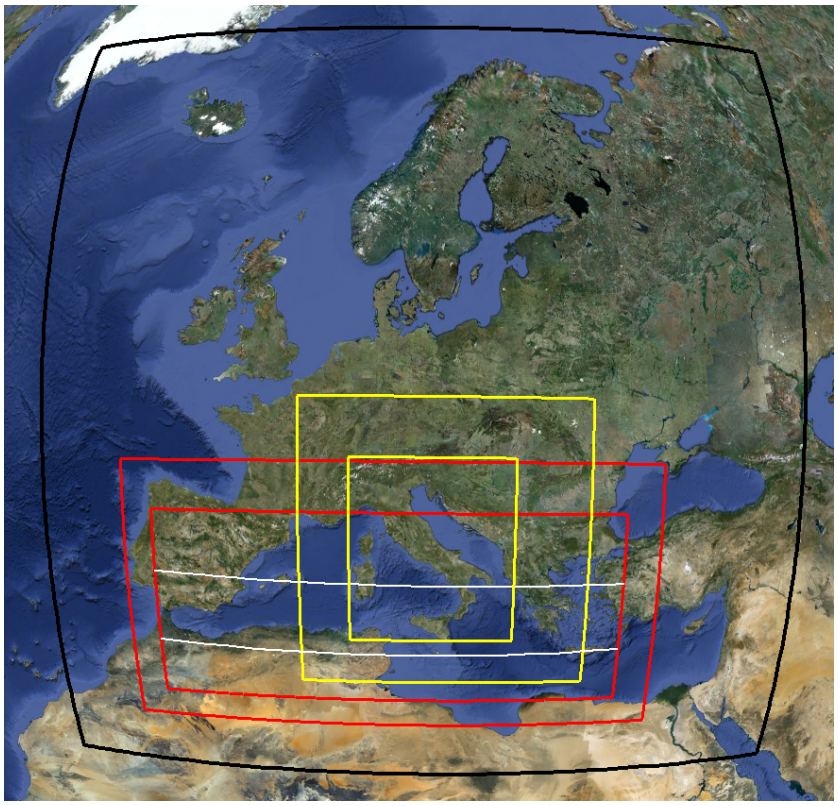

Figure 2.2: The largest modelling domain (black), and examples of the nested grids, for 2003 in red, and for 2005 in yellow. The two horizontal white lines in the smallest 2003 domain are the cross-sections at roughly 34 and 39°N described in section 2.4.3.

which take place in the atmosphere. A detailed description of these can be found in Skamarock *et al.* (2008), those used in this modelling study are as follows. The Purdue-Lin scheme was used for microphysics, it includes six classes of hydrometeors (water vapour, cloud water, rain, cloud ice, snow and graupel), the Mellor- Yamada-Janjic (MYJ) scheme was used for the Planetary Boundary Layer (PBL) parametrisation, this scheme describes vertical sub-grid-scale fluxes due to eddy transport in the whole atmospheric column, while the horizontal eddy diffusivity is calculated with a Smagorinsky 1st order closure. The surface layer parametrisation employed was the Eta surface layer scheme (it is based on similarity theory), the Land Surface model to describe interactions between the soil and atmosphere was Noah LSM (4 soil layers), the Kain-Fritsch scheme was used for cumulus parametrisation and the Rapid Radiative Transfer Model (RRTM) and Dudhia schemes for

long and shortwave radiation respectively. The period of the 2005 oceanographic campaign was simulated repeatedly using different combinations of parametrisations to assess how the choice influenced both model output and simulation time. The combination described above proved to be the most appropriate for the studies performed. It should be pointed out that the simulations performed in this study apply specifically to the Mediterranean summer and that the combination of parametrisations above may not be ideal in other cases.

Chemistry

The RADM2 (Regional Acid Deposition Model, version 2) mechanism (Stockwell *et al.*, 1990a) and the Madronich photolysis scheme (Madronich, 1987), were used in all the simulations, the photolysis rate constants were recalculated every 30 minutes.

Input data and Initialisation

The meteorological input data, obtained from the Research Data Archive (RDA), were the NCEP FNL (final) Global Operational Analyses, which are provided on a 1° by 1° grid at six hourly intervals. The data are converted to WRF input on the appropriate domain(s) using the WRF Preprocessing System (WPS). The chemical species concentrations were initialised using the idealised profile in WRF/Chem, and the model was allowed to spin-up for five days before the beginning of the observation period under study.

2.3.2 Emissions

The WRF/Chem model includes the option to calculate biogenic emissions on-line using the approach described by Guenther *et al.* (1993, 1994) and Simpson *et al.* (1995). During the simulations the biogenic emission fluxes were up-dated every 30 minutes. The anthropogenic emissions used in the model were obtained from the EMEP Centre for Emission Inventories and Projections (CEIP) (http://www.ceip.at/). The emissions used in EMEP models (Vestreng *et al.*, 2007) for the years corresponding to the measurement campaigns were used. As in Schürmann *et al.* (2009) a day - night temporal profile has been applied to the emissions following Simpson *et al.* (2003). The EMEP emissions were preferred because of their specificity to the Europe / Mediterranean region, and are available for individual years, and also the results obtained by Marmer *et al.* (2009) in a comparison of shipping emission inventories for the Mediterranean Sea. Marmer *et al.* (2009)

found that in their modelling study, at least in the Western Basin, the EMEP inventory gave the best match with the major part of the measurements with which they compared their simulations.

In-plume chemistry and artificial plume dilution

The perturbation caused by ship emissions to local photochemistry in the MBL began to be investigated in detail in the late 90s (Lawrence and Crutzen, 1999; Capaldo *et al.*, 1999). The direct inclusion of ship emissions in Chemical Transport Models (CTMs) can result in the instantaneous dilution of the emissions within the volume of the grid cell. In coarse resolution models this leads a to a false impression of the chemical composition in the cell, because the chemistry which occurs within the volume of the expanding plume, where the chemical composition is different to the air in the rest of the cell, is not taken into account (Charlton-Perez *et al.*, 2009; Huszar *et al.*, 2010; Vinken *et al.*, 2011). This can lead to errors in the simulation of NO_x and OH concentrations and in the simulated ozone production efficiency (OPE) (Charlton-Perez *et al.*, 2009). However a recent study of the effect of including non-linear chemistry for ship emissions in the GEOS-Chem model (Vinken *et al.*, 2011) indicates that the impact of dilution is less significant over more heavily polluted areas such as the North Sea, than it is in more pristine and remote areas of the MBL. Another aspect of plume emissions from shipping which has been considered recently in the literature is the influence on plume dilution resulting from the combination of boundary layer convection, the plume's buoyancy (it is hotter than the surrounding air) and the ship's speed and direction relative to the wind speed and direction (Chosson *et al.*, 2008). These factors influence both plume rise, which can be 2–10 times the actual stack height, and the shape of the plume (Chosson *et al.*, 2008). In the simulations described here the modelling domain resolution is higher than the emission inventory resolution, and the Mediterranean boundary layer is influenced by many other emission sources besides shipping, and therefore the emissions were interpolated directly into the modelling domain. Two emission height scenarios have however been used to investigate the possible effects of plume rise as described in section 2.3.3.

2.3.3 The simulations performed

The model resolution employed over the route taken by the R. V. Urania is 9 km by 9 km, while the resolution of the emissions database is 50 km by 50 km. Thus the introduction of the emissions into a model cell is different to most of the those cases described in section 2.3.2 where relatively highly

spatially resolved emissions are diluted in to a coarse resolution horizontal grid. The approach used here follows that of Huszar *et al.* (2010) where the emissions from the EMEP database are directly interpolated on to the model grid. Two emission height cases have been investigated for the shipping emissions to assess the importance of plume rise on the modelling results. In the EMEP unified model all emissions from SNAP (Selected Nomenclature for Air Pollution) sector 8 (other mobile sources and machinery, which includes shipping) are assumed to be emitted in the first model layer (0–92 m). The WRF/Chem simulations described here, given the synoptic conditions prevailing during the periods of the oceanographic campaigns investigated, generally had 5 vertical levels from sea level to roughly 400 m at sea level over the open Mediterranean. This is a fairly typical height of the Mediterranean MBL under summertime anticyclonic conditions. In the Em_low scenario the emissions are emitted into the first model level, while in the Em_hi scenario the emissions are distributed between levels 2 (≈30–90 m, 50 %), 3 (≈90–160 m 25 %) and 4 (≈160–250 m, 25 %).

To estimate the impact of ship emissions on O_3 production, the simulations descibed above were run again, using exactly the same parametrisations, but with a modified emissions database, in which all emissions from SNAP sector 8 over the Mediterranean had been removed.

2.4 Results and discussion

2.4.1 Model validation

Model results have been compared to data from the Med-Oceanor series of campaigns and data from the EMEP measurement stations present in the Mediterranean region. The comparison with EMEP data was performed considering those stations located within the highest resolution modelling domain. For some years only one station was within the boundaries of the smallest domain. The metrics listed in table 2.2 as they are defined in Chang and Hanna (2004) and Willmott *et al.* (1985) were used, where X_{mod} and X_{obs} are the modelled and observed values respectively, σ is the standard deviation and N the number of pairs.

The bias indicates the over or underestimation of the parameter in question in the units of the measurement. The root mean square error provides a measure of the model precision, and can be divided in to two parts, the systematic and unsystematic. The linear bias produced by a model is described by the systematic part of the RMSE, $\mathrm{RMSE_s}$ (Willmott *et al.*, 1985);

Metric	Definition
mean bias	$\mathrm{MB} = \overline{X}_{obs} - \overline{X}_{mod}$
correlation coefficient	$\mathrm{R} = \frac{\overline{(X_{obs}-\overline{X}_{obs})(X_{mod}-\overline{X}_{mod})}}{\sigma_{obs}\sigma_{mod}}$
root mean square error	$\mathrm{RMSE} = \sqrt{(\overline{X}_{obs} - X_{obs})^2}$
unsystematic fraction of RMSE	$\mathrm{UF}_{RMSE} = \frac{\mathrm{RMSE}_u^2}{\mathrm{RMSE}^2}$
index of agreement	$\mathrm{IOA} = 1 - \frac{\mathrm{N}\cdot\mathrm{RMSE}^2}{\sum_{i=1}^{N}(\lvert X_{mod}^{(i)}-\overline{X}_{mod}\rvert+\lvert X_{obs}^{(i)}-\overline{X}_{obs}\rvert)^2}$

Table 2.2: The metrics used to assess the model performance.

in tables 2.3 and 2.4 the unsystematic fraction of the RMSE is given, derived from:

$$\mathrm{RMSE}^2 = \mathrm{RMSE}_u^2 + \mathrm{RMSE}_s^2 \text{ (Willmott } \textit{et al.}\text{, 1985).} \tag{2.1}$$

The unsystematic fraction (UF) of the RMSE can take values between 0 and 1. The Index of Agreement, is a measure of the degree of agreement between the model and observations has values between 0 and 1, with 1 indicating perfect agreement.

Meteorological parameters

The performance statistics for the comparison between the modelled and measured hourly values of temperature (℃), wind speed ($\mathrm{m\,s^{-1}}$) and relative humidity (%) are shown in table 2.3. The relative humidity is calculated from the model output, water vapour $\mathrm{kg\,kg_{air}^{-1}}$ as described in Wallace and Hobbs (1977) using the vapour pressure definition from Lowe (1977). It should be noted that the calculation of the relative humidity requires the use of model output parameters, the temperature and pressure, which are themselves subject to uncertainty.

The quality of the comparison between the modelled and measured meteorological parameters is similar to results previously obtained using the WRF model (see for example (Grell *et al.*, 2005; de Meij *et al.*, 2009; Misenis and Zhang, 2010; Schürmann *et al.*, 2009; Tie *et al.*, 2007; Tuccella *et al.*, 2012)). The values for the RMSE of the wind speed are however generally somewhat higher than found in previous studies with values between 3.05

	2000	2003	2004	2005	2006	2009	2010
				Temperature			
MB [℃]	1.3	2.3	1.7	8.2	1.9	2.6	2.0
R	0.55	0.32	0.45	0.58	0.46	0.75	0.79
RMSE [℃]	1.9	2.9	2.1	8.9	2.2	3.1	2.4
UF-RMSE	0.43	0.25	0.18	0.02	0.18	0.26	0.30
IOA	0.64	0.46	0.54	0.44	0.44	0.63	0.71
				Wind speed			
MB [ms^{-1}]	-0.97	0.80	1.03	0.13	1.34	-0.9	-0.32
R	0.23	0.32	0.42	0.16	0.43	0.12	0.45
RMSE [ms^{-1}]	4.2	3.3	4.3	3.8	4.3	4.7	3.5
UF-RMSE	0.55	0.63	0.55	0.63	0.45	0.62	0.75
IOA	0.54	0.60	0.65	0.50	0.65	0.44	0.69
				Relative humidity			
MB [%]	-2.5	2.67	-10.8	9.0	-5.1	-2.4	
R	0.19	0.30	0.17	-0.01	0.23	0.34	
RMSE [%]	15.0	14.0	16.7	18.6	14.0	14.4	
UF-RMSE	0.75	0.35	0.19	0.51	0.71	0.88	
IOA	0.5	0.56	0.47	0.32	0.50	0.57	

Table 2.3: Comparison between the model output and meteorological parameters measured aboard the R. V. Urania. There was no relative humidity data available for 2010

and $4.66\,\mathrm{m\,s^{-1}}$, whereas it is more commonly around $2\,\mathrm{m\,s^{-1}}$ in the studies mentioned above. There are two main reasons for this, the first is the generally anticyclonic meteorological conditions which prevailed during the cruise campaigns, when the wind speed is often very low; the average wind speed during the whole series of Med-Oceanor oceanographic campaigns was around $6\,\mathrm{m\,s^{-1}}$. Low wind speeds are common in the Mediterranean region during the summer anticyclone and they prove difficult to model accurately, (de Meij *et al.*, 2009). The other common difficulty encountered in modelling the wind speed (and direction) in the Mediterranean is due to the very localised local circulation patterns which occur due to the complex orography near the coastline.

The 2003 campaign encountered some technical difficulties with the meteorological data collection during its second half which followed a route from Naples almost to the Strait of Gibraltar and returned to Livorno, and this had an impact on the quality of the overall comparison. Therefore only the first part of the campaign is considered, that is from 5–16 August, in the

validation of the meteorological variables obtained aboard the R. V. Urania.

During the 2005 Med-Oceanor campaign in the Adriatic the temperature is significantly underestimated. A closer look at the temperature data revealed that this occurred when the R. V. Urania entered the Adriatic Sea itself. The mean bias between the modelled and measured sea surface temperature for most of the campaigns is less than 1.5 ℃, and for the first part of the 2005 campaign, prior to entering the Adriatic the mean bias in SST was 0.7 ℃. However during the Adriatic part of the campaign the it was 3.7 ℃, and this affected the simulated temperature. However this did not seem to have a major effect on the modelled O_3, which compared well to the observations (section 2.4.1).

Ozone

Comparisons of modelled and measured ozone concentrations have been performed for the data obtained during the oceanographic campaigns, and also with measured ozone concentration data from stations in the EMEP monitoring network located within the smallest modelling domain, for each of the years (Hjellbrekke *et al.*, 2011). The agreement between the modelled concentrations and the observations are on a par with those from previous studies. A number of studies of ozone using WRF/Chem have been performed (for example, for regions in the US: Grell *et al.*, 2005; Fast *et al.*, 2006; Hu and Zhang, 2006; Zhang, 2008; Misenis and Zhang, 2010; Mexico City: Tie *et al.*, 2007; Zhang and Dubey, 2009; for regions in Europe: Schürmann *et al.*, 2009; de Meij *et al.*, 2009; Tuccella *et al.*, 2012; and also in China: Geng *et al.*, 2007). A summary of the statistical measures to assess the model's performance in reproducing the observations during the oceanographic measurement campaigns is presented in Table 2.4.

Table 2.4 includes the results from the two emission height scenarios Em_hi and Em_low (mentioned in section 2.3.2). The differences between these are discussed further in section 2.4.2, however as can be seen from table 2.4 the difference in the results in the first model layer are not very large.

The model does not consistently over or underestimate the ozone concentrations, the bias in some years is negative and others positive. Generally the model reproduces the measured O_3 concentrations reasonably well, although some campaigns were however reproduced less well than others. Figures 2.3, 2.4 and 2.5 show the modelled and measured O_3 concentrations for the 2000, 2005 and 2010 campaigns respectively. The rapid decreases in O_3 seen in the measurements occur when the R.V. Urania is directly influenced by plumes from ships passing close by, or when the ship is stationary to take water

	Em_low scenario					Em_hi scenario				
Year	MB (ppb)	R	RMSE (ppb)	UF	IOA	MB (ppb)	R	RMSE (ppb)	UF	IOA
2000	-3.7	0.51	11.0	0.59	0.69	0.66	0.59	9.6	0.68	0.76
2003	4.0	0.32	14.7	0.47	0.55	3.7	0.31	14.7	0.48	0.54
2004	15.1	0.02	18.5	0.07	0.39	16.1	-0.14	19.8	0.07	0.36
2005	3.0	0.55	13.8	0.80	0.73	4.57	0.56	13.5	0.69	0.72
2006	9.9	0.24	14.5	0.33	0.48	-8.8	0.19	14.3	0.40	0.49
2009	7.8	0.30	14.9	0.55	0.53	7.89	0.29	15.3	0.56	0.52
2010	-0.7	0.39	10.7	0.73	0.63	-1.2	0.38	10.9	0.73	0.63

Table 2.4: Comparison of the model results and the ozone concentrations measured aboard the R. V. Urania, see section 2.3.2 for the definition of the Em_low amd Em_hi emission scenarios. UF refers to the unsystematic fraction of the RMSE. The results for 2003 consider only the first half of the campaign, see section 2.4.1

column and sediment samples and the wind direction carries the ships own exhaust towards the O_3 analyser. When this occurs the high levels of NO decrease the O_3 concentration via reaction to form NO_2. This titration effect means that the correlation between the daily minimum observed and modelled O_3 concentrations was generally poor. The modelled and measured maximum daily values were better correlated, as were the daily mean values, with values of R over 0.7 in some cases.

As mentioned in section 2.4.1 the second half of the 2003 measurement campaign encountered some technical difficulties, and the comparison between the measured and modelled meteorological values was performed only for the first half of the campaign. For consistency the values in Table 2.4 refer to the first part of the campaign from 5–16 August. The direct influence of other ships on O_3 concentrations was particularly clear during the second period of the 2003 campaign (Naples – the Strait of Gibraltar – Livorno) when some of the lowest recorded during the series of Med-Oceanor campaigns were measured, below 20 ppb at times. The mean observed O_3 concentrations for the first and second periods are 65.6 ppb and 50.4 ppb respectively; such a difference is not evident in any of the other Med-Oceanor campaigns. The metrics reported in table 2.4, refer to the first eleven days of the campaign.

The results for the spring 2004 campaign are noticeably poorer than the campaigns which took place during the summer. The model underestimates the spring 2004 O_3 concentrations by 15 ppb throughout the modelling pe-

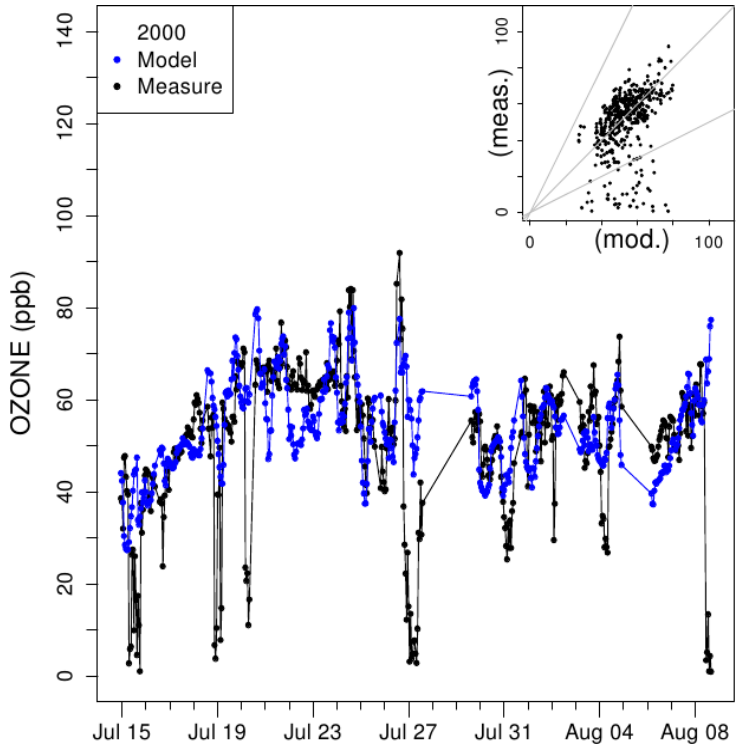

Figure 2.3: Measured and modelled O_3 concentration in ppb during the 2000 oceanographic campaign. Mean bias -3.7 ppb

riod. The results for this year show a much higher systematic component of the RMSE as can be seen from the low value of UF-RMSE. The reasons for this are not entirely clear but are likely to be related to the spring O_3 maximum, which seems, quoting Cristofanelli and Bonasoni (2009), *"mainly related (Monks, 2000; Vingarzan, 2004) to stratosphere-to-troposphere exchanges (STE) and long-range transport of* O_3 *precursors accumulating during winter in the Northern Hemispheric free troposphere, and its ensuing in situ photochemical production. In the free troposphere, the presence of the yearly* O_3 *double peak, frequently integrated in a broad spring–summer peak, is particularly evident for measurements carried out in high mountain areas."*

The comparison between the modelled O_3 concentrations and those measured at the EMEP stations, which were within the area bounded by the finest resolution modelling domain, gave results essentially similar to the comparison with the R. V. Urania, table 2.5. The most obvious difference between the results for land-based measurements and those obtained over the Mediterranean Sea, is that the model tended to overestimate the O_3 concentrations over land, with the exception of the simulations performed for

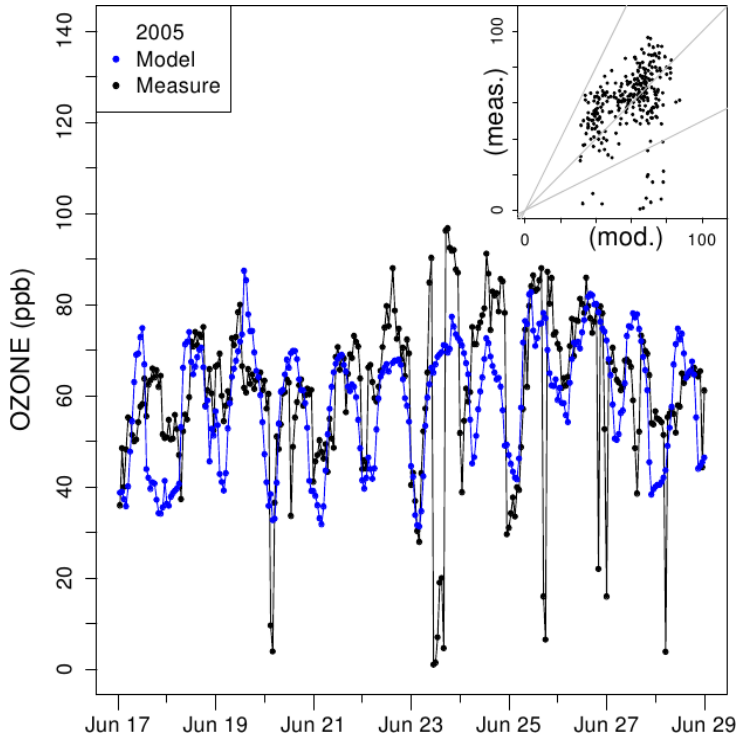

Figure 2.4: Measured and modelled O_3 concentration in ppb during the 2005 oceanographic campaign. Mean bias 3.0 ppb

the spring of 2004.

The comparison between the modelled and measured O_3 concentrations also reveals that the model does not reproduce well the amplitude of the day–night variation in concentration. This is very possibly due to difficulties in accurately modelling the temporal evolution of the boundary layer. If the nighttime boundary layer is too high in the model both the rate at which O_3 is deposited, and the rate at which it is titrated by species emitted at the surface would be underestimated. The daytime underestimate of the O_3 maximum may also be ascribed to the model's failure to correctly represent boundary layer dynamics as the mixing down of O_3 rich air plays an important role in the increase of the daytime O_3 concentration.

2.4.2 The influence of ship emission height in the model

As described in Sect. 2.3.2 two scenarios for the height at which ship emissions are introduced into the model have been studied. The first, Em_low, simply introduces all the ship emissions into the first model layer, while the second, Em_hi, distributes them between the second, third and fourth model

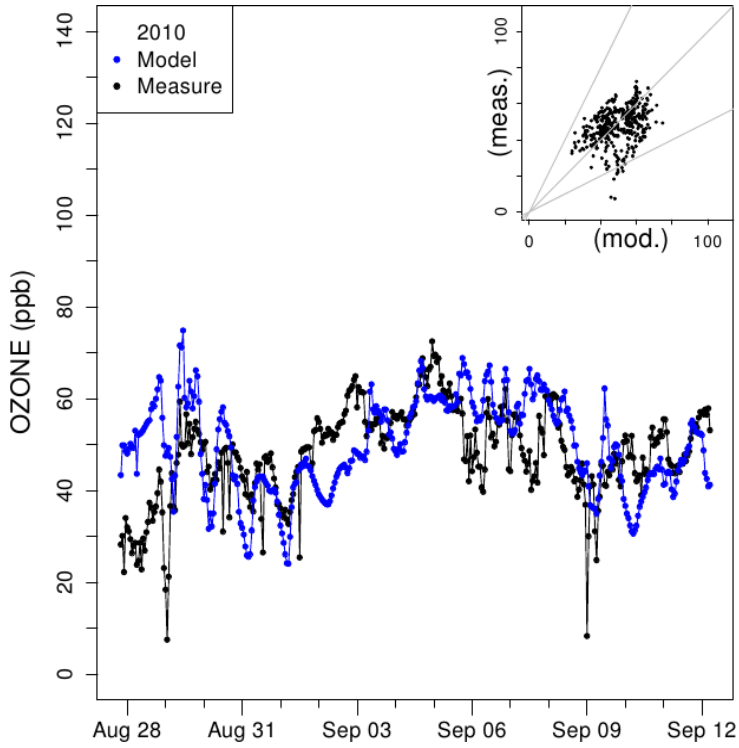

Figure 2.5: Measured and modelled O_3 concentration in ppb during the 2010 oceanographic campaign. Mean bias -0.7 ppb

layer, that is between 30 and 250 m, to examine the potential differences caused by plume rise (section 2.3.2). The results in tables 2.4 show that the comparison between the measured and modelled O_3 concentrations in both instances is very similar. The emission height does have an influence on the boundary layer as a whole however; table 2.6 shows the concentration differences for a number of chemical species both in the first model layer, and in the first six model layers over the marine part of the domain for the years 2005 and 2009. The top of the fifth model layer for the grid cells over the sea is close to 400 m and roughly coincides with the height of the MBL during summer anticyclonic conditions. The sixth model layer is at approximately 600 m over the Mediterranean and therefore certainly includes the whole of the MBL over the most part of the sea. The 2005 domain is more influenced by land based emissions because the cruise route was for the most part in the Adriatic Sea, the 2009 9 km by 9 km domain is significantly larger and has a higher percentage of open sea as can be seen from the route maps in figure 2.1.

Looking at at the O_3 concentration field at a given time can show up

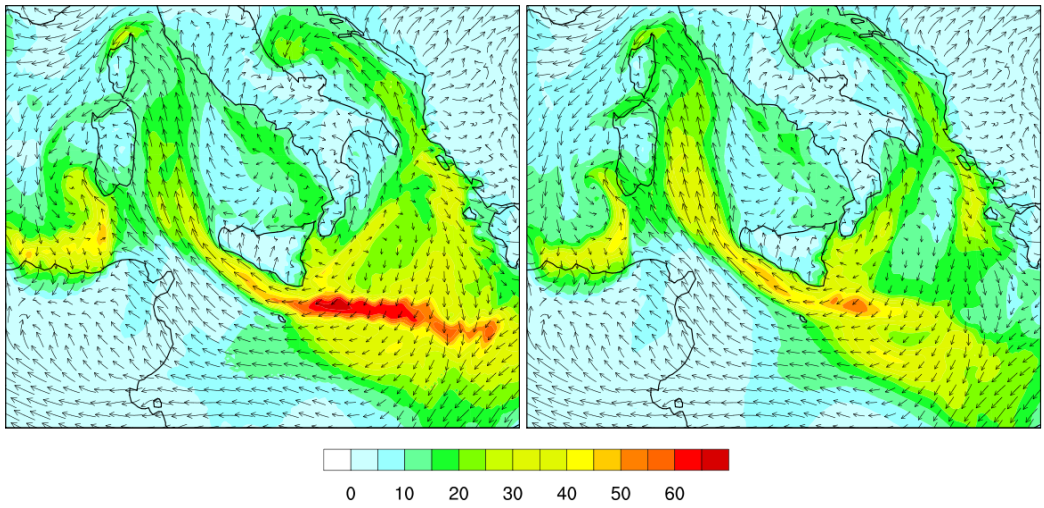

Figure 2.6: The influence of ship emission height on the modelled O_3 concentration in ppb, in the lowest model layer at midday on 16 June 2009. Left, Em_low scenario right, Em_hi scenario.

significant short term differences in the simulations. Figure 2.6 shows the modelled O_3 concentration and the wind arrows in the lowest model layer at midday on the 16 June 2009. The impact of the emission height on the O_3 concentrations is clear, as is the interaction between emission height and wind speed. In the Ionian Sea where the wind speed is low, emissions in the first layer influence the local O_3 more than emissions above the first layer. The same effect can be seen between Sardinia and the North African coast. However where wind speeds are higher the effect of emissions in higher model layers has a more widespread effect than emissions in the first model layer, as can be seen immediately to the west of Sardinia, where the yellow/orange area spreading northwards from the western tip of Sicily is greater in extent for the Em_hi simulation.

2.4.3 The influence of ship emissions

An emission inventory was prepared in which all the SNAP sector 8 emissions which occurred over the Mediterranean were removed from the database. The simulations described previously were rerun, on exactly the same domain and for exactly the same period. The simulations with all emissions have been denoted Tot_Emiss, and those without the contribution from shipping, No_ships. An overview of the results is presented in table 2.7 where the difference (in %) between the concentrations of O_3, NO and NO_2 for simulations with and without shipping emissions are given.

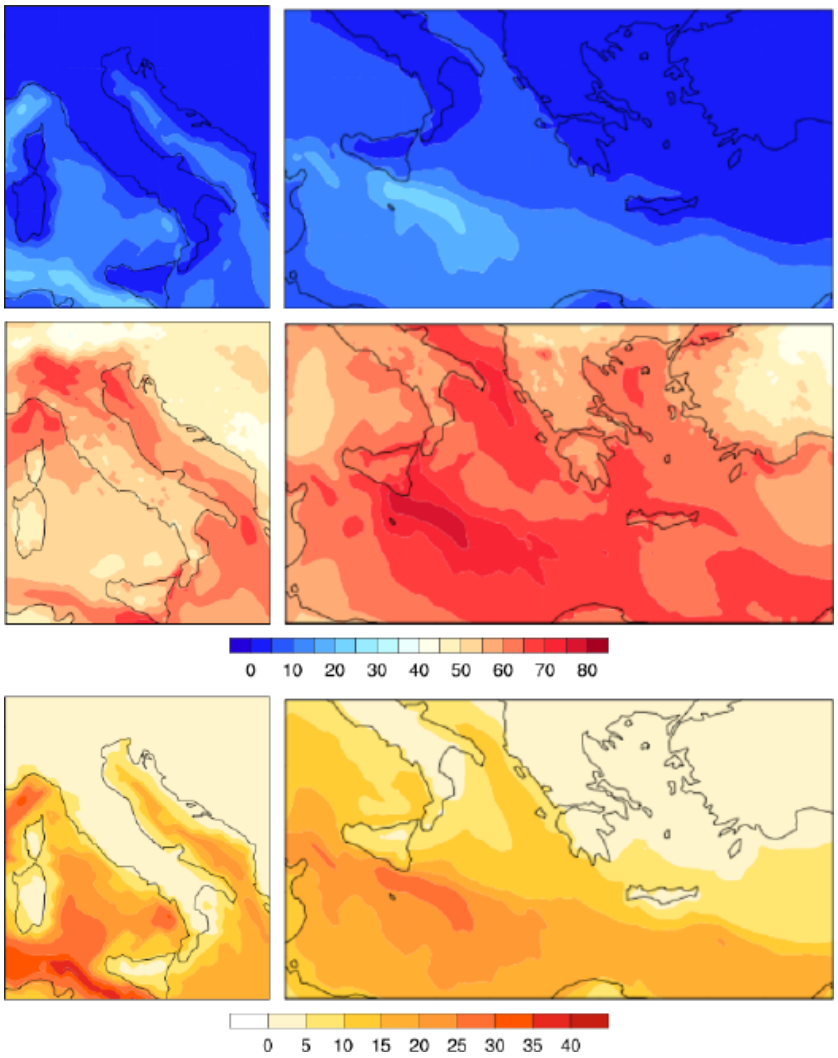

Figure 2.7: The average O_3 concentration and concentration difference in the first model layer for 2005 (left) and 2006 (right). Row one shows the difference Tot_Emiss – No_ships in ppb, row 2 the actual value in ppb and row 3 the difference in %.

Roughly speaking removing the emissions from ships results in a decrease in the modelled average O_3 concentration over the whole of the highest resolution domain by 5 or 6 ppb, and by 8 or 9 ppb over the Mediterranean Sea itself, for the simulation periods. These values are significant given the size of the domain and the length of time involved, however the effect of shipping emissions is clearly not uniform over the whole domain. While table 2.7 gives the average differences over the whole domain (and just the Mediterranean),

figure 2.7 shows the time averaged impact of shipping emissions for the 2005 (left column) and 2006 (right column) simulations.

Not unexpectedly the greatest impact is clearly over the sea in the shipping routes where the maritime traffic is most intense. The 2006 campaign covered a significantly wider area than the 2005 campaign and the difference in the modelled O_3 concentration along the shipping lane between the Strait of Sicily towards the entrance to the Suez Canal is easily seen. In figure2.7 the difference in O_3 concentrations between the two simulations can be 10 ppb or more in coastal areas, and it should be borne in mind that these are average concentrations. Figure 2.8 on the other hand illustrates the difference (Tot_emiss - No_ships) in the maximum O_3 concentrations simulated during the 2003 campaign has been plotted. The 2003 campaign was chosen because it covered the widest geographical area. The most extreme values, over 50 ppb occur in the Strait of Sicily and around the Alboran Sea. The coastal areas of North Africa exhibit significant differences between the two simulations, and the Mediterranean Spanish coastline and Sicily are also noticeably different in the two simulations.

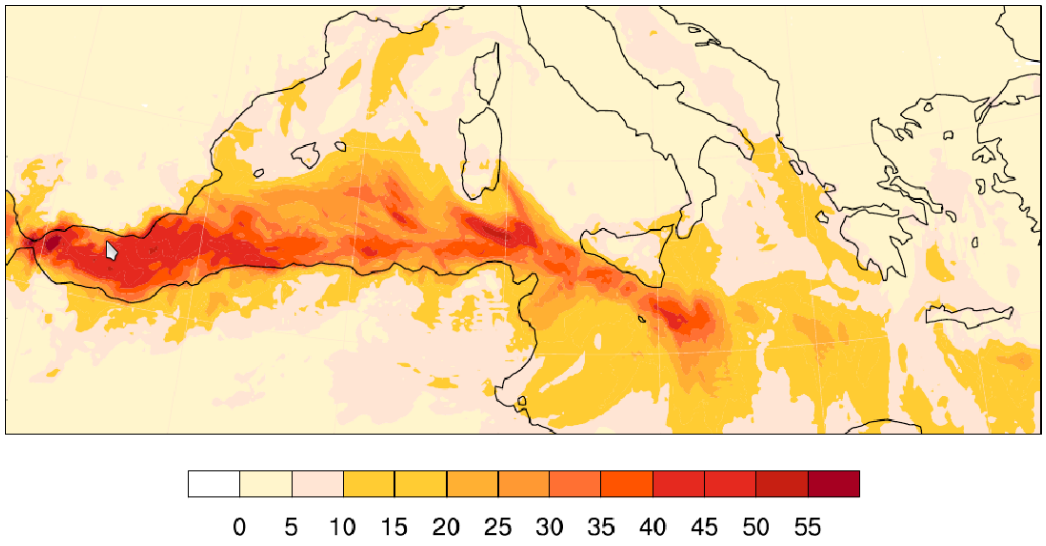

Figure 2.8: The difference (ppb) in the maximum O_3 concentrations between the Tot_emiss and No_ships simulations for the 2003 measurement campaign.

The vertical profile of the impact of ship emissions on the O_3 concentration is illustrated in figure 2.9. The figure shows the difference in O_3 concentrations for the two latitudinal sections indicated in figure 2.2. The Med-Oceanor 2003 campaign was again chosen to illustrate these profiles because it was the most wide-ranging of the cruise routes. Figure 2.9 shows

the vertical profile of O_3 concentration (middle column) and the differences in (O_3) in ppb (first column) and % (third column), between the Tot_Emiss and No_ships scenarios. In figure 2.9 the section passes through Southern Spain, across Corsica, Northern Calabria in Italy, Greece and to the Eastern side Turkey.

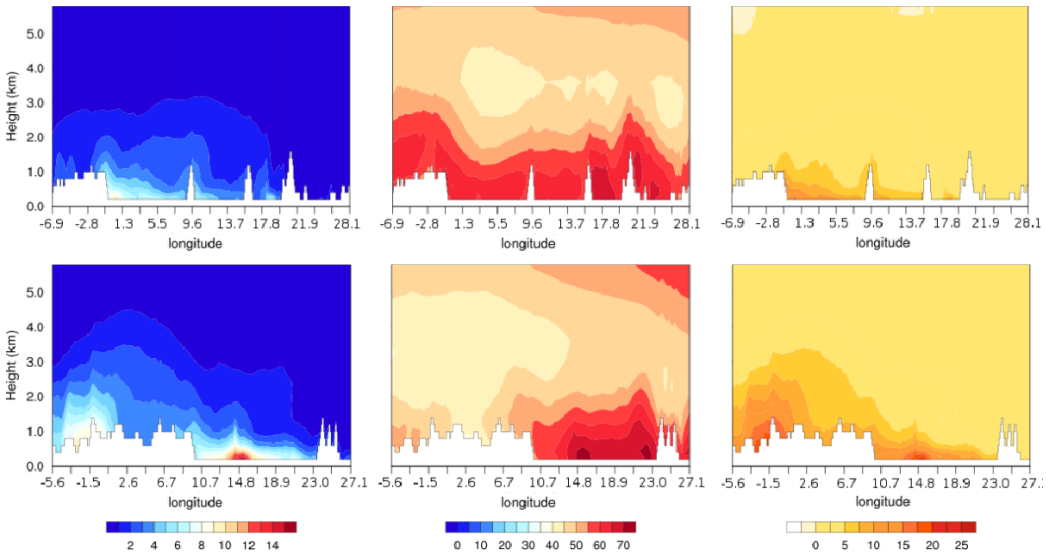

Figure 2.9: The vertical profile of O_3 concentration along ≈39° N (top row),and ≈34° N, bottom row. Column 1 shows the difference Tot_Emiss − No_ships in ppb, column 2 the actual value in ppb and column 3 the difference in %. The values are the average for the whole simulation period, 5 to 27 August 2003.

The contribution to O_3 concentrations is clearly seen to be highest in the Balearic Sea, in fact Valencia is the largest container port in the Mediterranean. However there is also a significant contribution in the Thyrrenian and Ionian Seas. Although the absolute concentrations in the Aegean Sea, (between ≈ 22° and 27°E along this section), are high, the contribution to these concentrations from shipping appears to be low. This is possibly due to the relatively high emissions from other sources in the region, both Athens and Istanbul being nearby. The more southerly cross-section shown in the lower row in figure 2.9 begins in Northern Morocco and meets the Mediterranean on the Gulf of Hammamet in Northern Tunisia, crosses the southern part of the Strait of Sicily and the southernmost Ionian Sea, then passes directly across Crete. At ≈15° E both the absolute O_3 and the contribution from shipping are high, this is the southern entrance to the Strait of Sicily. Again it can be seen that although absolute values are high to the eastern end

of the cross-section, (off the western coast of Crete) the contribution from shipping is less than in other areas. In this case this may well be because the major shipping lanes (toward Suez) are to the south of Crete and boundary layer flow during summer anticyclone conditions tends to be from north to south (Lelieveld *et al.*, 2002).

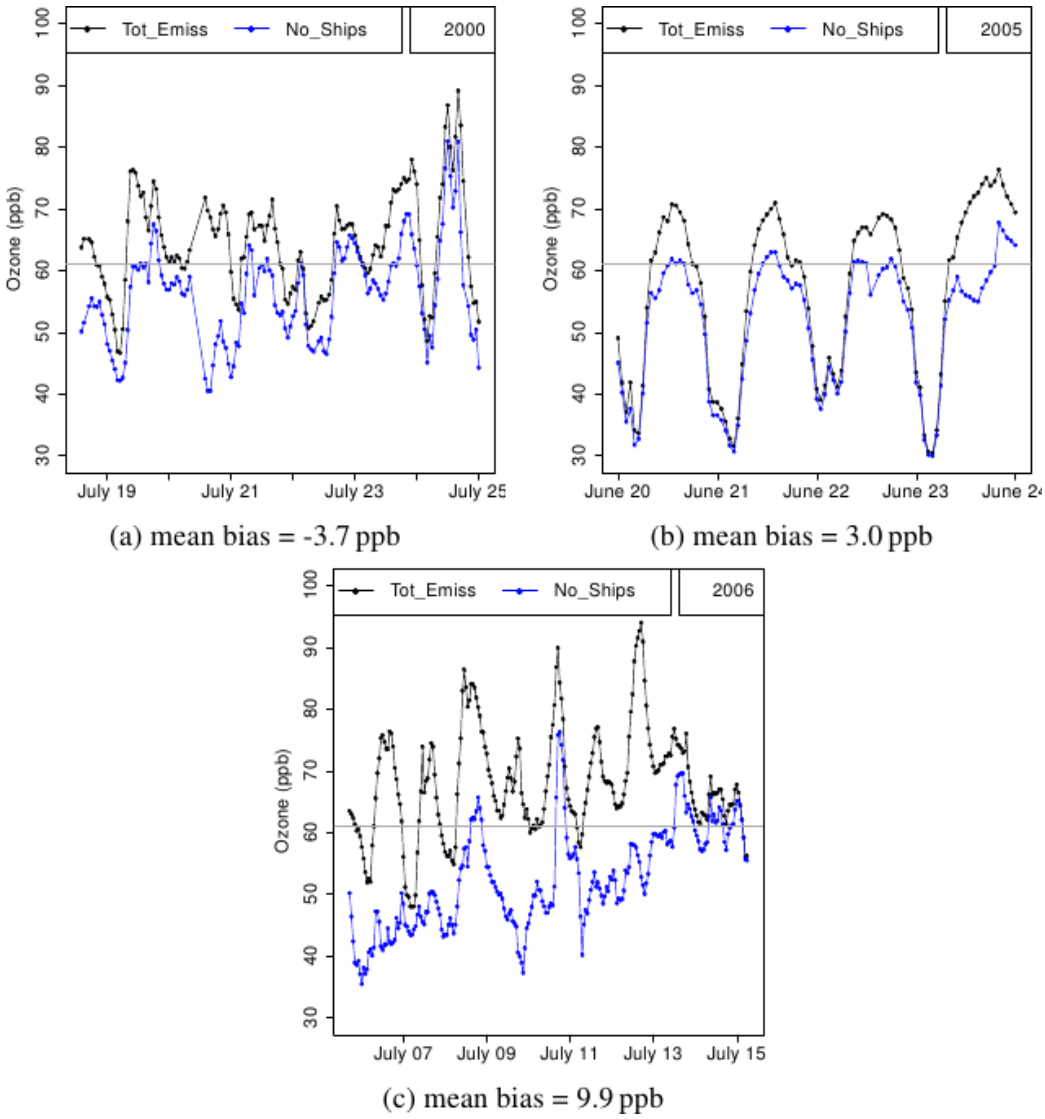

(a) mean bias = -3.7 ppb

(b) mean bias = 3.0 ppb

(c) mean bias = 9.9 ppb

Figure 2.10: Examples of the difference in O_3 concentration with and without ship emissions along the route of the R.V. Urania.

The noticeable O_3 differences over North Africa from roughly $-5°$ to $1°$ E are due to the morphology of the North African coastline near the Moroccan-

Algerian border. Where the Rif mountains in North-East Morocco, the Middle Atlas (Morocco) and the Tell Atlas (Algeria) mountain ranges converge there is a lower lying area, which allows the intense ship emissions in the Alboran Sea (the Mediterranean approach to the Gibraltar Strait), to make their way inland and influence O_3 concentrations, by more than 10 %, over 250 km inland. Large areas of the low-lying parts of the western coast of Tunisia are affected by ship emissions (in this case from the Strait of Sicily), the average O_3 concentration decreases by 5 to 10 ppb in these areas, ≈10–20 % when ship emissions are excluded. Where these decreases in O_3 concentrations occur over land the vertical scale of the impact is far greater than over the sea, as can be seen in figure 2.9 (lower row) over Morocco, Algeria and Tunisia. This suggests that ship emissions could contribute to the O_3 budget above the boundary layer, where due its role as a short-lived climate forcer it may have an impact on the regional radiation budget. To assess this possibility is beyond the scope of this paper but given that ship emissions also include black carbon, an investigation into the potential impact of ship emissions on regional climate may well be merited.

Comparison of the two simulations along the routes followed by the R.V. Urania shows on a number of occasions that the local contribution to O_3 makes a significant difference. Figure 2.10 shows the simulation results from three periods during the 2000, 2005 and 2006 campaigns where the difference due to the exclusion of the shipping emissions in the predicted O_3 concentrations is particularly noticeable. In figure 2.10 the horizontal line at ≈61 ppb is the mixing ratio equivalent of 120 μg m^{-3} at the atmospheric temperatures and pressures encountered during the oceanographic campaigns. This is the current EU directive on air quality (2008/50/CE) air quality standard for the maximum daily 8 h mean concentration of O_3. The figures also indicate the mean bias between observed and modelled results for the campaigns, and while the mean bias was relatively high, particularly in 2006, it can be seen that the O_3 concentration difference between the simulations with and without shipping emissions is greater. Longer term modelling studies of coastal regions near to major shipping lanes or ports would help in better defining the extent the impact of ship emissions on local and regional air quality.

2.5 Conclusions

The WRF/Chem model has been used to simulate O_3 concentrations for the periods of seven oceanographic research campaigns which took place in the Mediterranean Basin between 2000 and 2010. The results of the com-

parison between the model and observations are quantitatively similar to results obtained in previous studies using the WRF/Chem model. The results for the wind speed were not as good as previous studies, however the prevailing anticyclonic conditions during all but one of the simulation periods resulted in low wind speeds which are known to be difficult to reproduce. The results of the comparison between the modelled O_3 concentration with the exception of the spring 2004 campaign showed a reasonable agreement. The mean bias between measurements and the model was lower for shipboard measurements than for observations from the land based EMEP sites, while the correlation between the model and the measurements was higher for the EMEP sites. The model has some problems reproducing the variation between the day time maxima and the night-time minima at some of the EMEP sites, although the timing of the daily cycle, as reflected by the correlation coefficient, was reproduced well. The lower correlation between the model and shipboard measurements was in part due to the sporadic interception of relatively fresh ship plumes which caused noticeable decreases in the O_3 concentration as a result of titration by NO. Certainly during the 2003 cruise campaign which arrived almost at the Strait of Gibraltar there was a noticeable effect on O_3 close to the major shipping lanes in the Alboran Sea. Simulations performed to investigate the influence of emission height for ship plumes on the production and distribution of O_3 indicate that average O_3 concentrations are not greatly influenced by the way the emissions are distributed throughout the lowest model layers.

The average measured O_3 concentrations during the Med-Oceanor series of oceanographic measurement campaigns was 50–60 ppb, comparing simulations with and without shipping emissions showed differences of $\approx$3 and 12 ppb on the average concentrations of O_3 over the campaign periods. Ship emissions influence is mostly constrained to marine and coastal areas as a result of the low summer time Mediterranean MBL height and the steepness of much of the Mediterranean coastline. However the simulations with and without ship emissions showed differences in O_3 tens and even hundreds of km inland over the flatter coastal areas of North Africa.

Along the routes taken by the R.V. Urania the simulations suggest that ship emissions contribute significantly to exceedeances of the EU 8 h average concentration limit of 120 μg m^{-3}. As maritime traffic is projected to increase in the coming years, and as legislation leads to diminishing emissions from land based sources, the relative contribution of shipping to total O_3 precursor emissions will increase. Shipping emissions are likely to play an important role in local and regional air quality in Mediterranean coastal areas and beyond for the foreseeable future.

		Em_low scenario					Em_hi scenario				
Year	Station	MB [ppb]	R	RMSE [ppb]	UF	IOA	MB [ppb]	R	RMSE [ppb]	UF	IOA
2000	GR03	-6.1	0.53	17.1	0.84	0.68	1.0	0.53	14.2	0.87	0.72
	IT01	-12.3	0.24	30.4	0.36	0.53	-9.2	0.29	27.2	0.27	0.54
	MT01	-10.2	0.46	17.6	0.65	0.55	-9.9	0.20	19.7	0.64	0.44
2003	ES07	-5.5	0.20	15.8	0.54	0.50	-5.5	0.19	15.9	0.53	0.50
	ES12	-0.8	0.15	15.6	0.60	0.48	-1.2	0.14	15.8	0.59	0.48
	ES14	-3.8	0.26	15.1	0.39	0.52	-4.0	0.24	15.3	0.39	0.51
	GR02	-1.3	0.66	7.5	0.94	0.80	-1.4	0.66	7.6	0.93	0.79
	IT01	-13.4	0.61	24.5	0.29	0.68	-13.4	0.59	24.8	0.29	0.67
	MT01	-5.2	0.17	15.0	0.66	0.47	-5.9	0.16	15.8	0.66	0.45
2004	ES10	13.4	0.28	15.5	0.16	0.38	13.7	0.29	15.7	0.16	0.38
	ES14	5.2	0.31	11.5	0.53	0.53	5.1	0.32	11.4	0.53	0.53
	FR13	7.3	0.49	11.2	0.49	0.59	7.3	0.48	11.2	0.50	0.59
	FR16	14.6	0.59	15.6	0.04	0.44	14.5	0.58	15.5	0.04	0.44
	FR17	10.3	0.14	14.2	0.25	0.41	10.2	0.14	14.1	0.26	0.41
	IT01	-13.5	0.50	18.8	0.30	0.59	-13.9	0.52	18.9	0.27	0.59
	IT04	-6.5	0.64	13.6	0.42	0.74	-6.7	0.63	13.7	0.41	0.73
2005	IT01	-17.0	0.64	24.4	0.20	0.67	-17.1	0.64	24.4	0.20	0.67
	IT04	-25.3	0.78	29.6	0.20	0.69	-25.3	0.78	29.7	0.20	0.69
2006	IT01	-15.7	0.80	23.1	0.11	0.70	-16.2	0.80	23.3	0.10	0.70
	MT01	-16.4	0.25	22.1	0.44	0.28	-16.9	0.25	22.7	0.44	0.27
2009	IT01	-2.9	0.72	15.4	0.19	0.72	-3.0	0.72	15.4	0.19	0.72

Table 2.5: Comparison of the model results and the ozone concentrations measured at the EMEP stations within the highest resolution modelling domain, see section 2.3.2 for the description of the Em_low and Em_hi emission scenarios. The stations are ES07 Vznar, ES10 Cabo de Creus, ES12 Zarra, ES14 Els Torms, FR13 Peyrusse Vieille, FR16 Le Casset, FR17 Montfranc, GR02 Finokalia, GR03 Livadi, IT01 Montelibretti, IT04 Ispra,MT01 Giordan Lighthouse. The locations of the EMEP stations are shown in figure 2.1. UF refers to the unsystematic fraction of the RMSE

Year	Level	O_3 [ppb]	NO [ppt]	NO_2 [ppb]	SO_2 [ppb]	HO [molec. cm^{-3}]	HCHO [ppb]	HNO_3 [ppb]
2005	Av. conc. Em_low, level 1	57.3	72.9	1.2	1.4	4.7×10^5	6.0	0.94
	difference level 1	2.7	21.1	0.38	0.29	1.1×10^5	0.65	0.11
	difference levels 1–6	-1.1	-1.3	-0.026	-0.18	-1.4×10^4	-0.21	0.08
2009	Av. conc. Em_low, level 1	48.2	66.2	0.86	0.89	8.4×10^5	2.7	0.61
	difference level 1	1.8	11.3	0.19	0.20	6.3×10^4	0.33	0.05
	difference levels 1–6	0.01	-1.5	-0.021	-0.026	-1.9×10^5	0.12	0.02
					percentage differences			
2005	level 1	4.6	28.9	31.4	20.5	23.6	11.6	1.4
	levels 1–6	-1.7	-4.4	-6.1	-11.3	-3.8	-3.8	-6.9
2009	level 1	3.7	17.1	22.5	22.8	-7.4	12.1	8.5
	levels 1–6	0.0	-4.7	-5.8	2.6	-27.6	4.4	2.7

Table 2.6: Concentration differences between the Em_low and Em_hi scenarios, over the marine part of the 9 km modelling domain (Em_low - Em_hi). (Percentage differences calculated as (Em_low - Em_hi)/Em_low $\times$ 100 %)

		Whole domain						Mediterranean Sea					
		Em_low			Em_hi			Em_low			Em_hi		
Year	Level	O_3	NO	NO_2	O_3	NO	NO_2	O_3	NO	NO_2	O_3	NO	NO_2
2000	1	11.4	22.9	21.9	8.8	15.1	14.2	15.2	40.3	43.9	10.7	27.7	29.7
	1–6	4.3	10.1	10.1	5.5	11.2	11.9	4.8	18.2	20.3	6.2	20.0	23.2
2003	1	9.3	17.9	16.3	9.6	13.0	12.5	11.7	40.4	42.0	12.3	31.8	34.4
	1–6	6.5	9.8	10.2	7.0	10.3	11.0	7.5	23.7	27.2	8.2	24.9	28.9
2004	1	9.5	30.7	21.3	8.7	21.0	15.0	13.9	57.9	53.9	12.4	44.8	42.6
	1–6	5.5	16.0	13.0	5.9	1.0	14.4	9.1	45.5	44.6	9.3	43.8	43.3
2005	1	10.5	19.4	16.0	8.3	9.2	7.6	17.0	44.2	44.5	13.1	25.6	26.0
	1–6	3.6	5.7	6.1	4.5	6.9	7.4	7.5	27.7	30.3	8.2	25.0	27.7
2006	1	11.7	27.4	25.8	10.6	19.5	18.3	14.4	42.4	45.5	12.9	32.1	35.0
	1–6	4.3	11.2	11.5	5.3	12.2	13.1	7.5	27.7	31.6	8.3	26.9	30.9
2009	1	16.3	36.5	34.2	15.1	31.2	28.2	19.9	55.3	57.8	17.4	46.9	47.4
	1–6	8.3	19.1	20.1	9.1	20.2	21.8	11.8	41.1	45.2	11.6	42.6	46.0
2010	1	9.0	20.0	16.7	9.7	16.3	12.3	10.5	35.7	36.4	11.3	31.2	31.9
	1–6	7.1	15.7	14.1	7.7	15.9	13.8	9.1	30.1	32.6	9.8	30.1	32.7

Table 2.7: The influence (%) of shipping emissions on the average concentrations of O_3, NO and NO_2 in the lowest model layer and on the first six layers (over the marine parts of the modelling domain). Calculated as (Tot_Emiss - No_Ships) / Tot_Emiss $\times$ 100 %

Chapter 3

Atmospheric mercury modelling: a Mediterranean area investigation

Mercury is a global pollutant which has come under increasing scrutiny over recent years (UNEP, 2013b; Mason *et al.*, 2012; Driscoll *et al.*, 2013). The Mediterranean region has a long history of mercury mining dating back to before Roman times, and the area contains around 65% of the world's cinnabar deposits, although the impact of mineral deposits on Hg in the Sea itself is not entirely clear (Cossa and Coquery, 2005). The Mediterranean Sea itself, while not having particularly high concentrations of Hg or its compounds in its waters, does have high concentrations of Hg in its fish, particularly those towards the top of the food chain such as tuna and swordfish (Cossa and Coquery, 2005; Storelli *et al.*, 2002, 2005). Importantly almost all Hg in Mediterranean fish is present as methylmercury (MeHg) (Storelli *et al.*, 2002, 2005, 2010).

Chemical Transport Models (CTMs) are a useful tools for investigate the mercury pollution, and can evaluate the Hg dispersion over long distances giving more detailed information on mercury cycle. While in broad terms global Hg CTMs have helped to constrain Hg budgets in environmental media, and the rates at which Hg is exchanged between media (Seigneur *et al.*, 2004; Selin *et al.*, 2007; Selin, 2009), it remains difficult to reproduce the variations in Hg species concentrations and fluxes on a regional scale (Lin *et al.*, 2006; Ryaboshapko *et al.*, 2007a,b; Bullock *et al.*, 2008, 2009; Baker and Bash, 2012). To date regional models used to simulate the emission, transport, transformation and deposition of Hg have all been off-line models. That is to say that the CTM makes use of pre-calculated meteorological variables, and interpolates these (in time or space or both) to calculate the

change in Hg species concentrations resulting from transport. This is done separately from the calculation of the change in Hg species concentrations which occur as a result of chemical production and loss reactions. A version of the on-line regional CTM WRF/Chem (Grell *et al.*, 2005) has been developed which includes gas phase Hg chemistry and a parametrised approach to Hg aqueous phase chemistry. An on-line CTM simulates the transport and chemistry which determine a chemical species' concentration in the same model time step. This approach means that there is no interpolation in either space or time of the transport term. It also means the parametrisations used to describe the physical phenomena controlling transport are the same for the meteorological and chemical parts of the model. This is not necessarily the case if output from a meteorological model is used as input for an off-line CTM. Although on-line models require longer calculation times than off-line models, advances in computational speeds means that this is significantly less of a problem than it was some years ago. A further advantage of the WRF/Chem model is that it has been coupled with the Kinetic PreProcessor (KPP) (Damian *et al.*, 2002; Sandu *et al.*, 2003; Sandu and Sander, 2006). KPP enables the user to define a chemical mechanism, which using the WKC (WRF/Chem-KPP Coupler, Salzmann and Lawrence (2006)) can be directly included into the WRF/Chem framework. This flexibility permits simulations using a number of variations of a chemical scheme to be performed with ease.

A parametrisation of air-sea exchange of Hg has been included which is consistent with the global Hg model ECHMERIT (Jung *et al.* (2009); De Simone *et al.* (2013) and Appendix A). ECHMERIT has been used to furnish boundary and initial conditions for this version of WRF/Chem, including the Hg boundary and initial conditions. As shown by Pongprueksa *et al.* (2008) the boundary conditions used by regional models have a major influence on modelling results. While using the output from global Hg CTMs to provide temporally and spatially varying boundary conditions should provide a more realistic modelling framework, the use of different global models can lead to significant variations in regional model outcomes, as shown by Bullock *et al.* (2008, 2009).

In this chapter, based on Gencarelli *et al.* (2013a), simulations with WRF/Chem including Hg have been performed to investigate Hg fate, transport and deposition in the Mediterranean area, for the year 2009. The results have been compared to the measurements performed during an intensive oceanographic campaign in June aboard the Italian Research Council's R. V. Urania, and also to measurements throughout the year from the European Monitoring and Evaluation Programme (EMEP) measurement network. The emission and deposition during the year to the from and to the surface

of the Mediterranean Sea have been calculated.

3.1 Model Description

The non-hydrostatic mesoscale chemical transport model WRF/Chem (Grell *et al.* (2005) and section 2.3) offers a number of parametrisation options to represent the physical processes which take place in the atmosphere. A detailed description of these can be found in Skamarock *et al.* (2008) and references therein. The physics options used for these simulations were as follows; the Purdue-Lin scheme was used for microphysics, which includes six classes of hydrometeors (water vapour, cloud water, rain, cloud ice, snow and graupel). The Mellor-Yamada-Janjic (MYJ) scheme was used for the Planetary Boundary Layer (PBL) parametrisation, this scheme describes vertical sub-grid-scale fluxes due to eddy transport in the whole atmospheric column, while the horizontal eddy diffusivity is calculated with a Smagorinsky 1st order closure. The surface layer parametrisation employed was the Eta surface layer scheme, the land surface model to describe interactions between the soil and atmosphere was Noah LSM (4 soil layers), and the Kain-Fritsch scheme was used for cumulus parametrisation. The Rapid Radiative Transfer Model (RRTM) and the Dudhia schemes were used for long and shortwave radiation, respectively.

WRF/Chem version 3.4 was used, with the RADM2 (Regional Acid Deposition Model, version 2) mechanism (Stockwell *et al.*, 1990b) modified to include Hg chemistry. Photolysis rates were calculated using the Fast-J photolysis scheme (Wild *et al.*, 2000) and updated every 30 min. All pollutant species normally simulated in the standard RADM2 mechanism are also simulated in WRF/Chem with Hg.

3.1.1 Modelling domains

Three domains, one coarse and two nested, have been used in the simulations. The coarse domain covers Europe and the Mediterranean, and includes parts of North Africa and the Middle East at a resolution of 81 km by 81 km. The first nested domain (middle domain) covers most of Europe and includes the Mediterranean Sea with a resolution of 27 km by 27 km. This domain was chosen to include as many EMEP stations which measure Hg, either atmospheric or in precipitation, as possible while still maintaining a domain size that did not result in excessive computational times. The second nested domain (fine domain, 9 km by 9 km) covers the route of the R. V. Urania during the oceanographic measurement campaign, see figure 3.1.

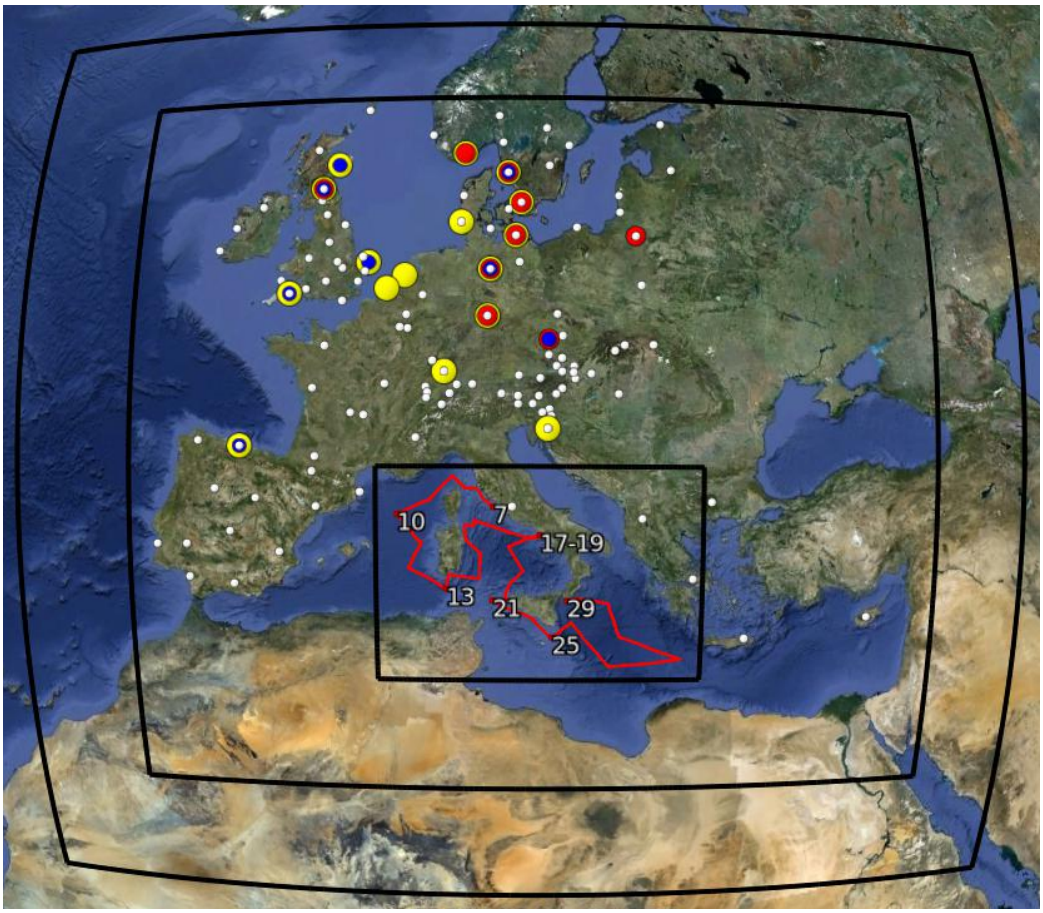

Figure 3.1: Model domains, location of the EMEP measurement stations (yellow points for wet deposition flux, red for TGM, blue for Hg^P, white for ozone concentrations) and Med-Oceanor 2009 route (red line). The numbers over the route represent the June data.

All three domains have 28 sigma vertical levels from the surface to 50 hPa. Meteorological input was from the Global Forecast System (GFS) (1°by 1°) at six hourly intervals. Chemical boundary and initial conditions were taken from the global on-line Hg model ECHMERIT (Jung *et al.*, 2009; De Simone *et al.*, 2013). The NCAR Earth System Laboratory Atmospheric Chemistry Division, (`http://www.acd.ucar.edu/wrf-chem/`) has made available a preprocessor to make use of MOZART output to provide chemical initial and spatially and temporally varying boundary conditions (IC/BC) for WRF/Chem. This preprocessor was adapted to read in and process the output from ECHMERIT in order to provide the chemical initial and boundary conditions for this Hg version of WRF/Chem.

3.1.2 The chemical mechanism

Gaseous elementary mercury (Hg^0 or GEM), Hg associated with particulate matter (Hg^P), gaseous oxidised mercury (Hg^{II} or GOM) and the aqueous phase oxidised Hg ($Hg^{II}_{(aq)}$) have been added to the RADM2 chemical mechanism in WRF/Chem with Hg using KPP (Damian *et al.*, 2002; Sandu *et al.*, 2003; Sandu and Sander, 2006) and the WKC coupler (Salzmann and Lawrence, 2006). The species Hg^P (or Particulate Bound Mercury, PBM) is used as a tracer to follow primary anthropogenic emissions of Hg associated with particulate matter. $Hg^{II}_{(aq)}$ is used to refer to oxidised Hg species in the aqueous phase (in the presence of liquid water in the atmosphere); if this species is not deposited by precipitation (i.e. a cloud evaporates) it is then considered to be associated with the residual aerosol left after droplet evaporation and transported/deposited as such. The gas phase oxidation of Hg^0 by O_3 (with rate constant from Hall (1995)) and by OH (rate constant from Sommar *et al.* (2001b)) have been included in the chemical mechanism. In particular at the RADM2 mechanism equations have been added these:

$$Hg^0 + O_3 \longrightarrow \frac{1}{2}\, Hg^{II} + \frac{1}{2}\, Hg^{II}_{(aq)} \tag{3.1}$$

$$Hg^0 + OH \longrightarrow \frac{1}{2}\, Hg^{II} + \frac{1}{2}\, Hg^{II}_{(aq)} \tag{3.2}$$

$$Hg^0_{(aq)} + O_{3(aq)} \longrightarrow Hg^{II}_{(aq)} \tag{3.3}$$

The aqueous phase chemistry of Hg has been parametrised for simplicity and also to ensure reasonable simulation times in this first version of the model. When the Liquid Water Content (LWC) in a model cell exceeds a threshold value of $10^{-7}\,m^3_{aq}\,m^{-3}_{air}$ it is assumed that a cloud is present in the model cell (Jacobson, 2005), and the model assumes that the concentrations of both $Hg^0_{(aq)}$ and $O_{3(aq)}$ are in equilibrium with their respective gas phase concentrations. The rate of production of $Hg^{II}_{(aq)}$ via oxidation of $Hg^0_{(aq)}$ by $O_{3(aq)}$ is calculated using the aqueous phase rate constant $k = 4.7 \cdot 10^7 M^{-1}$ from Munthe (1992) as:

$$\frac{d\left[Hg^{II}_{(aq)}\right]}{dt} = k \cdot \left[Hg^0_{(aq)}\right] \cdot \left[O_{3(aq)}\right] \cdot \mathrm{LWC}$$

In the model the species $Hg^{II}_{(aq)}$ is considered to be in the aqueous phase if cloud water or rainfall is present in the model cell, but if the cell is dry the species is considered to be associated with particulate matter. If $Hg^{II}_{(aq)}$

is advected from a dry cell to a model cell where liquid water is present it is assumed to completely scavenged into the atmospheric aqueous phase.

3.1.3 Dry and wet deposition

Dry deposition of gas phase species in WRF/Chem is treated using the approach developed by Wesely (1989) (see Grell *et al.* (2005)) and calculated as described in Lin *et al.* (2006). The original WRF/Chem routines have been adapted to include the deposition of Hg compounds, the deposition flux is calculated from the product of the deposition velocity and Hg species gaseous concentration in the lowermost model level. For Hg^{II} the deposition velocity has been assumed to be equal to that of $HNO_{3(g)}$ due to the similarity in their solubility (Seigneur *et al.*, 2004), while for Hg^{P} and $Hg^{II}_{(aq)}$ (recalling that the species $Hg^{II}_{(aq)}$ in cells with a liquid water below the threshold value (see section 3.1.2) is considered to be bound to atmospheric particulate) the dry deposition flux is calculated using WRF/Chem particulate deposition parametrisations. Both Hg^{P} and $Hg^{II}_{(aq)}$ are assumed to be in the coarse mode.

Wet deposition of Hg species has been implemented adding the Hg compounds to the scheme in WRF/Chem for gas and particulate convective transport and wet deposition. In-cloud and below-cloud scavenging of Hg species have been also been included adapting an already available module in WRF/Chem, based on the approach described by Neu and Prather (2012). In the model the fraction of the grid box exposed to scavenging is calculated using the algorithm described in Neu and Prather (2012), and the Hg species scavenging rate is assumed to be the same as that for $HNO_{3(g)}$.

Dry deposition of Hg^{0} and its re-emission has recently been reviewed by Zhang and Dubey (2009). There is still quite a large uncertainty associated with the net Hg^{0} flux (and its direction) over terrestrial surfaces, and therefore in this first version of the model it has not been included.

3.1.4 Emissions

Anthropogenic emissions used in the model were obtained from the RETRO (`http://www.retro.enes.org/`) and EDGAR v4 (`http://www.edgar.jrc.ec.europa.eu/`) databases using the WRF/Chem emissions preprocessor (Freitas *et al.*, 2011). The emissions preprocessor package (Freitas *et al.*, 2011) was modified to read the Arctic Monitoring and Assessment Programme (AMAP) mercury emissions inventory (Pacyna *et al.*, 2005) for the year 2000 (the $0.5\,^{\circ} \times 0.5\,^{\circ}$ inventory was used, `http://amap.no/Resources/`

`HgEmissions/`). The AMAP inventory provides emissions over three height ranges which were distributed between the appropriate model vertical levels. The total anthropogenic AMAP Hg emission to air are shown for the Mediterranean basin area in figure 3.2. The elevated Hg emission in central Europe is evident.

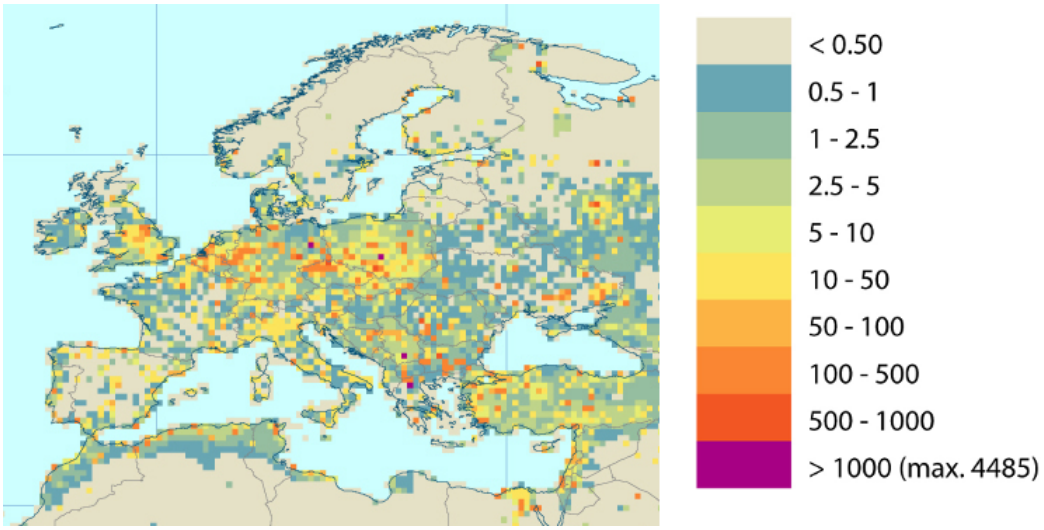

Figure 3.2: Total anthropogenic AMAP Hg emission to air (g km^{-2}). Image adapted from http://amap.no/.

Mercury emissions from biomass burning and evasion of Hg^0 from the sea surface have also been included. Hg emissions from biomass burning input files were prepared using the preprocessor developed at NCAR, `http://www.acd.ucar.edu/wrf-chem/`. This preprocessor makes use of the Fire Inventory from NCAR (FINN v1, Wiedinmyer *et al.* (2011)). In this first version of the model an enhancement ratio of 1.0×10^{-7} ppb Hg/ppb CO has been used (Friedli *et al.*, 2009) for all vegetation categories.

Evasion of Hg^0 from the sea surface has been implemented using a parametrisation based on Wanninkhof (1992), following the methodology of Gårdfeldt *et al.* (2003), assuming a constant Dissolved Gaseous Mercury (DGM) concentration of 150 fmol l^{-1} (Andersson *et al.*, 2007, 2011) and using the expression for the Henry's Law constant of Hg^0 from Andersson *et al.* (2008). Specifically, in the model the Hg^0 fluxes are computed using the two-layer gas exchange model introduced by Liss and Slater (1974):

$$F = K_w(C_w - C_a/H(T)) \tag{3.4}$$

where F is the Hg^0 flux, in ng m^{-2} h^{-1}, K_w is the water-side mass transfer coefficient, in m h^{-1}, $H(T)$ is the Henry's Law constant corrected for the

temperature T, and C_w and C_a, both expressed in ng m^{-3}, are the Hg^0 concentrations in seawater and in air, respectively. The water-side mass transfer coefficient K_w was calculated by using the parameterization of Wanninkhof (1992):

$$K_w = 0.31 \times u_{10}^2 (Sc_{Hg}/Sc_{CO})^{-0.5} \tag{3.5}$$

where u_{10} is the wind speed 10 meter above sea surface and Sc_{Hg} and Sc_{CO} are the Schmidt number of mercury and Carbon Oxide, respectively. The parameterization of Andersson *et al.* (2008) was used to calculate the temperature dependent Henry's law constant:

$$H(T) = e^{(\frac{-2404.3}{T} + 6.92)} \tag{3.6}$$

A positive value of F indicates a net Hg flux from the ocean to atmosphere whereas a negative flux would indicate deposition to the ocean. Due to the (gener- ally) supersaturated DGM concentrations, the oceans represent a net source of Hg to the atmosphere. In the present version of the model, since the deposition (both dry and wet) is computed separately by deposition routines, only positive fluxes are taken in account.

The marine and biomass emissions are emitted into the lowest model level, however for the biomass burning emissions the plume rise module already in WRF/Chem (Grell *et al.*, 2011) has been adopted. Parameterizations to include natural emissions and soil reemissions of previously deposited Hg have not been included in this model version. The WRF/Chem option to calculate biogenic emissions on-line with the Guenther scheme (Guenther *et al.*, 1993, 1994) has been used. During the simulations the biogenic emission fluxes were updated every 30 min.

Annual emission totals for the different Hg emission sources are shown in table 3.1 for the middle modelling domain, which covers the Mediterranean region. The relative importance of the Mediterranean Sea as a source of Hg^0 is very clear.

3.2 Measurements

The model has been run for the year 2009. For this year Hg measurements were available from 18 European Monitoring and Evaluation Programme (EMEP, `http://www.nilu.no/projects/ccc/emepdata.html`) stations and ozone concentrations from 111 (see supplementary information for the location of the sites). Specifically, monthly measurements of Hg wet deposition and precipitation amount were available from 16 stations, Hg^0 concentrations from 9 and Hg^P from 8 (see figure 3.1). During 2009 observations from

Source	Specie	Hg emissions	Speciation (%)	Percentage of total (%)
Anthropogenic	Hg^0	106.6	47	
	Hg^{II}	57.9	25	
	Hg^P	64.1	28	
Total Anthropogenic	Hg	228.6		59
Marine evasion (Mediterranean)	Hg^0	151.5 (67.5)		39 (17)
Biomass Burning	Hg^0	6.6		2
Total	Hg	391.8		

Table 3.1: Hg emissions (Mg year^{-1}) in the middle model domain. The proportions of Hg^0, Hg^{II} and Hg^P are from the anthropogenic emission database (Pacyna *et al.*, 2005).

the oceanographic campaign Med-Oceanor (descibed in section 2.1.2) were available. The campaign took place between the 7^{th} and 29^{th} June. During this campaign measurements were performed aboard the CNR's R. V. Urania, mostly in the Tyrrhenian Sea. The measurements made during oceanographic campaigns are described in Sprovieri *et al.* (2003, 2010). Briefly, collection and analysis of Hg^0, Hg^{II} and Hg^P were performed using an automated Tekran (Toronto, Canada) Model 2537A CVAFS (Cold Vapour Atomic Fluorescence Spectrophotometry), coupled to a Tekran Model 1130 speciation unit, and a Tekran Model 1135 system. The measurement frequency was 5 minutes for Hg^0, and 2 hours for Hg^{II} and Hg^P. Under the operating conditions employed the detection limit for Hg^{II} and Hg^P was less than $2\,\mathrm{pg\,m^{-3}}$.

3.3 Results

The skill of the WRF/Chem model using the RADM2 mechanism in reproducing meteorological and air quality parameters has been assessed in a number of previous studies (Schürmann *et al.*, 2009; Grell *et al.*, 2005; Tie *et al.*, 2007; Tuccella *et al.*, 2012; Fast *et al.*, 2006; Geng *et al.*, 2007). Thus the principal aim of this study is to analyse the model's performance in terms of Hg species concentrations in air and the Hg wet deposition flux. Having said this, because O_3 is of particularly relevance to Hg oxidation (see section 3.1.2) and the balance between emission and deposition is of interest, the agreement between the modelled and measured O_3 concentrations, particularly in coastal areas, was also investigated. The modelled values have been compared to the monthly mean values from the EMEP monitoring sites. Most sites measure Total Gaseous Mercury (TGM) thus the modelled concentrations of Hg^0 and Hg^{II} have been summed in order to perform the comparison. The site at Waldhof in Germany is the only site for which speciated Hg measurements were available for 2009. However, during the Med-Oceanor campaign speciated measurements were performed throughout the 23 days thus for this period it was possible to compare the atmospheric Hg species separately.

3.3.1 Ozone concentrations

The modelled concentrations of O_3 have a particular relevance for the modelled Hg species, firstly because O_3 is an oxidant of Hg^0, and secondly because the photolysis of O_3 leads to the production of OH radicals which are also an Hg^0 oxidant. As oxidised Hg compounds dominate both dry and

wet deposition fluxes, O_3 concentrations are a major factor in determining the atmospheric cycle of Hg. Hourly ozone concentrations from the EMEP stations within the middle domain (see figure 3.1) were compared to the model results for the whole year. Figure 3.3 shows box and whisker plots of the modelled and measured mean, bias (as defined in Myers *et al.* (2013)) both for the whole of 2009 and also only for the summer months (June, July and August). The Pearson's correlation coefficient (R) is also shown if figure 3.3. There is good agreement between the model values and the measurements in the most part of the monitoring sites, with a better estimate of the mean value and a higher value of the correlation in summer months. As can be seen in figure 3.3, the correlation is higher for the coastal sites (ES17, ES07, ES12, ES14, ES10, IT01, SI08, MK07, GR01, GR02, CY02, see the site map in the Supplementary Information). The quality of the comparison over the year between all the EMEP sites in the 27 km by 27 km domain are comparable to the results obtained by Tuccella *et al.* (2012) using a slightly smaller domain at 30 km by 30 km resolution.

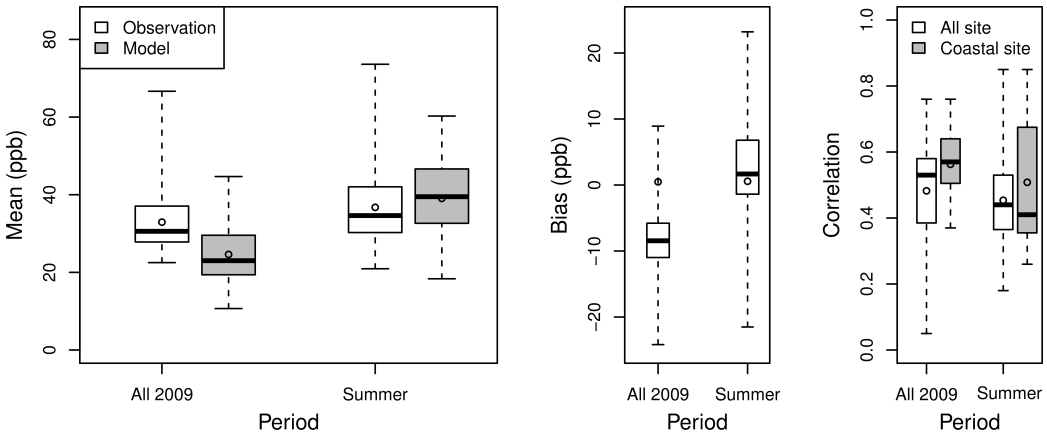

Figure 3.3: Box and whisker plots of hourly ozone concentration metrics for the 111 EMEP sites. Points represent the mean value. The correlation for just the 11 EMEP coastal sites is also shown.

Comparing the hourly value of ozone concentrations during the Med-Oceanor campaign (figure 3.4, the route is shown in figure 3.1) with the results from the fine domain (9 km by 9 km) it can be seen that the model reproduces the O_3 trend reasonably well near the coastline (the south of Sardinia, in the Gulf of Naples and close to Sicily). However the comparison is less satisfactory when the R. V. Urania was in areas further from land, where the relative impact from ship emissions is greater. The presence of fresh ship exhaust in the marine boundary layer will often result in titration

of O_3 by NO in the ship plume (see for example Vinken *et al.* (2011)) leading to localised areas of lower O_3 concentrations which the model, with its time independent emissions cannot reproduce accurately. Considering only the measurements near the coastline (the grey box in figure 3.4, around a third of all the campaign model-measurement pairs) the correlation coefficient between the model and observations is 0.72.

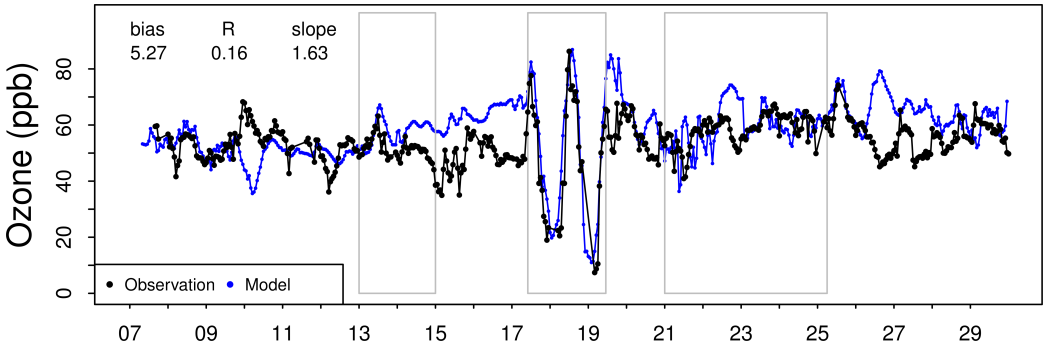

Figure 3.4: Ozone concentrations measured (black) and modelled (blue) during the Med-Oceanor measurement campaign and values of metrics (bias is in ppb). Grey boxes contain the model-measurements pairs near the coastal area.

3.3.2 Atmospheric Hg concentrations over Europe

Measurements of atmospheric Hg were performed at a number of EMEP monitoring stations within the 27 km by 27 km domain during 2009. Nine monitoring stations measured Hg in the gas phase and 8 measured Hg concentrations in atmospheric particulate matter. Not all the stations distinguish between Hg^0 and Hg^{II} and therefore these species in the model results are summed to give TGM for comparison with observations. The frequency of measurements is not the same at all the sites and therefore monthly averaged values of TGM observations have been used (Hjellbrekke, 2003) and the corresponding average calculated from the model output. The comparison between observed and modelled concentrations is shown in figure 3.5 whiles some statistical parameters of the comparison for the full year are summarised in Table 3.2. The station at Kosetice (CZ03) in the Czech Republic proved difficult to reproduce in the simulations and has a mean TGM concentration significantly lower than all the other stations and indeed below the generally accepted hemispheric background concentration of $\approx 1.7\,\mathrm{ng\,m^{-3}}$. The reason for this is not clear.

station	$M_{meas} \pm SD_{meas}$	$M_{mod} \pm SD_{mod}$	R	bias
CZ03	0.68 ± 0.62	1.53 ± 0.11	0.12	0.85
DE02	1.69 ± 0.13	1.61 ± 0.11	0.43	-0.08
DE08	1.70 ± 0.17	1.52 ± 0.11	0.40	-0.18
DE09	1.48 ± 0.22	1.64 ± 0.09	0.75	0.16
GB48	1.11 ± 0.34	1.54 ± 0.04	0.48	0.43
NO01	1.68 ± 0.18	1.55 ± 0.07	-0.07	-0.13
PL05	1.25 ± 0.25	1.66 ± 0.14	0.72	0.41
SE11	1.40 ± 0.14	1.67 ± 0.10	0.69	0.27
SE14	1.51 ± 0.11	1.60 ± 0.09	0.65	0.09

Table 3.2: TGM concentration statistical analysis in the EMEP stations. Mean (M), Standard Deviation (SD) and bias are in $\mathrm{ng\,m^{-3}}$.

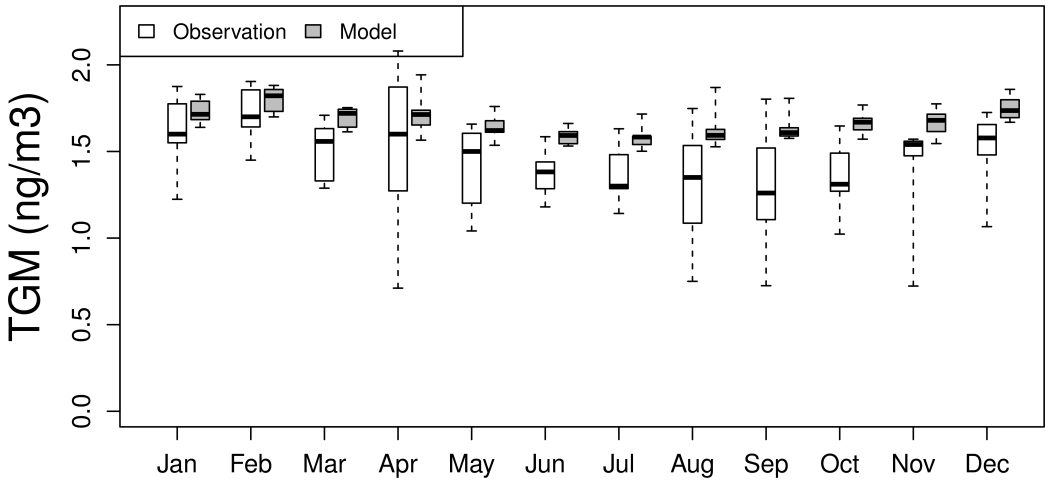

Figure 3.5: Monthly distribution of measured and modelled TGM concentrations at EMEP measurement stations.

Generally, as seen in figure 3.5 the model tends to slightly overestimate the monthly averaged TGM concentrations and the bias for the individual monitoring sites ranges from around -0.2 to $0.4\,\mathrm{ng\,m^{-3}}$ (with the exception of site CZ03). As can be seen from table 3.2 of the 9 sites, only 3 showed a negative bias. The seasonal variation, slightly lower values in the summer than the winter seen in the observations is also seen in the model results, although it is less marked. It can also be seen from figure 3.5 that the variability in the observations is greater than the variability seen in the model results, (see also the standard deviations in table 3.2). The correlation coefficients in table 3.2 are reasonable at most sites, with the the sites at Birkenes (NO01) and Kosetice (CZ03) being the obvious exceptions. The other results

are similar to those obtained by Ryaboshapko *et al.* (2007a, 2003).

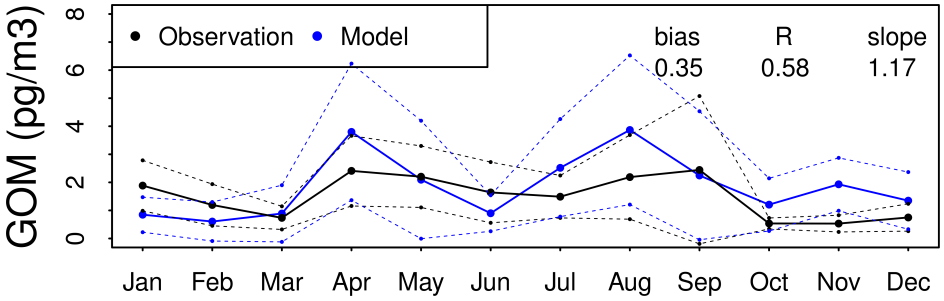

Figure 3.6: Monthly RGM concentrations measured (black) and modelled (blue) at Waldhof station. The metrics (bias is in $\mathrm{pg\,m^{-3}}$) of the comparison and the standard deviation of the data (dashed line) are also shown.

As mentioned earlier hourly values of TGM and two hourly values of Hg^{II} are available for the site at Waldhof (DE02) in Germany. The daily averaged observed and modelled values of TGM are plotted in figure 3.8, where it can be clearly seen that the short term variability in the observations is not reproduced by the model. However the bias is low -0.06 $\mathrm{ng\,m^{-3}}$, and the slope of the linear regression between the two datasets is 0.94. The correlation is however low on a daily basis, ≈ 0.20. The Hg^{II} results are similar, the bias is low -1.6 $\mathrm{pg\,m^{-3}}$, but the correlation is also low on a daily basis. However as shown in figure 3.6 the model does seem to be able to capture the Hg^{II} trend during the year. The statistical parameters in figure 3.6 refer to monthly average values of the observations and model results.

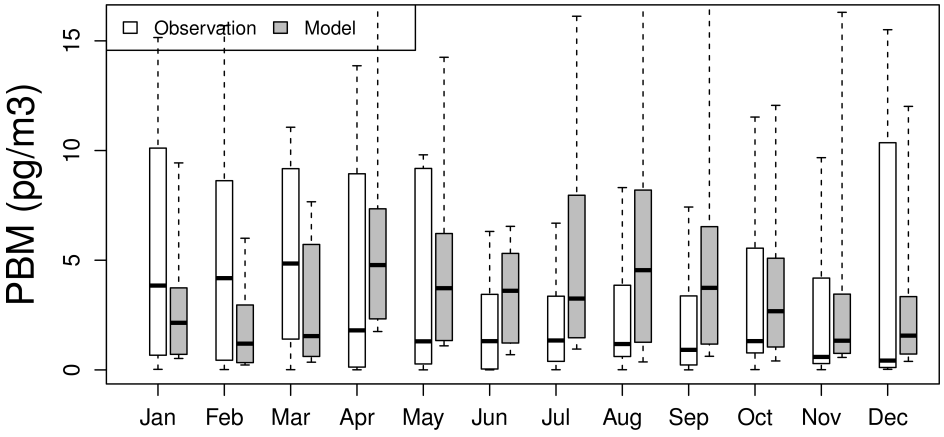

Figure 3.7: Monthly distribution of measured and modelled PBM concentrations at EMEP stations.

The box and whisker plot in figure 3.7 shows the monthly averaged distribution of modelled and measured Hg^P concentrations at the eight stations where it was measured. The measured values generally show more variation during the winter than the summer, the model however predicts higher variability during the summer.

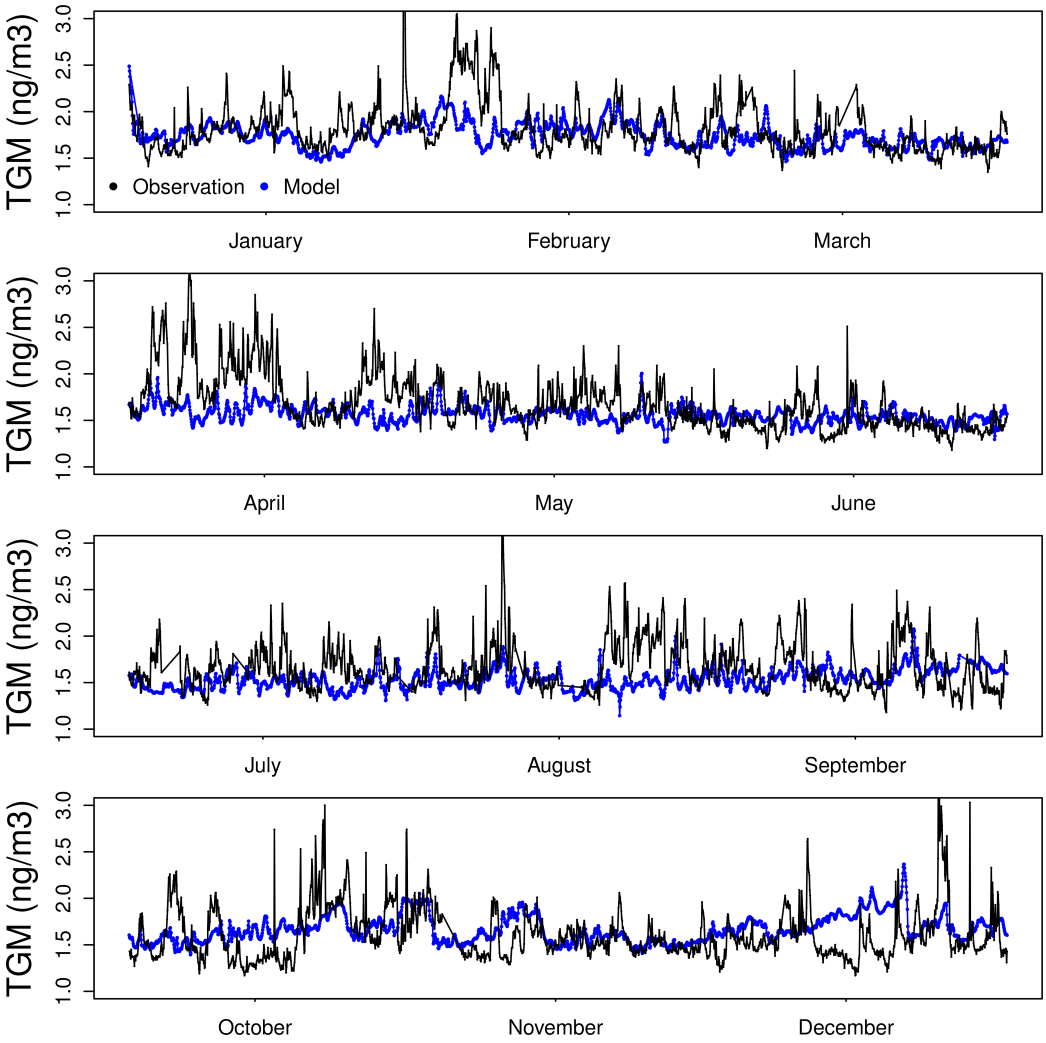

Figure 3.8: Hourly TGM concentrations measured (black) and modelled (blue) at Waldhof station.

3.3.3 Marine Boundary Layer air concentrations

For the Med-Oceanor campaign in June 2009 the daily average observations and model results have been compared. Figure 3.9 shows observed

and simulated values of Hg^0, Hg^{II} and Hg^P, with the respective metrics. Although the model reflects in part the qualitative trend in Hg^{II} and Hg^P, it overestimates both. The variation seen in the Hg^0 concentrations, particularly towards the end of the measurement campaign are not reflected in the model results. However over the whole of the campaign the bias was ≈ 0, and the slope of the regression line between model results and observations was close to 1. One complication in the marine boundary layer which can cause models to overestimate oxidised Hg species concentrations is the presence of sea salt and non-sea-salt sulphate aerosols. These aerosols are ubiquitous in the marine boundary layer and can be a sink for gas phase Hg^{II} and Hg^{II} in particulates (Hedgecock and Pirrone, 2004; Holmes *et al.*, 2009). The inclusion of Hg species scavenging by marine aerosols in the MBL is foreseen in the next phase of the model development.

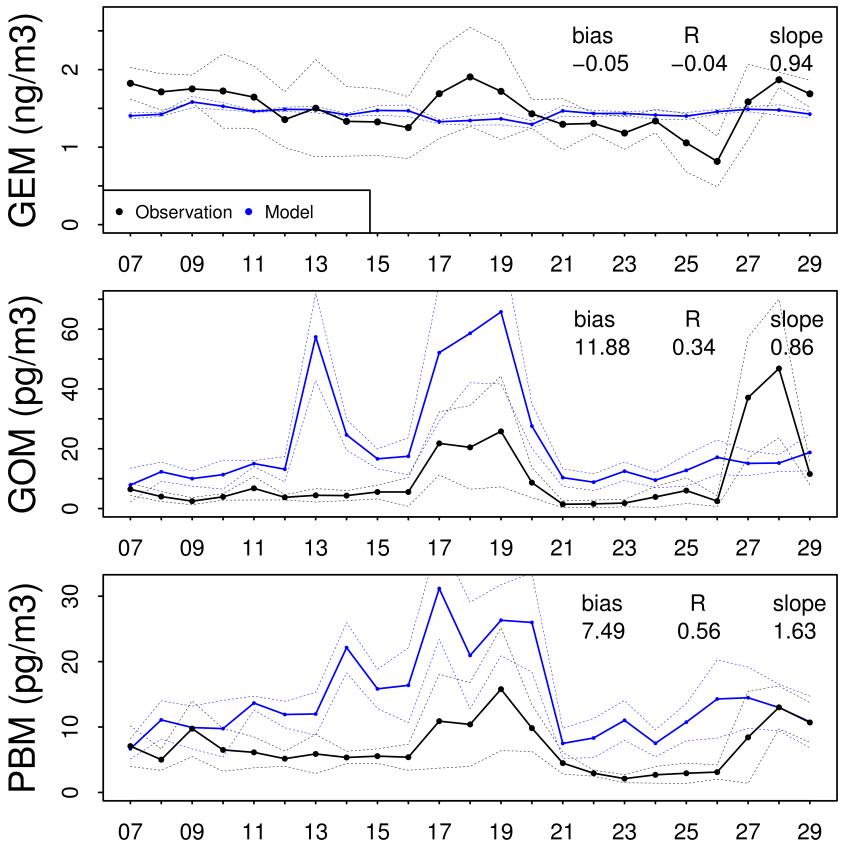

Figure 3.9: Mercury concentrations measured (black) during the MedOceanor campaign and modelled values (blue). The time axis indicates the day in June while the bias is in $ng\,m^{-3}$ for GEM and in $pg\,m^{-3}$ for RGM and PBM. Dashed line represents the standard deviations to the data.

3.3.4 Mercury deposition

Measurements of Hg in precipitation are available from 16 EMEP sites in the model 27 km by 27 km domain for the year 2009, the comparison of measured and model values is shown in figure 3.10.

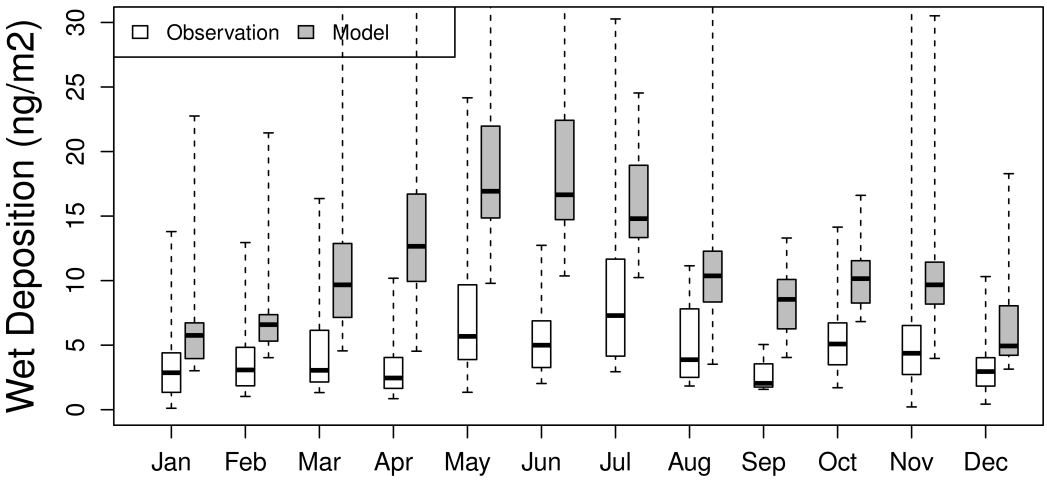

Figure 3.10: Monthly mean of the mercury wet deposition flux at EMEP sites and in the correspondenting model cells.

The model overestimates the wet deposition flux especially in hot months, when photochemical oxidant production peaks. The model overestimates the rate of Hg^{II} formation and this is then scavenged by clouds and rainfall. In part the overestimation of the wet deposition flux is also caused by the slight overestimation of the rainfall at the sites (Bullock Jr. and Brehme, 2002), as shown in figure 3.11. Clearly though this is not the major factor. Looking at the modelled and observed monthly averaged concentration of Hg in precipitation, figure 3.12, it is clear that the overestimation of the wet deposition flux occurs in late Spring / early Summer. Exactly why this should be will be investigated in future studies. The Hg deposition fluxes obtained are however similar to those from previous modelling model studies (Bullock *et al.*, 2009; Ryaboshapko *et al.*, 2007b).

The dry deposition flux of Hg is very difficult to measure directly. The most common approach is to use surrogate surfaces (Lyman *et al.*, 2009; Peterson *et al.*, 2012; Gustin *et al.*, 2012), these methods are however still under development, (see also the review by Zhang and Dubey (2009) on the dry deposition of atmospheric Hg). The dry deposition velocities calculated by the model for values for Hg^{II} are similar to those obtained by Baker and Bash (2012), with values between $0.5\,\mathrm{cm\,s^{-1}}$ for the 10^{th} percentile and

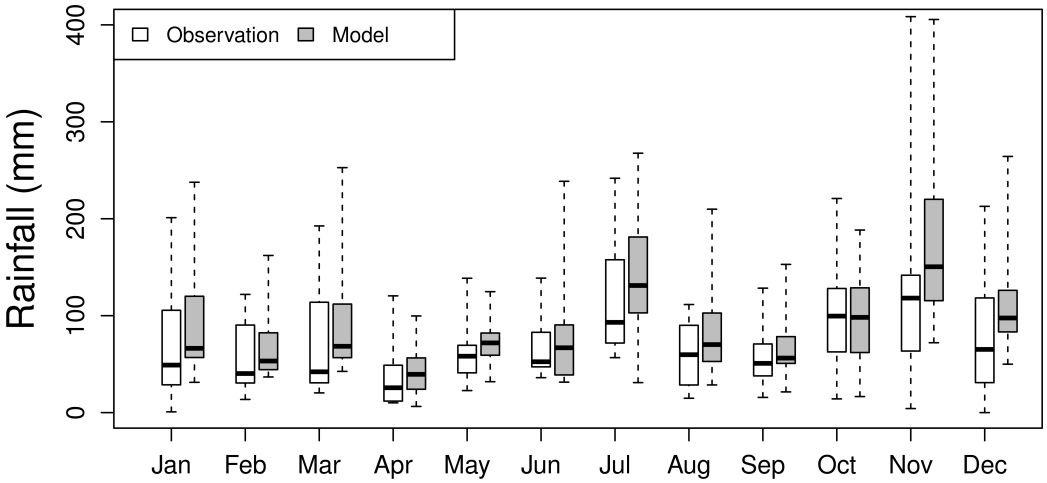

Figure 3.11: Monthly rainfall at EMEP stations and and in the corresponding model cells.

$4.0\,\mathrm{cm\,s^{-1}}$ for the 90^{th}. For particulate dry deposition velocity the modelled values are lower (between $0.1\,\mathrm{cm\,s^{-1}}$ and $3.7\,\mathrm{cm\,s^{-1}}$), according to Zhang and Dubey (2009).

Figure 3.13 shows the annual Hg deposition flux over the middle domain. As well as the total, total dry and total wet deposition of Hg, the figure illustrates the quantity of Hg deposited as Hg^{II} and Hg^{P} in both the wet and dry fluxes. As in Zhang *et al.* (2012b) the relative contributions of dry and wet deposition to the total deposition over the whole domain are similar (dry 48%, wet 52%). Scavenging of Hg^{II} accounts for 46% of the wet deposition flux, whereas scavenging of Hg^{P} contributes 6%. These two species contribute equally to the calculated dry deposition flux in the modelling domain (24% and 24%).

The contribution of wet deposition to the total deposition flux is greater in the North of the domain and over the mountain ranges of the Alps and Pyrenees. Wet deposition also dominates over some coastal areas of the Adriatic and Turkey. Dry deposition dominates over North Africa and continental European, especially near emission sources.

3.3.5 Mediterranean flux

The WRF/Chem with Hg model also calculates the Hg^{0} evasion flux from the Mediterranean Sea, section 3.1.4. Combining the modelled deposition flux and emission for the Mediterranean it is possible to estimate the net flux from the Sea itself. Figure 3.14 shows the monthly accumulated

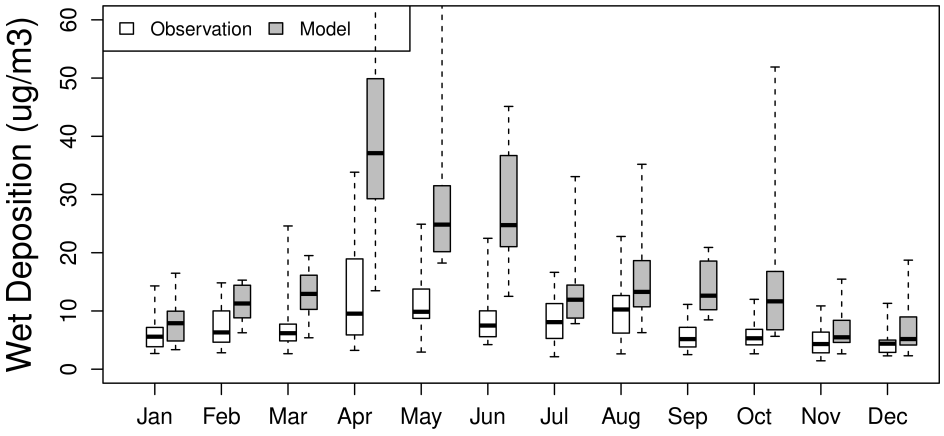

Figure 3.12: Monthly mean to the mercury wet deposition concentrations in EMEP sites and in correspondents model cells.

	Wet deposition		Dry deposition		Sea evasion	Net flux
	Particulate	Gaseous	Particulate	Gaseous		
	0.65	18.94	8.16	9.97		
Total	19.59		18.13		67.51	29.79

Table 3.3: Mercury Mediterranean Sea evasion and deposition ($\mathrm{Mg\,year^{-1}}$).

Hg deposition fluxes and the monthly accumulated Hg evasion. With the exception of April (when there the model shows no net flux) it is clear that the Mediterranean is a net source of Hg to the atmosphere. The yearly totals for deposition and evasion and the net annual flux are shown in table 3.3. Thus for the modelled year (2009) the results suggest that the contribution to atmospheric Hg^0 from the Mediterranean Sea was nearly 30 Mg. This estimate is significantly less than our previous modelling estimate (Hedgecock *et al.*, 2006) which was of a net evasive flux of nearly $70\,\mathrm{Mg\,yr^{-1}}$. The reason for this is that in this study the deposition flux is higher, and the evasive flux from the ocean is lower than in the previous investigation. How much this difference depends on the chemical mechanism, and the treatment of the species $Hg^{II}_{(aq)}$ as particulate in dry cells, and how much variation can be expected as a result of year to year variation in meteorological conditions is the subject of continuing studies.

The Hg emission from the Mediterranean Sea is greatest in December and lowest in May. Figure 3.15 shows that the monthly mean marine emission in these months have different spatial patterns, reflecting the influence of meteorological parameters and to a lesser extent Hg^0 concentrations on marine emissions of Hg.

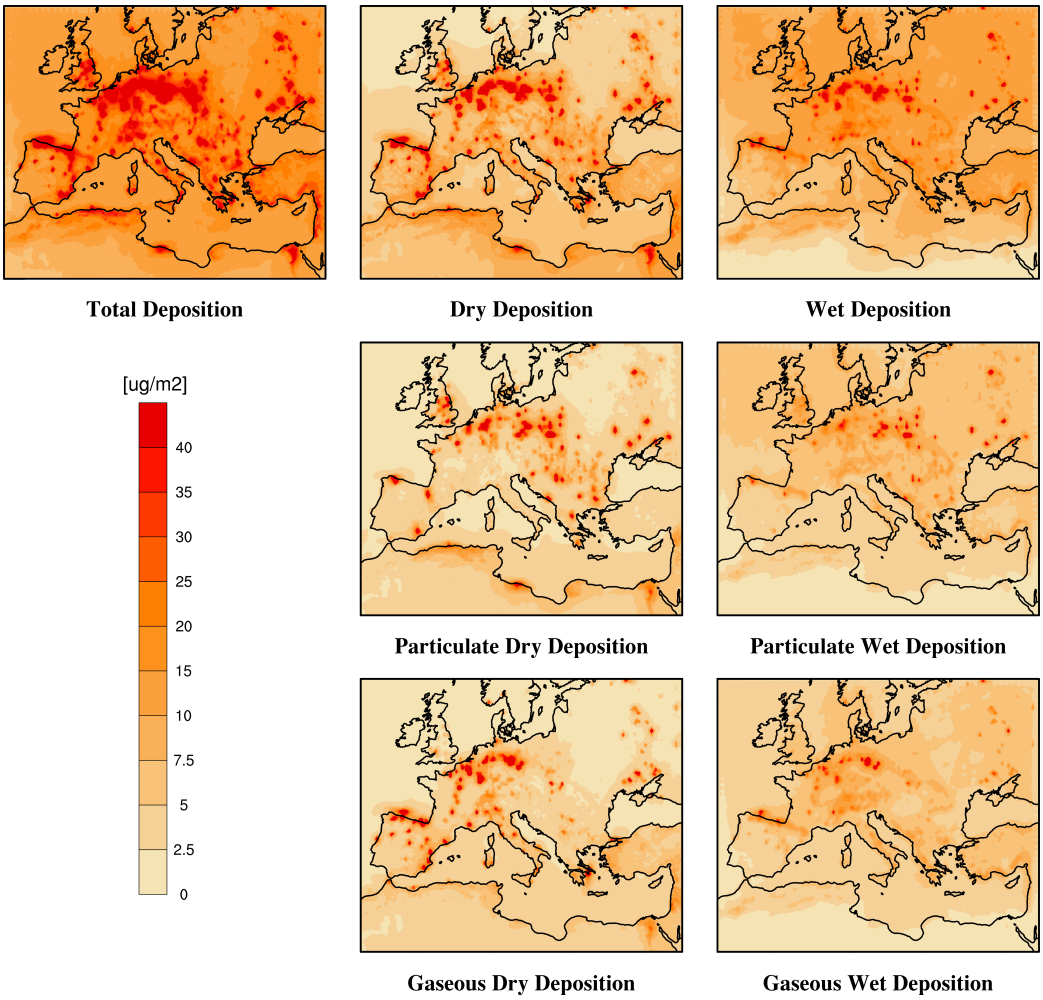

Figure 3.13: Mercury deposition in model domain. Note that the colour scale is not linear.

3.4 Discussion

This study has brought to light a number of issues concerning the regional modelling of Hg atmospheric emission, transport and deposition. The speciation of Hg included in emission inventories in regional models needs to be reconsidered because different regions may use different Hg emission reduction methods, and these methods influence the relative proportions of the Hg species in flue gases. Emissions from oceans and seas would benefit from long term data on DGM concentrations in the surface layer. The chemistry of Hg in the atmosphere and in particular its redox reactions are still uncertain, and the possibility of the atmospheric importance of Br con-

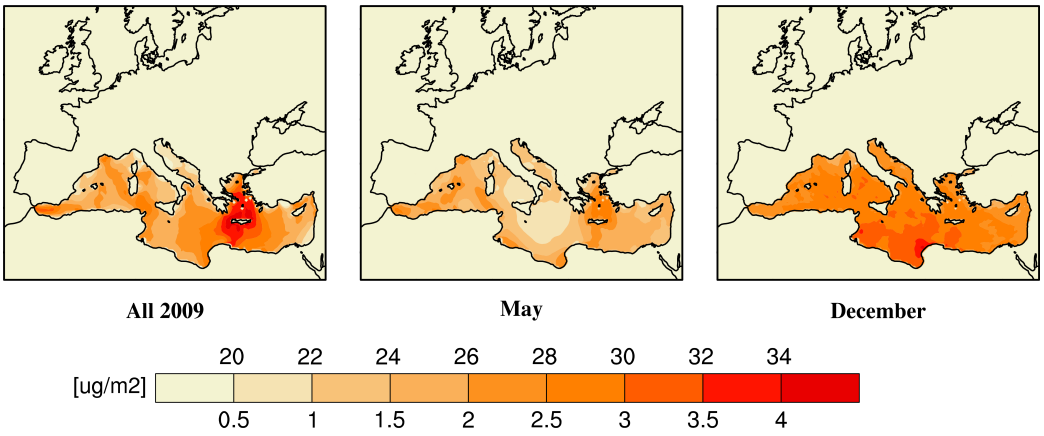

Figure 3.14: Mediterranean Sea evasions. The upper colour scale is for the "All 2009" image, while the lower is for evasion to May and December. Note that the colour scale is not linear.

taining compounds and also heterogeneous reaction pathways leads to some uncertainty in models (see the recent review by Subir *et al.* (2011, 2012)). The role of atmospheric chemical processes has also been discussed in relation to the fate of oxidised Hg compounds in the plumes of large industrial combustion facilities. It has been suggested that some commonly emitted reductants such as CO or SO_2 could alter the proportions of Hg species before the plume is fully diluted, altering the "effective" speciation of the emissions, see Pongprueksa *et al.* (2008) and Zhang *et al.* (2012a). In the particular case of the Mediterranean Sea understanding the role of year on year changes in meteorological conditions on the exchange of Hg between the atmosphere and the sea surface is important. The levels of Hg found in Mediterranean fish is clearly a reason for this, but this exchange also makes up an important fraction of the Mediterranean Sea Hg budget, (see Žagar *et al.* (2013)). Currently simulations are underway for the other years in which Med-Oceanor campaigns were performed in the Mediterranean. The cruise data is of great importance for these simulations as they allow the results to be compared with open sea observations.

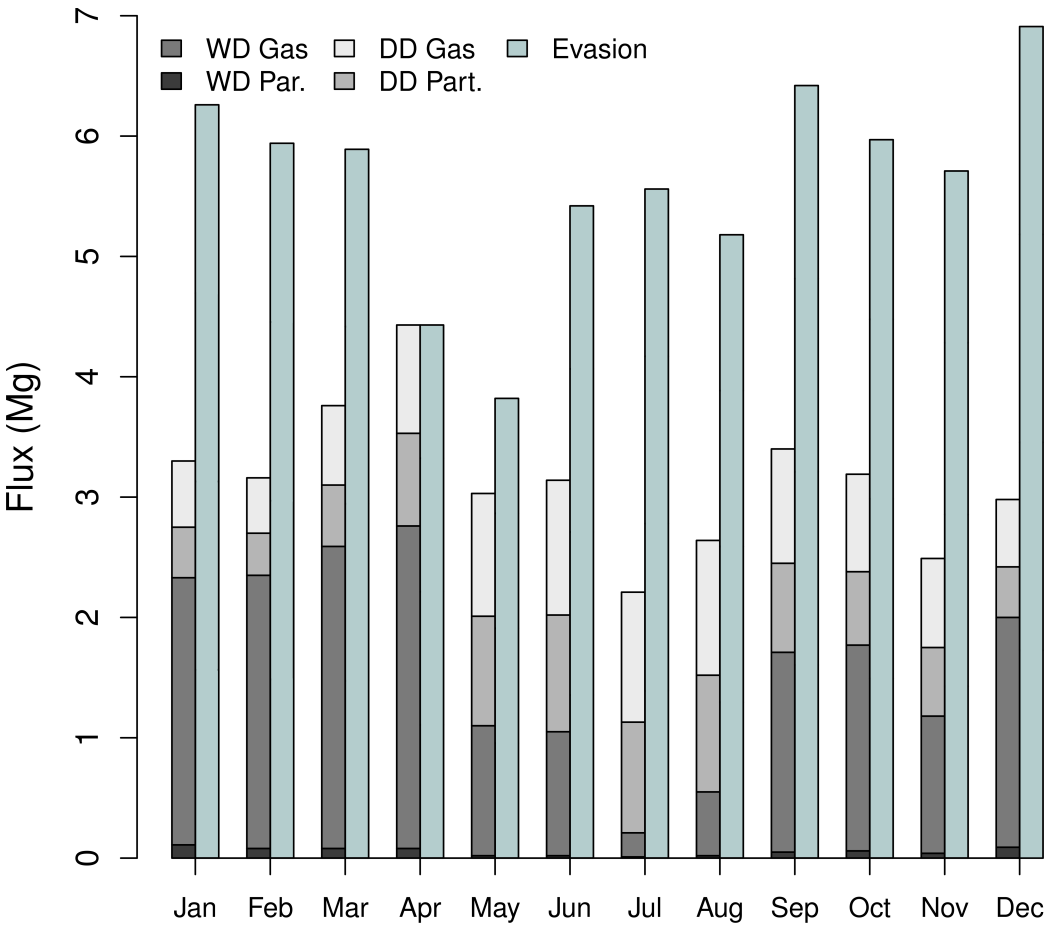

Figure 3.15: Mediterranean sea Hg mass balance. For every month the Hg sea evasion is shown on the right and the deposition on the left. Deposition is divided into gas and particulate wet deposition (WD) and dry deposition (DD).

3.5 Conclusions

A modified version of the WRF/Chem model has been developed with the aim of simulating atmospheric Hg chemistry. Thus modules and routines to include Hg emissions from anthropogenic and natural sources, Hg chemical interactions in the atmosphere and Hg deposition processes have been added to WRF/Chem. The model reproduces the seasonal variation in TGM concentration at continental sites in Europe, with a slight positive bias, and overestimates the monthly averages at 6 out of the 9 monitoring stations for which data were available. In the MBL the model results reproduce the qualitative trend in the Hg^{II} and Hg^{P} measurements. The magnitude of the Hg deposition flux in the model domain from wet and dry deposition processes are similar, but with very different spatial distributions. Wet deposition is greater in the area characterised by high precipitation as expected, however even in those regions with a damp climate, dry deposition dominates in areas near major Hg emission sources. Hg evasion from the sea surface has been implemented in the model using an on-line parametrisation. Within the modelling domain which covers Europe the marine emission source contributes 39% of the total annual Hg emitted. The Mediterranean alone contributes almost half of this and accounts for 17% of the Hg emitted within the domain. Comparing the magnitude of dry and wet deposition with evasion flux from the Mediterranean sea the results suggest that the Mediterranean Sea emits $\approx$67 Mg year^{-1}, and receives $\approx$37 Mg year^{-1} from dry and wet deposition. The net flux of Hg to the atmosphere from the Mediterranean Sea is thus estimated to be $\approx$30 Mg year^{-1}.

3.6 Appendix A: ECHMERIT global atmospheric model

ECHMERIT is a fully coupled on-line model, based on the Atmospheric General Circulation Model ECHAM5 (Roeckner *et al.*, 2003, 2006), and a MERcury chemistry module, developed at the Institute for Atmospheric Pollution of the Italian National Research Council (CNR-IIA) in Rende, ITaly (Jung *et al.*, 2009).

Different schemes for advection, convection and vertical diffusion are already implemented in the model. It has a highly customisable chemistry mechanism designed to facilitate the investigation of both aqueous and gas phase atmospheric mercury chemistry. Recently it has been updated and improved with a new air-sea exchange parameterisation (De Simone *et al.*, 2013).

A number of off-line CTMs have been developed in recent years (De Simone *et al.* (2013) and references therein), but ECHMERIT differs from almost all other global Hg models in that it is an on-line model.

An important application of global models is to provide the boundary and the initial conditions (BC/IC) to regional mercury models which perform simulations at higher spatial resolutions. Regional CTM simulations of atmospheric Hg chemistry and deposition have been shown to be particularly sensitive to the BC/IC which are used (Pongprueksa et al, 2008). Boundary conditions for regional simulations are generally more important than initial conditions for regional Hg CTMs, and therefore recently most regional models make use of time and space varying BCs from global model output. However there can be some variation in the regional modelling results depending on which global model output is used (Bullock et al, 2008, 2009; Harris et al, 2012).

ECHMERIT transports 27 chemical species, including four mercury species: Hg^0, Hg^P, Hg^{II} and $Hg^{II}_{(aq)}$. The model uses a spectral grid with horizontal resolution of T42 grid (roughly 2.8° by 2.8°). Whereas in the vertical the model is discretised with a hybrid-sigma pressure system with 19 or 31 non-equidistant levels up to 10 hPa.

To reproduce real meteorological conditions the nudging routine already implemented in ECHAM5 using reanalysis data from the ERA-INTERIM project (ECMWF) has been used. Averaged values obtained from previous multi-year long model simulations are used to initialise the concentrations of all species.

Chapter 4

Mediterranean mass balance

The Mediterranean Sea area is subject to mercury pollution from anthropogenic and natural sources. A large part (approximately 65%) of the world Hg reserves are in the cinnabar belt underlying the Mediterranean area (Bernhard and Buffoni, 1982). Mercury in the Mediterraneanoriginates from past mining activities (Idrija in Slovenia, Monte Amiata in Italy and Almaden in Spain), coal and oil combustion, cement production and chloralkali plants (Kocman *et al.*, 2013).

Recently several studies have been dedicated to the Hg transformation processes in the water column (Monperrus *et al.*, 2007; Cossa *et al.*, 2009), soil sediment (Hines *et al.*, 2006; Monperrus *et al.*, 2007; Ogrinc *et al.*, 2007), atmosphere (Pirrone *et al.*, 2003; Wängberg *et al.*, 2001a, 2008; Sprovieri *et al.*, 2010), and in the marine boundary layer (Hedgecock *et al.*, 2003, 2005, 2006; Sprovieri *et al.*, 2010).

In several Mediterranean fish species, notably tuna and swordfish, were found elevated Hg levels, due at the MeHg bioaccumulation, although the total Hg (HgT) concentrations in water are not significantly higher than in the Atlantic Ocean (Cossa *et al.*, 1997; Cossa and Coquery, 2005; Storelli *et al.*, 2002, 2005; Mason *et al.*, 1998; Mason and Sullivan, 1999; Mason *et al.*, 2001; Žagar *et al.*, 2013). Although all recent studies indicate the presence of elevated mercury concentrations in fish (Cossa and Coquery, 2005; Storelli *et al.*, 2002, 2005), and in spite of several sampling campaigns and published studies on the concentrations of Hg and its compounds in the various environmental compartments of the Mediterranean Sea, relatively little is known of the actual distribution of Hg in the area (Cinnirella *et al.*, 2013). Calculation of the mass balance of contaminants can provide useful information on the processes, which influence their concentration in any given environmental compartment. They can help indicate the most important sources, sinks and also the equilibrium or non-equilibrium state of the contaminant

intercompartmental exchange processes. Often, a relatively good estimate on the future trends of pollutant concentrations and therefore impacts on the environment can be made on the basis of a well defined mass balance modelling system (Žagar *et al.*, 2013).

Recently many numerical models have been developed and used in order to simulate mercury transport, fluxes and transformations in both water and the atmosphere (Kallos *et al.*, 2001; Žagar *et al.*, 2007; Selin, 2009; Sunderland *et al.*, 2009; Mason *et al.*, 2012; Gencarelli *et al.*, 2013a) and several mass balances have been established for the Mediterranean and its component seas and basins (Cossa *et al.*, 1997; Rajar *et al.*, 2007).

Due to the recently obtained measurement data (Kotnik *et al.*, 2013), the continuing development of numerical models and increasing understanding of Hg transformation processes (Mason *et al.*, 2012), it has been possible to update the recent HgT mass balance (Žagar *et al.*, 2013). Using the most recent data it has also been possible to calculate an approximate MeHg mass balance which had not been established previously and which is by far the most important organic Hg compound entering the food web (Žagar *et al.*, 2013).

4.1 Processes in Marine Boundary Layer

The Mediterranean established to be an interesting place to study the atmospheric oxidation of elemental mercury and ozone production. Particularly in summertime the Mediterranean MBL is characterised by atmospheric stability, high temperatures and abundant sunshine that provide good conditions for ozone formation, and the combination of high ozone concentrations, strong sunlight and the humidity of the MBL also leads to the production of OH. Both OH and ozone are thought to be oxidants of atmospheric Hg^0 (Hall (1995); Sommar *et al.* (2001b); Pal and Ariya (2004); Subir *et al.* (2011) and section 1.2.1). The Mediterranean MBL therefore provides the ideal location to assess the importance of the reactions between Hg and these oxidants in the atmospheric Hg cycle. Measurements obtained during an oceanographic campaign in the Adriatic in 2005 were compared to simulations obtained using a box model of multiphase MBL photochemistry (Sprovieri *et al.*, 2010). The ozone concentrations were high during this particular campaign, averaging over 60 ppb during the cruise. Various simulations were performed in which O_3/OH and Br/BrO were assumed to be the Hg^0 oxidants. The simulations with O_3/OH as oxidants considerably overestimated the concentrations of Hg^{II} and also failed to reproduce the magnitude of the diurnal cycle, probably because the O_3 concentration remained high during the night-

time. The simulations which assumed Br was the Hg^0 oxidant reproduced the measurements far better, and given the results of other studies (Holmes *et al.*, 2010; Tas *et al.*, 2012), it seems likely that, in the MBL at least, Br is the most important GEM oxidant.

4.2 Model intercomparison of the air-water fluxes

Oxidised Hg compounds are significantly less volatile and more soluble than elemental Hg, and subsequently are taken up by clouds and also dry deposited more readily than elemental Hg. Simulation with global model ECHMERIT (Jung *et al.* (2009); De Simone *et al.* (2013) and Appendix A) and WRF/Chem with Hg regional model (Gencarelli *et al.* (2013a) and chapter 3) have been used to estimate the deposition of atmospheric mercury to the Mediterranean Sea. In a previous regional modelling study (Hedgecock *et al.*, 2006), it was estimated that the Mediterranean Sea was a net emitter of approximately 70 Mg of Hg^0 a year. There are uncertainties on the average DGM concentration in the Mediterranean, and this quantity is important in the mechanism of air-water exchange (section 3.1.4). The ECHMERIT global model has been run in tracer mode to evaluate the net emission and deposition from the Mediterranean assuming uniform concentrations of 10, 20, 30 and 40 pg l^{-1} for the years 2008 and 2009. Table 4.1 resume the model results.

Model	MECAWEx	PCFLOW3D	ECHMERIT		WRF/Chem
year	1999	2004	2008	2009	2009
Dry dep.	13.2				18
Wet dep.	7.4				20
Total dep.	20.6	23	50/51	46/43	38
Emission	90.4	50	65/47	69/50	68
Net evasion	≈ 70	≈ 27	$\approx 24/4$	$\approx 23/7$	≈ 30

Table 4.1: Hg deposition and evasion obtained by atmospheric and hydrological models in the Mediterranean area. All values are in Mg $year^{-1}$. Table from Žagar *et al.* (2013).

The difference between the earliest model result (MECAWEx, Hedgecock *et al.* (2006)) and the most recent simulations (ECHMERIT and WRF/Chem) is notable in terms of the lower emissions totals, but also in the deposition fluxes. The WRF/Chem result suggests that the MECAWEx wet deposition

estimate is severely low. Furthermore, both the evasion and deposition calculated by the coupled atmospheric and water models (Žagar *et al.*, 2007) are thought to be too low, although the net evasion is not significantly different than in the most recent simulations. The deposition totals from WRF/Chem and ECHMERIT are similar. The emissions from WRF/Chem and ECHMERIT are also similar and both lower than MECAWEx (the two values for ECHMERIT in table 4.1 are simulations in which DGM was assumed to be 40 and 30 pg l^{-1}, respectively, while the WRF/Chem simulation used a constant 30 pg l^{-1}). ECHMERIT has the advantage that it is global, and therefore, the sum of all the marine emissions can be calculated. Using a DGM value of 30 pg l^{-1} gives total global emission estimates which are in line with current estimates from other modelling groups and recent estimates from compartmental models (Selin, 2009; Mason *et al.*, 2012).

4.3 Conclusion regarding the Mediterranean mass balance

The GEM evasion and deposition from the most recent simulations (68 and 38 Mg $year^{-1}$, respectively for WRF/Chem with Hg) were considered. However, the net flux is the important factor for the mass balance, and a relatively good agreement between the results of all recent estimates (PCFLOW3D (Žagar *et al.*, 2007), ECHMERIT and WRF/Chem) was obtained with regard to this quantity. Similar net fluxes of approximately 25-30 Mg $year^{-1}$ give us a certain amount of confidence, even though the actual deposition and evasion in each simulation vary due to differences in individual processes parameterisations.

Numerous authors suggest that MeHg deposition is extremely low and usually not exceeding 1% of the Hg^0 deposition (Hammerschmidt *et al.*, 2007; Graydon *et al.*, 2008; Guo *et al.*, 2008; Heimbrger *et al.*, 2011). Due to low precipitation (Boukthir and Barnier, 2000; Rajar *et al.*, 2007) and the absence of gaseous MeHg species in the surface layer (Horvat *et al.* (2003); Kotnik *et al.* (2007); Heimbürger *et al.* (2010)), the estimated value of MeHg deposition is about 400 kg $year^{-1}$, while MeHg evasion is negligible (Žagar *et al.*, 2013).

4.4 Bromine oxidation in WRF/Chem with Hg

WRF/Chem with Hg simulations have been performed to investigate mercury oxidation by Bromine-compounds in the Mediterranean MBL (Gencarelli *et al.*, 2012, 2013b). In this section the preliminary results of this model application are shown.

The WRF/Chem with Hg model described in section 3.1 has been modified to include the gas phase oxidation of Hg^0 by Br (with the rate constant from Ariya *et al.* (2002)) and by BrO (rate constant from Spicer *et al.* (2002)). In this way equations 3.1-3.3 are subsitued as:

$$Hg^0 + Br \longrightarrow \frac{1}{2} Hg^{II} + \frac{1}{2} Hg^{II}_{(aq)} \tag{4.1}$$

$$Hg^0 + BrO \longrightarrow \frac{1}{2} Hg^{II} + \frac{1}{2} Hg^{II}_{(aq)} \tag{4.2}$$

The aqueous phase mechanism for this oxidation scheme are under preparation. WRF/Chem model does not include atmospheric Bromine chemistry. One major problem is the lack of a Br emissions inventory and uncertainty in marine emissions of organic Br compounds. Thus specific tools are been developed for include the Br and BrO concentrations from the AMCOTS (Atmospheric Chemistry Model Over The Sea) box model (Hedgecock *et al.*, 2005; Sprovieri *et al.*, 2010) in the WRF/Chem with Hg. The AMCOTS model was initially developed to investigate the atmospheric chemistry of Hg in the gas and deliquesced aerosol phases in the MBL (Hedgecock *et al.*, 2005). It contains a detailed mechanism to describe gas phase chemistry, photolysis, aqueous phase chemistry in deliquesced sea salt and non-sea salt sulphate aerosol, and the transfer of chemical species between the phases.

4.4.1 Result using Bromine-compounds oxidation

The same model domains and physics options used in chapter 3 have been used for investigate the Bromine compound oxidation. This simulations were performed for June 2009, in order to use the measurements from the Med-Oceanor campaign for validate the model results.

Figure 4.1 shows the observed and simulated values of Hg^0 and Hg^{II} along the Med-Oceanor measurement route, with the respective metrics. The results for the two different oxidation mechanisms using O_3/OH or Br/BrO as GEM oxidants are shown.

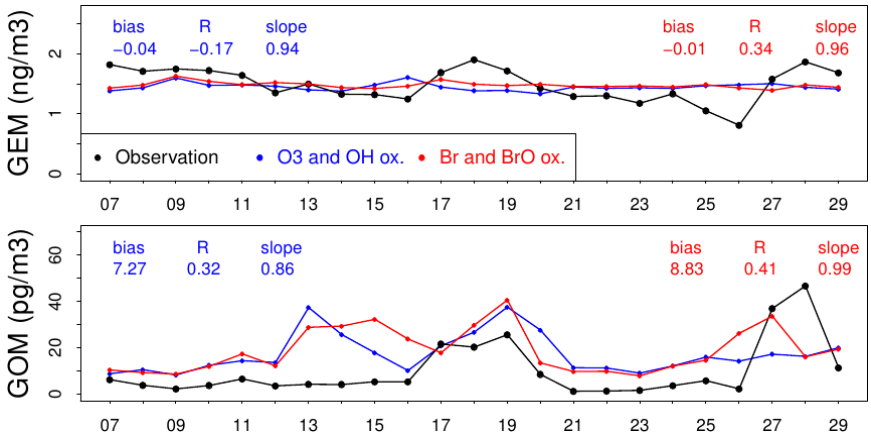

Figure 4.1: Mercury concentrations measured (black) during the Med-Oceanor campaign and modelled values (blue for O_3/OH oxidation and red for Br/BrO oxidation). The time axis indicates the day in June while the bias is in ng m^{-3} for GEM and in pg m^{-3} for RGM.

Using the oxidation by Br and BrO mechanisms the model simulations reproduce in part the qualitative trend in Hg^{II} concentrations. The bias for Hg^0 over the whole campaign is ≈ 0, and the slope of the regression line between model results and observations was close to 1.

The differences between the two oxidation patterns are also evident in the Hg deposition. Figure 4.2 shows the spatial distribution of Hg deposition (wet and dry) in the period of simulation. While Hg deposition is more evenly distributed over the domains for O_3/OH oxidations, it is located prevalently near the Hg emission sources in the Br/BrO oxidation case.

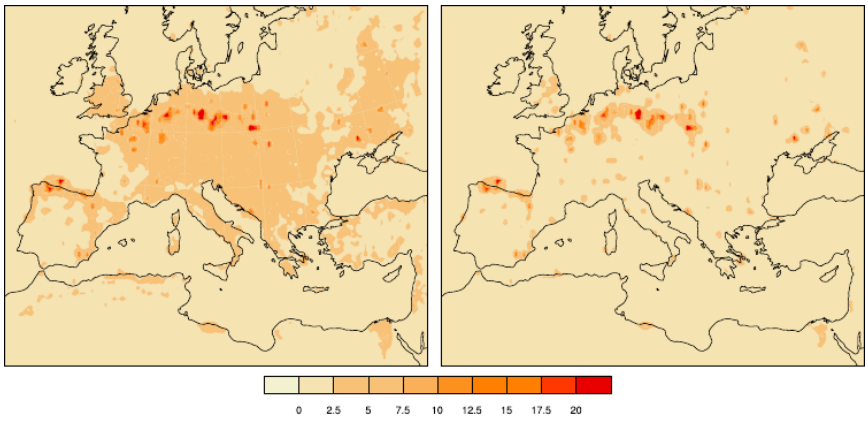

Figure 4.2: Model Hg deposition (μg m^{-2}) for June 2009. On the left for oxidation by O_3 and OH and on the right for oxidation by Br and BrO.

The investigation of Hg oxidation in the MBL by Bromine compounds is still in progress. However these preliminary results appear to confirm that in the Mediterranean MBL Br and BrO are important GEM oxidants, giving better agreement between the modelled and observed GEM and GOM values.

Chapter 5

Summary and conclusions

This work has presented a modelling study to investigate the atmospheric air quality, and in particular the pollution by ozone and mercury in Mediterranean area.

Initially the WRF/Chem model was used to simulate O_3 concentrations for the periods of seven oceanographic research campaigns which took place in the Mediterranean Basin between 2000 and 2010. The results of the comparison between the model and observations O_3 concentration showed a reasonable agreement. Having demonstrated the model's ability to reproduce the O_3 concentrations, it was used to evaluate the impact of shipping emissions on the air quality to the Mediterranean area. Considering that the average measured O_3 concentrations during the Med-Oceanor series of oceanographic measurement campaigns was 50 – 60 ppb, shipping emissions can contribute between ≈3 and 12 ppb to the long-term average concentrations of O_3. Shipping emissions will therefore continue to play an important role in local and regional air quality in Mediterranean coastal areas and beyond for the foreseeable future.

To investigate the atmospheric mercury cycle a modified version of the WRF/Chem model has been developed. Thus modules and routines to include Hg emissions from anthropogenic and natural sources, Hg chemical interactions in the atmosphere and the Hg deposition processes have been added to WRF/Chem. These modules include Hg emission from biomass burning, both from biofuel use and from wildfires and Hg exchange at the sea/ocean surface. The model is able to reproduce the seasonal variation in TGM concentration at continental sites in Europe, while in the MBL the model results reproduce the qualitative trend in Hg^{II} and Hg^{P} measurements. The magnitude of the Hg deposition flux in the model domain from wet and dry deposition processes are similar, but with very different spatial distributions. Wet deposition is greater in the area characterised by high

precipitation as expected, however even in those regions with a damp climate, dry deposition dominates in areas near major Hg emission sources. Hg evasion from the sea surface has been implemented in the model using an online parametrisation, and estimates of the annual flux have calculated. Comparing the magnitude of dry and wet deposition with evasion flux from the Mediterranean Sea the results suggest that the Mediterranean Sea emits $\approx$67 Mg year^{-1}, and receives $\approx$37 Mg year^{-1} from dry and wet deposition. The net flux of Hg to the atmosphere from the Mediterranean Sea is thus estimated to be $\approx$30 Mg year^{-1} (Gencarelli *et al.*, 2013a).

The estimates obtained for the net evasion flux with WRF/Chem have been compared with other recent estimates obtained with other model (ECH-MERIT (De Simone *et al.*, 2013), PCFLOW3D/RAMS-HG (Žagar *et al.*, 2007), MECAWEX (Hedgecock *et al.*, 2006)) to the net flux, being an important factor for the investigation to the Mediterranean mass balance. Using also these results an estimated MeHg flux has also been calculated, with around 400 kg of MeHg deposited in a year over the whole basin (Žagar *et al.*, 2013).

The WRF/Chem with Hg model has been adapted for include the gas phase oxidation of Hg^0 by Br and BrO. This work is still in progress, but preliminary results indicate that in the Mediterranean MBL Br-containing compounds are an important GEM oxidant.

Bibliography

Adame, J. A., Serrano, E., Bolívar, J. P., and de la Morena, B. A. (2009). On the tropospheric ozone variations in a coastal area of southwestern europe under a mesoscale circulation. *J. Appl. Meteor. Climatol.*, **49**(4), 748–759.

Andersson, M. E., Gårdfeldt, K., Wängberg, I., Sprovieri, F., Pirrone, N., and Lindqvist, O. (2007). Seasonal and daily variation of mercury evasion at coastal and off shore sites from the mediterranean sea. *Marine Chemistry*, **104**, 214 – 226.

Andersson, M. E., Grdfeldt, K., Wängberg, I., and Strmberg, D. (2008). Determination of henrys law constant for elemental mercury. *Chemosphere*, **73**(4), 587–592.

Andersson, M. E., Sommar, J., Grdfeldt, K., and Jutterstrm, S. (2011). Airsea exchange of volatile mercury in the north atlantic ocean. *Marine Chemistry*, **125**(14), 1 – 7.

Ariya, P. A., Khalizov, A., and Gidas, A. (2002). Reactions of gaseous mercury with atomic and molecular halogens: Kinetics, product studies, and atmospheric implications. *The Journal of Physical Chemistry A*, **106**(32), 7310–7320.

Ariya, P. A., Peterson, K., Snider, G., and Amyot, M. (2009). Mercury chemical transformations in the gas, aqueous and heterogeneous phases: state-of-the-art science and uncertainties. In N. Pirrone and R. P. Mason, editors, *Mercury Fate and Transport in the Global Atmosphere: Emissions, Measurements and Models*, chapter 15, pages 459–501. Springer.

Auvray, M. and Bey, I. (2005). Long-range transport to europe: Seasonal variations and implications for the european ozone budget. *J. Geophys. Res.*, **110**(D11), D11303–.

Baker, K. R. and Bash, J. O. (2012). Regional scale photochemical model evaluation of total mercury wet deposition and speciated ambient mercury. *Atmospheric Environment*, **49**(0), 151 – 162.

Bernhard, M. and Buffoni, G. (1982). Mercury in the mediterranean, an overview. In *Proceedings of the International Conference on Environmental Pollution 1981*, pages 458 – 484. University of Thessaloniki.

Bonasoni, P., Stohl, A., Cristofanelli, P., Calzolari, F., Colombo, T., and Evangelisti, F. (2000). Background ozone variations at mt. cimone station. *Atmospheric Environment*, **34**(29-30), 5183 – 5189.

Boukthir, M. and Barnier, B. (2000). Seasonal and inter-annual variations in the surface freshwater flux in the mediterranean sea from the ecmwf re-analysis project. *Journal of Marine Systems*, **24**(34), 343–354.

Bullock, O. R., Atkinson, D., Braverman, T., Civerolo, K., Dastoor, A., Davignon, D., Ku, J.-Y., Lohman, K., Myers, T. C., Park, R. J., Seigneur, C., Selin, N. E., Sistla, G., and Vijayaraghavan, K. (2008). The north american mercury model intercomparison study (nammis): Study description and model-to-model comparisons. *Journal of Geophysical Research: Atmospheres*, **113**(D17), n/a–n/a.

Bullock, O. R. J., Atkinson, D., Braverman, T., Civerolo, K., Dastoor, A., Davignon, D., Ku, J. Y., Lohman, K., Myers, T. C., Park, R. J., Seigneur, C., Selin, N. E., Sistla, G., and Vijayaraghavan, K. (2009). An analysis of simulated wet deposition of mercury from the north american mercury model intercomparison study. *J. Geophys. Res.*, **114**(D8), D08301–.

Bullock Jr., O. R. and Brehme, K. A. (2002). Atmospheric mercury simulation using the {CMAQ} model: formulation description and analysis of wet deposition results. *Atmospheric Environment*, **36**(13), 2135 – 2146.

Capaldo, K., Corbett, J. J., Kasibhatla, P., Fischbeck, P., and Pandis, S. N. (1999). Effects of ship emissions on sulphur cycling and radiative climate forcing over the ocean. *Nature*, **400**(6746), 743–746.

Chang, J. C. and Hanna, S. R. (2004). Air quality model performance evaluation. *Meteorology and Atmospheric Physics*, **87**, 167–196.

Charlton-Perez, C. L., Evans, M. J., Marsham, J. H., and Esler, J. G. (2009). The impact of resolution on ship plume simulations with no$_x$ chemistry. *Atmospheric Chemistry and Physics*, **9**(19), 7505–7518.

Chosson, F., Paoli, R., and Cuenot, B. (2008). Ship plume dispersion rates in convective boundary layers for chemistry models. *Atmospheric Chemistry and Physics*, **8**(16), 4841–4853.

Cinnirella, S., Graziano, M., Pon, J., Murciano, C., Albaigs, J., and Pirrone, N. (2013). Integrated assessment of chemical pollution in the mediterranean sea: Driver-pressures-state-welfare analysis. *Ocean & Coastal Management*, **xx**, xx.

Clarkson, T. W. and Magos, L. (2006). The toxicology of mercury and its chemical compounds. *Critical Reviews in Toxicology*, **36**, 609–662.

Corbett, J. J., Winebrake, J. J., Green, E. H., Kasibhatla, P., Eyring, V., and Lauer, A. (2007). Mortality from ship emissions: A global assessment. *Environmental Science & Technology*, **41**(24), 8512–8518.

Corbitt, E. S., Jacob, D. J., Holmes, C. D., Streets, D. G., and Sunderland, E. M. (2011). Global sourcereceptor relationships for mercury deposition under present-day and 2050 emissions scenarios. *Environmental Science & Technology*, **45**(24), 10477 – 10484.

Cossa, D. and Coquery, M. (2005). The mediterranean mercury anomaly, ageochemical or abiologocal issue. In A. Saliot, editor, *The Mediterranean Sea*, volume 5K of *Handbook of Environmental Chemistry*, pages 177–208. Springer Berlin Heidelberg.

Cossa, D., Martin, J.-M., Takayanagi, K., and Sanjuan, J. (1997). The distribution and cycling of mercury species in the western mediterranean. *Deep Sea Research Part II: Topical Studies in Oceanography*, **44**(3-4), 721–740.

Cossa, D., Averty, B., and Pirrone, N. (2009). The origin of methylmercury in open Mediterranean waters. *Limnology and oceanography*, **54**(5), 837–844.

Cristofanelli, P. and Bonasoni, P. (2009). Background ozone in the southern europe and mediterranean area: Influence of the transport processes. *Environmental Pollution*, **157**(5), 1399 – 1406.

Cristofanelli, P., Bonasoni, P., Carboni, G., Calzolari, F., Casarola, L., Sajani, S. Z., and Santaguida, R. (2007). Anomalous high ozone concentrations recorded at a high mountain station in italy in summer 2003. *Atmospheric Environment*, **41**(7), 1383 – 1394.

Dalsøren, S. B., Eide, M. S., Endresen, Ø., Mjelde, A., Gravir, G., and Isaksen, I. S. A. (2009). Update on emissions and environmental impacts from the international fleet of ships: the contribution from major ship types and ports. *Atmospheric Chemistry and Physics*, **9**(6), 2171–2194.

Damian, V., Sandu, A., Damian, M., Potra, F., and Carmichael, G. (2002). The kinetic preprocessor kpp-a software environment for solving chemical kinetics. *Computers and Chemical Engineering*, **26**(11), 1567–1579.

de Meij, A., Gzella, A., Cuvelier, C., Thunis, P., Bessagnet, B., Vinuesa, J. F., Menut, L., and Kelder, H. M. (2009). The impact of mm5 and wrf meteorology over complex terrain on chimere model calculations. *Atmospheric Chemistry and Physics*, **9**(17), 6611–6632.

De Simone, F., Gencarelli, C. N., Hedgecock, I. M., and Pirrone, N. (2013). Global atmospheric cycle of mercury: a model study of the impact of oxidation mechanisms. *Environmental Science and Pollution Research*.

Derwent, R. G., Stevenson, D. S., Doherty, R. M., Collins, W. J., Sanderson, M. G., Johnson, C. E., Cofala, J., Mechler, R., Amann, M., and Dentener, F. J. (2005). The contribution from shipping emissions to air quality and acid deposition in europe. *AMBIO: A Journal of the Human Environment*, **34**(1), 54–59.

Driscoll, C. T., Mason, R. P., Chan, H. M., Jacob, D. J., and Pirrone, N. (2013). Mercury as a global pollutant: Sources, pathways, and effects. *Environmental Science & Technology*.

Duncan, B. N., West, J. J., Yoshida, Y., Fiore, A. M., and Ziemke, J. R. (2008). The influence of european pollution on ozone in the near east and northern africa. *Atmospheric Chemistry and Physics*, **8**(8), 2267–2283.

Durnford, D. A., Dastoor, A. P., Steen, A. O., Berg, T., Ryzhkov, A., Figueras-Nieto, D., Hole, L. R., Pfaffhuber, K. A., and Hung, H. (2012). How relevant is the deposition of mercury onto snowpacks? part 1: A statistical study on the impact of environmental factors. *Atmospheric Chemistry and Physics Discussions*, **12**(1), 387 – 439.

EC (2008). Directive 2008/50/EC of the European Parliament and of the Council on ambient air quality and cleaner air for Europe.

EEA (2013). Air quality in Europe. Technical report, European Environment Agency.

Eyring, V., Köhler, H. W., van Aardenne, J., and Lauer, A. (2005). Emissions from international shipping: 1. the last 50 years. *J. Geophys. Res.*, **110**(D17), D17305–.

Eyring, V., Stevenson, D. S., Lauer, A., Dentener, F. J., Butler, T., Collins, W. J., Ellingsen, K., Gauss, M., Hauglustaine, D. A., Isaksen, I. S. A., Lawrence, M. G., Richter, A., Rodriguez, J. M., Sanderson, M., Strahan, S. E., Sudo, K., Szopa, S., van Noije, T. P. C., and Wild, O. (2007). Multi-model simulations of the impact of international shipping on atmospheric chemistry and climate in 2000 and 2030. *Atmospheric Chemistry and Physics*, **7**(3), 757–780.

Eyring, V., Isaksen, I. S., Berntsen, T., Collins, W. J., Corbett, J. J., Endresen, O., Grainger, R. G., Moldanova, J., Schlager, H., and Stevenson, D. S. (2010). Transport impacts on atmosphere and climate: Shipping. *Atmospheric Environment*, **44**(37), 4735 – 4771.

Fast, J. D., Gustafson, William I., J., Easter, R. C., Zaveri, R. A., Barnard, J. C., Chapman, E. G., Grell, G. A., and Peckham, S. E. (2006). Evolution of ozone, particulates, and aerosol direct radiative forcing in the vicinity of houston using a fully coupled meteorology-chemistry-aerosol model. *J. Geophys. Res.*, **111**(D21), D21305–.

Ferrara, R., Ceccarini, C., Lanzillotta, E., Gårdfeldt, K., Sommar, J., Horvat, M., Logar, M., Fajon, V., and Kotnik, J. (2003). Profiles of dissolved gaseous mercury concentration in the mediterranean seawater. *Atmospheric Environment*, **37, Supplement 1**(0), 85 – 92.

Freitas, S. R., Longo, K. M., Alonso, M. F., Pirre, M., Marecal, V., Grell, G., Stockler, R., Mello, R. F., and Sánchez Gácita, M. (2011). Prep-chem-src – 1.0: a preprocessor of trace gas and aerosol emission fields for regional and global atmospheric chemistry models. *Geoscientific Model Development*, **4**(2), 419–433.

Friedli, H. R., Radke, L. F., Lu, J. Y., Banic, C. M., Leaitch, W. R., and MacPherson, J. I. (2003). Mercury emissions from burning of biomass from temperate north american forests: laboratory and airborne measurements. *Atmospheric Environment*, **37**(2), 253 – 267.

Friedli, H. R., Arellano, A. F., Cinnirella, S., and Pirrone, N. (2009). Initial estimates of mercury emissions to the atmosphere from global biomass burning. *Environmental Science & Technology*, **43**(10), 3507–3513.

Gårdfeldt, K., Sommar, J., Strmberg, D., and Feng, X. (2001). Oxidation of atomic mercury by hydroxyl radicals and photoinduced decomposition of methylmercury species in the aqueous hase. *Atmospheric Environment*, **35**, 3039 – 3047.

Gårdfeldt, K., Sommar, J., Ferrara, R., Ceccarini, C., Lanzillotta, E., Munthe, J., Wängberg, I., Lindqvist, O., Pirrone, N., Sprovieri, F., Pesenti, E., and Strömberg, D. (2003). Evasion of mercury from coastal and open waters of the atlantic ocean and the mediterranean sea. *Atmospheric Environment*, **37, Supplement 1**(0), 73 – 84.

Gårdfeldt, K. and Jonsson, M. (2003). Is bimolecular reduction of hg(ii) complexes possible in aqueous systems of environmental importance. *The Journal of Physical Chemistry A*, **107**(22), 4478 – 4482.

Gencarelli, C. N., De Simone, F., Hedgecock, I. M., Sprovieri, F., and Pirrone, N. (2012). Development of a regional scale atmospheric hg model based on wrf-chem: results of preliminary studies. In *E3S Web of Conferences*, volume 1. EDP Sciences.

Gencarelli, C. N., De Simone, F., Hedgecock, I. M., Sprovieri, F., and Pirrone, N. (2013a). Development and application of a regional scale atmospheric mercury model based on wrf/chem: a mediterranean area investigation. *Environmental Science and Pollution Research*.

Gencarelli, C. N., De Simone, F., Hedgecock, I. M., and Pirrone, N. (2013b). Development and application of a regional scale atmospheric mercury model on-line based on wrf/chem. In *11th International Conference on Mercury as a Global Pollutant, Edinburgh*.

Geng, F., Zhao, C., Tang, X., Lu, G., and Tie, X. (2007). Analysis of ozone and vocs measured in shanghai: A case study. *Atmospheric Environment*, **41**, 989–1001.

Gerasopoulos, E., Kouvarakis, G., Vrekoussis, M., Kanakidou, M., and Mihalopoulos, N. (2005). Ozone variability in the marine boundary layer of the eastern mediterranean based on 7-year observations. *J. Geophys. Res.*, **110**(D15), D15309–.

Goodsite, M. E., Plane, J. M. C., and Skov, H. (2012). Correction to a theoretical study of the oxidation of hg0 to hgbr2 in the troposphere. *Environmental Science & Technology*, **46**(9), 5262–5262.

Graydon, J., St Louis, V., Hintelman, H., Lindberg, S., Sandilands, K., Rudd, J., Kelly, C., Hall, B., and Mowat, L. (2008). Long-term wet and dry deposition of total and methyl mercury in the remote boreal ecoregion of canada. *Environ Sci Technol*, **42**, 83458351.

Grell, G., Freitas, S. R., Stuefer, M., and Fast, J. (2011). Inclusion of biomass burning in wrf-chem: impact of wildfires on weather forecasts. *Atmospheric Chemistry and Physics*, **11**(11), 5289–5303.

Grell, G. A., Knoche, R., Peckham, S. E., and McKeen, S. A. (2004). Online versus offline air quality modeling on cloud-resolving scales. *Geophys. Res. Lett.*, **31**.

Grell, G. A., Peckham, S. E., Schmitz, R., McKeen, S. A., Frost, G., Skamarock, W. C., and Eder, B. (2005). Fully coupled "online" chemistry within the wrf model. *Atmospheric Environment*, **39**, 6957–6975.

Guenther, A., Zimmerman, P., and Wildermuth, M. (1994). Natural volatile organic compound emission rate estimates for u.s. woodland landscapes. *Atmospheric Environment*, **28**(6), 1197 – 1210.

Guenther, A. B., Zimmerman, P. R., Harley, P. C., Monson, R. K., and Fall, R. (1993). Isoprene and monoterpene emission rate variability: Model evaluations and sensitivity analyses. *J. Geophys. Res.*, **98**(D7), 12609–12617.

Guo, Y., Feng, X., Li, Z., He, T., Yan, H., Meng, B., Zhang, J., and Qiu, G. (2008). Distribution and wet deposition fluxes of total and methyl mercury in wujiang river basin, guizhou, china. *Atmosperic Environment*, **42**, 70967103.

Gustin, M. S., Weiss-Penzias, P. S., and Peterson, C. (2012). Investigating sources of gaseous oxidized mercury in dry deposition at three sites across florida, usa. *Atmospheric Chemistry and Physics*, **12**(19), 9201–9219.

Hall, B. (1995). The gas phase oxidation of elemental mercury by ozone. *Water, Air, and Soil Pollution*, **80**(1-4), 301–315.

Hammerschmidt, C., Lamborg, C., and Fitzgerald, W. (2007). Aqueous phase methylation as a potential source of methylmercury in wet deposition. *Atmosperic Environment*, **41**, 16631668.

Harris, R., Pollman, C., Landing, W., Evans, D., Axelrad, D., Hutchinson, D., Morey, S. L., Rumbold, D., Dukhovskoy, D., Adams, D. H., Vijayaraghavan, K., Holmes, C., Atkinson, R. D., Myers, T., and Sunderland, E. (2012). Mercury in the gulf of mexico: Sources to receptors. *Environmental Research*, **119**(0), 42–52.

Hedgecock, I. M. and Pirrone, N. (2004). Chasing quicksilver: Modeling the atmospheric lifetime of hg0(g) in the marine boundary layer at various latitudes. *Environmental Science & Technology*, **38**(1), 69–76.

Hedgecock, I. M., Pirrone, N., Sprovieri, F., and Pesenti, E. (2003). Reactive gaseous mercury in the marine boundary layer: modelling and experimental evidence of its formation in the Mediterranean region. *Atmospheric Environment*, **37**(Supplement 1), 41 – 49.

Hedgecock, I. M., Trunfio, G. A., Pirrone, N., and Sprovieri, F. (2005). Mercury chemistry in the MBL: Mediterranean case and sensitivity studies using the AMCOTS (Atmospheric Mercury Chemistry over the Sea) model. *Atmospheric Environment*, **39**(38), 7217 – 7230.

Hedgecock, I. M., Pirrone, N., Trunfio, G. A., and Sprovieri, F. (2006). Integrated mercury cycling, transport, and air-water exchange (MECAWEx) model. *Journal Of Geophysical Research - Atmospheres*, **111**(D20), D20302–.

Hedgecock, I. M., Pirrone, N., and Sprovieri, F. (2008). Chasing quicksilver northward: mercury chemistry in the arctic troposphere. *Environmental Chemistry*, **5**(2), 131–134.

Hedgecock, I. M., Gencarelli, C. N., Schürmann, G. J., Sprovieri, F., and Pirrone, N. (2012). Measurements and modelling of ozone in the mediterranean mbl: an investigation of the importance of ship emissions to local ozone production. *Atmospheric Chemistry and Physics Discussions*, **12**(7), 16557–16602.

Heimbürger, L.-E., Cossa, D., Marty, J.-C., Migon, C., Averty, B., Dufour, A., and Ras, J. (2010). Methyl mercury distributions in relation to the presence of nano- and picophytoplankton in an oceanic water column (ligurian sea, north-western mediterranean). *Geochimica et Cosmochimica Acta*, **74**(19), 5549 – 5559.

Heimbrger, L., Mignon, C., and Cossa, D. (2011). Impact of atmospheric deposition of anthropogenic and natural trace metals on northwestern

mediterranean surface waters: a box model assessment4. *Environ Pollut*, **159**, 16291634.

Hines, M. E., Faganeli, J., Adatto, I., and Horvat, M. (2006). Microbial mercury transformations in marine, estuarine and freshwater sediment downstream of the idrija mercury mine, slovenia. *Applied Geochemistry*, **21**(11), 1924–1939.

Hjellbrekke, A.-G. (2003). Data report 2001. *Acidifying and eutrophying compounds, EMEP/CCC-Report*.

Hjellbrekke, A.-G., Solberg, S., and Fjæraa, A. M. (2011). Ozone measurements 2009, emep/ccc-report 2/2011. Technical report, EMEP (European Monitoring and Evaluation Programme). Reports on measurement data for all years are available from http://www.nilu.no/projects/ccc/reports.html.

Holmes, C. D., Jacob, D. J., and Yang, X. (2006). Global lifetime of elemental mercury against oxidation by atomic bromine in the free troposphere. *Geophys. Res. Lett.*, **33**, L20808.

Holmes, C. D., Jacob, D. J., Mason, R. P., and Jaffe, D. A. (2009). Sources and deposition of reactive gaseous mercury in the marine atmosphere. *Atmospheric Environment*, **43**(14), 2278 – 2285.

Holmes, C. D., Jacob, D. J., Corbitt, E. S., Mao, J., Yang, X., Talbot, R., and Slemr, F. (2010). Global atmospheric model for mercury including oxidation by bromine atoms. *Atmospheric Chemistry and Physics*, **10**(24), 12037 – 12057.

Horvat, M., Kotnik, J., Logar, M., Fajon, V., Zvonaric, T., and Pirrone, N. (2003). Speciation of mercury in surface and deep-sea waters in the mediterranean sea. *Atmospheric Environment*, **37**(Supplement 1), 93 – 108.

Hu, X. and Zhang, Y. (2006). Implementation and testing of a new aerosol module in wrf/chem. In *14th Joint Conference on the Applications of Air Pollution Meteorology with the Air and Waste Management Assoc.*

Huszar, P., Cariolle, D., Paoli, R., Halenka, T., Belda, M., Schlager, H., Miksovsky, J., and Pisoft, P. (2010). Modeling the regional impact of ship emissions on no_x and ozone levels over the eastern atlantic and western europe using ship plume parameterization. *Atmospheric Chemistry and Physics*, **10**(14), 6645–6660.

Hynes, A. J., Donohoue, D. L., Goodsite, M. E., and Hedgecock, I. M. (2009). Our current understanding of major chemical and physical processes affecting mercury dynamics in the atmosphere and at the air-water/terrestrial interfaces. In N. Pirrone and R. P. Mason, editors, *Mercury Fate and Transport in the Global Atmosphere: Emissions, Measurements and Models*, chapter 14, pages 427–457. Springer.

Im, U. and Kanakidou, M. (2011). Summertime impacts of eastern mediterranean megacity emissions on air quality. *Atmospheric Chemistry and Physics Discussions*, **11**(9), 26657–26690.

IPCC (2007). Climate change 2007: The physical science basis, the fourth assessment report of the ipcc. Technical report, Intergovernmental Panel on Climate Change (IPCC).

Jacobson, M. (2005). *Fundamentals of Atmospheric Modeling*. Cambridge University Press.

Jung, G., Hedgecock, I. M., and Pirrone, N. (2009). Echmerit v1.0 – a new global fully coupled mercury-chemistry and transport model. *Geoscientific Model Development*, **2**(2), 175–195.

Kalabokas, P., Mihalopoulos, N., Ellul, R., Kleanthous, S., and Repapis, C. (2008). An investigation of the meteorological and photochemical factors influencing the background rural and marine surface ozone levels in the central and eastern mediterranean. *Atmospheric Environment*, **42**(34), 7894 – 7906.

Kalabokas, P. D., Volz-Thomas, A., Brioude, J., Thouret, V., Cammas, J.-P., and Repapis, C. C. (2007). Vertical ozone measurements in the troposphere over the eastern mediterranean and comparison with central europe. *Atmospheric Chemistry and Physics*, **7**(14), 3783–3790.

Kallos, G., Voudouri, A., Pytharoulis, I., and Kakaliagou, O. (2001). Modelling framework for atmospheric mercury over the mediterranean region: Model development and applications. In S. Margenov, J. Waśniewski, and P. Yalamov, editors, *Large-Scale Scientific Computing*, volume 2179 of *Lecture Notes in Computer Science*, pages 281–290. Springer Berlin Heidelberg.

Kanakidou, M., Mihalopoulos, N., Kindap, T., Im, U., Vrekoussis, M., Gerasopoulos, E., Dermitzaki, E., Unal, A., Koak, M., Markakis, K., Melas, D., Kouvarakis, G., Youssef, A. F., Richter, A., Hatzianastassiou, N., Hilboll,

A., Ebojie, F., Wittrock, F., von Savigny, C., Burrows, J. P., Ladstaetter-Weissenmayer, A., and Moubasher, H. (2011). Megacities as hot spots of air pollution in the east mediterranean. *Atmospheric Environment*, **45**(6), 1223 – 1235.

Kocman, D., Horvat, M., Pirrone, N., and Cinnirella, S. (2013). Contribution of contaminated sites to the global mercury budget. *Environmental Research*.

Kotnik, J., Horvat, M., Tessier, E., Ogrinc, N., Monperrus, M., Amouroux, D., Fajon, V., Gibičar, D., Žižek, S., Sprovieri, F., and Pirrone, N. (2007). Mercury speciation in surface and deep waters of the mediterranean sea. *Marine Chemistry*, **107**(1), 13 – 30.

Kotnik, J., Sprovieri, F., Ogrinc, N., Horvat, M., and Pirrone, N. (2013). Mercury in the mediterranean. part 1: spatial and temporal trends. *Environ Sci Pollut Res*.

Landis, M. S. and Keeler, G. J. (2002). Atmospheric mercury deposition to lake michigan during the lake michigan mass balance study. *Environmental Science & Technology*, **36**(21), 4518 – 4524.

Lawrence, M. G. and Crutzen, P. J. (1999). Influence of nox emissions from ships on tropospheric photochemistry and climate. *Nature*, **402**(6758), 167–170.

Lelieveld, J., Berresheim, H., Borrmann, S., Crutzen, P. J., Dentener, F. J., Fischer, H., Feichter, J., Flatau, P. J., Heland, J., Holzinger, R., Korrmann, R., Lawrence, M. G., Levin, Z., Markowicz, K. M., Mihalopoulos, N., Minikin, A., Ramanathan, V., de Reus, M., Roelofs, G. J., Scheeren, H. A., Sciare, J., Schlager, H., Schultz, M., Siegmund, P., Steil, B., Stephanou, E. G., Stier, P., Traub, M., Warneke, C., Williams, J., and Ziereis, H. (2002). Global air pollution crossroads over the mediterranean. *Science*, **298**(5594), 794–799.

Lin, C.-J., Pongprueksa, P., Lindberg, S. E., Pehkonen, S. O., Byun, D., and Jang, C. (2006). Scientific uncertainties in atmospheric mercury models i: Model science evaluation. *Atmospheric Environment*, **40**(16), 2911 – 2928.

Liss, P. S. and Slater, P. G. (1974). Flux of gases across the air-sea interface. *Nature*, **247**, 181–184.

Lowe, P. R. (1977). An approximating polynomial for the computation of saturation vapor pressure. *Journal of Applied Meteorology*, **16**, 100–103.

Lyman, S., Gustin, M., Prestbo, E., Kilner, P., Edgerton, E., and Hartsell, B. (2009). Testing and application of surrogate surfaces for understanding potential gaseous oxidized mercury dry deposition. *Environ Sci Technol*, **46**, 62356241.

Madronich, S. (1987). Photodissociation in the atmosphere 1. actinic flux and the effects of ground reflections and clouds. *J. Geophys. Res.*, **92**(D8), 9740–9752.

Marmer, E. and Langmann, B. (2005). Impact of ship emissions on the mediterranean summertime pollution and climate: A regional model study. *Atmospheric Environment*, **39**(26), 4659 – 4669.

Marmer, E., Dentener, F., Aardenne, J. v., Cavalli, F., Vignati, E., Velchev, K., Hjorth, J., Boersma, F., Vinken, G., Mihalopoulos, N., and Raes, F. (2009). What can we learn about ship emission inventories from measurements of air pollutants over the mediterranean sea? *Atmospheric Chemistry and Physics*, **9**(18), 6815–6831.

Mason, R., Fitzgerald, W., and Morel, F. (1994). The biogeochemical cycling of elemental mercury: Anthropogenic influences. *Geochimica et Cosmochimica Acta*, **58**(15), 3191 – 3198.

Mason, R., Rolfhus, K., and Fitzgerald, W. (1998). Mercury in the north atlantic. *Marine Chemistry*, **61**(1-2), 37–53.

Mason, R. P. (2009). Mercury emissions from natural processes and their importance in the global mercury cycle. In N. Pirrone and R. P. Mason, editors, *Mercury Fate and Transport in the Global Atmosphere: Emissions, Measurements and Models*, chapter 7, pages 173–191. Springer.

Mason, R. P. and Sullivan, K. A. (1999). The distribution and speciation of mercury in the south and equatorial atlantic. *Deep Sea Research Part II: Topical Studies in Oceanography*, **46**(5), 937 – 956.

Mason, R. P., Lawson, N. M., and Sheu, G. R. (2001). Mercury in the atlantic ocean: factors controlling air-sea exchange of mercury and its distribution in the upper waters. *Deep Sea Research Part II: Topical Studies in Oceanography*, **48**(13), 2829 – 2853.

Mason, R. P., Choi, A. L., Fitzgerald, W. F., Hammerschmidt, C. R., Lamborg, C. H., Soerensen, A. L., and Sunderland, E. M. (2012). Mercury biogeochemical cycling in the ocean and policy implications. *Environmental Research*, **119**, 101 – 117.

Matthias, V., Bewersdorff, I., Aulinger, A., and Quante, M. (2010). The contribution of ship emissions to air pollution in the north sea regions. *Environmental Pollution*, **158**(6), 2241 – 2250.

Mergler, D., Anderson, H. A., Chan, L. H. M., Mahaffey, K. R., Murray, M., Sakamoto, M., and Stern, A. H. (2007). Methylmercury exposure and health effects in humans: A worldwide concern. *Ambio*, **36**, 3–11.

Millán, M. M., Sanz, M. J., Salvador, R., and Mantilla, E. (2002). Atmospheric dynamics and ozone cycles related to nitrogen deposition in the western mediterranean. *Environmental Pollution*, **118**(2), 167 – 186.

Miola, A. and Ciuffo, B. (2011). Estimating air emissions from ships: Meta-analysis of modelling approaches and available data sources. *Atmospheric Environment*, **45**(13), 2242 – 2251.

Misenis, C. and Zhang, Y. (2010). An examination of sensitivity of wrf/chem predictions to physical parameterizations, horizontal grid spacing, and nesting options. *Atmospheric Research*, **97**, 315–334.

Monks, P., Granier, C., Fuzzi, S., Stohl, A., Williams, M., Akimoto, H., Amann, M., Baklanov, A., Baltensperger, U., Bey, I., Blake, N., Blake, R., Carslaw, K., Cooper, O., Dentener, F., Fowler, D., Fragkou, E., Frost, G., Generoso, S., Ginoux, P., Grewe, V., Guenther, A., Hansson, H., Henne, S., Hjorth, J., Hofzumahaus, A., Huntrieser, H., Isaksen, I., Jenkin, M., Kaiser, J., Kanakidou, M., Klimont, Z., Kulmala, M., Laj, P., Lawrence, M., Lee, J., Liousse, C., Maione, M., McFiggans, G., Metzger, A., Mieville, A., Moussiopoulos, N., Orlando, J., O'Dowd, C., Palmer, P., Parrish, D., Petzold, A., Platt, U., Pöschl, U., Prévôt, A., Reeves, C., Reimann, S., Rudich, Y., Sellegri, K., Steinbrecher, R., Simpson, D., ten Brink, H., Theloke, J., van der Werf, G., Vautard, R., Vestreng, V., Vlachokostas, C., and von Glasow, R. (2009). Atmospheric composition change global and regional air quality. *Atmospheric Environment*, **43**(33), 5268 – 5350.

Monks, P. S. (2000). A review of the observations and origins of the spring ozone maximum. *Atmospheric Environment*, **34**, 3545–3561.

Monperrus, M., Tessier, E., Amouroux, D., Leynaert, A., Huonnic, P., and Donard, O. (2007). Mercury methylation, demethylation and reduction rates in coastal and marine surface waters of the mediterranean sea. *Marine Chemistry*, **107**(1), 49–63.

Munthe, J. (1992). The aqueous oxidation of elemental mercury by ozone. *Atmospheric Environment. Part A. General Topics*, **26**(8), 1461 – 1468.

Munthe, J. and McElroy, W. (1992). Some aqueous reactions of potential importance in the atmospheric chemistry of mercury. *Atmospheric Environment. Part A. General Topics*, **26**(4), 553 – 557.

Munthe, J., Wängberg, I., Pirrone, N., Iverfeldt, Å., Ferrara, R., Ebinghaus, R., Feng, X., Gårdfeldt, K., Keeler, G., Lanzillotta, E., Lindberg, S. E., Lu, J., Mamane, Y., Prestbo, E., Schmolke, S., Schroeder, W. H., Sommar, J., Sprovieri, F., Stevens, R. K., Stratton, W., Tuncel, G., and Urba, A. (2001). Intercomparison of methods for sampling and analysis of atmospheric mercury species. *Atmospheric Environment*, **35**(17), 3007 – 3017.

Myers, T., Atkinson, R. D., Bullock Jr., O. R., and Bash, J. O. (2013). Investigation of effects of varying model inputs on mercury deposition estimates in the southwest us. *Atmospheric Chemistry and Physics*, **13**(2), 997–1009.

Neu, J. L. and Prather, M. J. (2012). Toward a more physical representation of precipitation scavenging in global chemistry models: cloud overlap and ice physics and their impact on tropospheric ozone. *Atmospheric Chemistry and Physics*, **12**(7), 3289–3310.

Nolle, M., Ellul, R., Heinrich, G., and Gsten, H. (2002). A long-term study of background ozone concentrations in the central mediterraneandiurnal and seasonal variations on the island of gozo. *Atmospheric Environment*, **36**(8), 1391 – 1402.

Nriagu, J. O. and Pacyna, J. M. (1988). Quantitative assessment of worldwide contamination of air, water and soils by trace metals. *Nature*, **333**(6169), 134–139.

Ogrinc, N., Monperrus, M., Kotnik, J., Fajon, V., Vidimova, K., Amouroux, D., Kocman, D., Tessier, E., Žižek, S., and Horvat, M. (2007). Distribution of mercury and methylmercury in deep-sea surficial sediments of the mediterranean sea. *Marine Chemistry*, **107**(1), 31–48.

Pacyna, E., Pacyna, J., Sundseth, K., Munthe, J., Kindbom, K., Wilson, S., Steenhuisen, F., and Maxson, P. (2010). Global emission of mercury to the atmosphere from anthropogenic sources in 2005 and projections to 2020. *Atmospheric Environment*, **44**(20), 2487 – 2499.

Pacyna, E. G., Pacyna, J. M., and Pirrone, N. (2001). European emissions of atmospheric mercury from anthropogenic sources in 1995. *Atmospheric Environment*, **35**(17), 2987 – 2996.

Pacyna, J., Wilson, S., Steenhuisen, F., and Pacyna., E. (2005). Spatially distributed inventories of global anthropogenic emissions of mercury to the atmosphere.

Pacyna, J. M. and Keeler, G. J. (1995). Sources of mercury in the arctic. *Water, Air, and Soil Pollution*, **80**, 621–632.

Pacyna, J. M. and Pacyna, E. (2000). Assessment of emissions/discharges of mercury reaching the arctic environment. *Norwegian Institute for Air Research Reports.*

Pacyna, J. M. and Pacyna, P. (1996). Global emissions of mercury to the atmosphere. emission from anthropogenic sources. Technical report, Report for the arctic monitoring and assessment programme (AMAP), Oslo.

Pal, B. and Ariya, P. A. (2004). Gas-phase ho-initiated reactions of elemental mercury: Kinetics, product studies, and atmospheric implications. *Environmental Science & Technology*, **38**(21), 5555 – 5566.

Petersen, G., Munthe, J., Pleijel, K., Bloxam, R., and Kumar, A. V. (1998). A comprehensive eulerian modeling framework for airborne mercury species: Development and testing of the tropospheric chemistry module (tcm). *Atmosperic Environment*, **29**, 829–843.

Peterson, C., Alishahi, M., and Gustin, M. S. (2012). Testing the use of passive sampling systems for understanding air mercury concentrations and dry deposition across florida, usa. *Science of The Total Environment*, **424**(0), 297 – 307.

Pirrone, N. and Keating, T. (2010a). *Hemispheric Transport of Air Pollution 2010. Part B, Mercury.* United Nations, New York ; Geneva.

Pirrone, N. and Keating, T. (2010b). *Hemispheric Transport of Air Pollution 2010. Part B, Mercury.* United Nations, New York ; Geneva.

Pirrone, N. and Mason, R. (2009). *Mercury Fate and Transport in the Global Atmosphere: Emissions, Measurements and Models.* Springer US.

Pirrone, N. and Wichmann-Fiebig, M. (2003). Some recommendations on mercury measurements and research activities in the european union. *Atmospheric Environment*, **37**(Supplement 1), 3 – 8.

Pirrone, N., Keeler, G. J., and Nriagu, J. O. (1996). Regional differences in worldwide emissions of mercury to the atmosphere. *Atmospheric Environment*, **30**(17), 2981 – 2987.

Pirrone, N., Allegrini, I., Keeler, G. J., Nriagu, J. O., Rossmann, R., and Robbins, J. A. (1998). Historical atmospheric mercury emissions and depositions in north america compared to mercury accumulations in sedimentary records. *Atmospheric Environment*, **32**(5), 929 – 940.

Pirrone, N., Hedgecock, I., and Forlano, L. (2000). The role of the ambient aerosol in the atmospheric processing of semi-volatile contaminants: A parameterised numerical model (gaspar). *Journal Of Geophysical Research*, **105**, 9773–9790.

Pirrone, N., Munthe, J., Barregrd, L., Ehrlich, H. C., Petersen, G., Fernandez, R., and ..., Wichmann-Fiebig, M. (2001). Eu ambient air pollution by mercury (hg)-position paper. *Office for Official Publications of the European Communities.*

Pirrone, N., Ferrara, R., Hedgecock, I. M., Kallos, G., Mamane, Y., Munthe, J., Pacyna, J. M., Pytharoulis, I., Sprovieri, F., Voudouri, A., and Wängberg, I. (2003). Dynamic processes of mercury over the mediterranean region: results from the mediterranean atmospheric mercury cycle system (mamcs) project. *Atmospheric Environment*, **37**(Supplement 1), 21 – 39.

Pirrone, N., Cinnirella, S., Feng, X., Finkelman, R. B., Friedli, H. R., Leaner, J., Mason, R., Mukherjee, A. B., Stracher, G. B., Streets, D. G., and Telmer, K. (2010). Global mercury emissions to the atmosphere from anthropogenic and natural sources. *Atmospheric Chemistry and Physics*, **10**(13), 5951–5964.

Pirrone, N., Aas, W., Cinnirella, S., Ebinghaus, R., Hedgecock, I. M., Pacyna, J., Sprovieri, F., and Sunderland, E. M. . (2013). Toward the next generation of air quality monitoring: Mercury. *Atmosperic Environment.*

Pleijel, K. and Munthe, J. (1995). Modeling the atmospheric chemistry of mercury. in mercury as a global pollutant. *Springer Netherlands.*, pages 317–324.

Pongprueksa, P., Lin, C.-J., Lindberg, S. E., Jang, C., Braverman, T., Jr., O. R. B., Ho, T. C., and Chu, H.-W. (2008). Scientific uncertainties in atmospheric mercury models iii: Boundary and initial conditions, model grid resolution, and hg(ii) reduction mechanism. *Atmospheric Environment*, **42**(8), 1828 – 1845.

Rajar, R., Četina, M., Horvat, M., and Žagar, D. (2007). Mass balance of mercury in the mediterranean sea. *Marine Chemistry*, **107**(1), 89–102.

Roeckner, E., Bäuml, G., Bonaventura, L., Brokopf, R., Esch, M., Giorgetta, M., Hagemann, S., Kirchner, I., Kornblueh, L., Manzini, E., Rhodin, A., Schlese, U., Schulzweida, U., and A., T. (2003). The atmospheric general circulation model echam 5. part i: Model description. Technical report, Max Planck Institute for Meteorology (MPI-M), Hamburg, Germany. MPI-Report No. 349.

Roeckner, E., Brokopf, R., Esch, M., Giorgetta, M., Hagemann, S., Kornblueh, L., Manzini, E., Schlese, U., and Schulzweida, U. (2006). Sensitivity of simulated climate to horizontal and vertical resolution in the echam5 atmosphere model. *Journal of Climate*, **19**(16), 3771–3791.

Ryaboshapko, A., Artz, R., Bullock, R., Christensen, J., Cohen, M., Dastoor, A., Davignon, D., Draxler, R., Ebinghaus, R., Ilyin, I., *et al.* (2003). Intercomparison study of numerical models for long-range atmospheric transport of mercury. *Stage II. Comparison of modeling results with observations obtained during short-term measuring campaigns. MSC-E Technical report.*

Ryaboshapko, A., Bullock, O. R., Jr., Christensen, J., Cohen, M., Dastoor, A., Ilyin, I., Petersen, G., Syrakov, D., Travnikov, O., Artz, R. S., Davignon, D., Draxler, R. R., Munthe, J., and Pacyna, J. (2007a). Intercomparison study of atmospheric mercury models: 2. modelling results vs. long-term observations and comparison of country deposition budgets. *Science of The Total Environment*, **377**(2-3), 319 – 333.

Ryaboshapko, A., Bullock Jr., R. O., Christensen, J., Cohen, M., Dastoor, A., Ilyin, I., Petersen, G., Syrakov, D., Travnikov, O., Artz, R. S., Davignon, D., Draxler, R. R., Munthe, J., and Pacyna, J. (2007b). Intercomparison study of atmospheric mercury models: 2. modelling results vs. long-term observations and comparison of country deposition budgets. *Science of The Total Environment*, **377**(2 - 3), 319 – 333.

Saliba, M., Ellul, R., Camilleri, L., and Gsten, H. (2008). A 10-year study of background surface ozone concentrations on the island of gozo in the central mediterranean. *Journal of Atmospheric Chemistry*, **60**, 117–135. 10.1007/s10874-008-9112-3.

Salzmann, M. and Lawrence, M. G. (2006). Automatic coding of chemistry solvers in WRF-Chem using KPP. In *7th WRF Users Workshop*, Boulder, Colorado, USA.

Sandu, A. and Sander, R. (2006). Technical note: Simulating chemical systems in fortran90 and matlab with the kinetic preprocessor kpp-2.1. *Atmospheric Chemistry and Physics*, **6**(1), 187–195.

Sandu, A., Daescu, D. N., and Carmichael, G. R. (2003). Direct and adjoint sensitivity analysis of chemical kinetic systems with kpp: Part i - theory and software tools. *Atmospheric Environment*, **37**(36), 5083 – 5096.

Scheuhammer, A. M., Meyer, M. W., Sandheinrich, M. B., and Murray, M. W. (2007). Effects of environmental methylmercury on the health of wild birds, mammals, and fish. *Ambio*, **36**, 12–18.

Schroeder, W. H. and Munthe, J. (1998). Atmospheric mercury–an overview. *Atmospheric Environment*, **32**(5), 809 – 822.

Schürmann, G. J., Algieri, A., Hedgecock, I. M., Manna, G., Pirrone, N., and Sprovieri, F. (2009). Modelling local and synoptic scale influences on ozone concentrations in a topographically complex region of southern italy. *Atmospheric Environment*, **43**, 4424–4434.

Seigneur, C., Vijayaraghavan, K., Lohman, K., Karamchandani, P., and Scott, C. (2004). Global source attribution for mercury deposition in the united states. *Environmental Science & Technology*, **38**(2), 555–569.

Seigneur, C., Vijayaraghavan, K., and Lohman, K. (2006). Atmospheric mercury chemistry: Sensitivity of global model simulations to chemical reactions. *Journal of Geophysical Research D: Atmospheres*, **111**(22), D22306.

Selin, N. E. (2009). Global biogeochemical cycling of mercury: A review. *Annual Review of Environment and Resources*, **34**(1), 43–63.

Selin, N. E., Jacob, D. J., Park, R. J., Yantosca, R. M., Strode, S., Jaeglé, L., and Jaffe, D. (2007). Chemical cycling and deposition of atmospheric mercury: Global constraints from observations. *Journal Of Geophysical Research - Atmospheres*, **112**(D2), D02308–.

Simpson, D., Guenther, A., Hewitt, C. N., and Steinbrecher, R. (1995). Biogenic emissions in europe 1. estimates and uncertainties. *J. Geophys. Res.*, **100**(D11), 22875–22890.

Simpson, D., Fagerli, H., Jonson, J., Tsyro, S., Wind, P., and Tuovinen, J. (2003). Trans-boundary acidication and eutrophication and ground level ozone in europe: Unied emep model description, emep status report 1/03 part i. Technical report, Norwegian Meteorological Institute, Oslo, Norway.

Skamarock, W. C., Klemp, J. B., Dudhia, J., Gill, D. O., Barker, D. M., Duda, M. G., Huang, X.-Y. Wang, W., and Powers, J. G. (2008). A description of the advanced research wrf version 3. Technical report, National Center for Atmospheric Research.

Slemr, F., Schuster, G., and Seiler, W. (1985). Distribution, speciation, and budget of atmospheric mercury. *Journal of Atmospheric Chemistry*, **3**(4), 407–434.

Smith-Downey, N. V., Sunderland, E. M., and Jacob, D. J. (2010). Anthropogenic impacts on global storage and emissions of mercury from terrestrial soils: Insights from a new global model. *Journal of Geophysical Research: Biogeosciences*, **115(G3)**, 20052012.

Soerensen, A. L., Sunderland, E. M., Holmes, C. D., Jacob, D. J., Yantosca, R. M., Skov, H., Christensen, J. H., Strode, S. A., and Mason, R. P. (2010). An improved global model for air-sea exchange of mercury: High concentrations over the north atlantic. *Environmental Science & Technology*, **44**(22), 8574 – 8580.

Sommar, J., Gårdfeldt, K., Strömberg, D., and Feng, X. (2001a). A kinetic study of the gas-phase reaction between the hydroxyl radical and atomic mercury. *Atmospheric Environment*, **35**(17), 3049 – 3054.

Sommar, J., Gårdfeldt, K., Strömberg, D., and Feng, X. (2001b). A kinetic study of the gas-phase reaction between the hydroxyl radical and atomic mercury. *Atmospheric Environment*, **35**(17), 3049 – 3054.

Song, S.-K., Shon, Z.-H., Kim, Y.-K., Kang, Y.-H., Oh, I.-B., and Jung, C.-H. (2010). Influence of ship emissions on ozone concentrations around coastal areas during summer season. *Atmospheric Environment*, **44**(5), 713 – 723.

Spicer, C. W., Satola, J., Abbgy, A. A., and Plastridge, R. A.and Cowen, K. A. (2002). Kinetics of Gas-Phase Elemental Mercury Reactions With Halogen Species, Ozone and Nitrate Radical Under Atmospheric Conditions. *Florida Department of Environmental Protection*.

Sprovieri, F., Pirrone, N., Gårdfeldt, K., and Sommar, J. (2003). Mercury speciation in the marine boundary layer along a 6000km cruise path around the mediterranean sea. *Atmospheric Environment*, **37**(Supplement 1), 63 – 71.

Sprovieri, F., Pirrone, N., Ebinghaus, R., Kock, H., and Dommergue, A. (2010). A review of worldwide atmospheric mercury measurements. *Atmospheric Chemistry and Physics*, **10**(17), 8245–8265.

Stockwell, W. R., Middleton, P., Chang, J. S., and Taang, X. (1990a). The second-generation regional acid deposition model chemical mechanism for

regional air quality modelling. *Journal of Geophysical Research*, **95**, 16343–16367.

Stockwell, W. R., Middleton, P., Chang, J. S., and Taang, X. (1990b). The second-generation regional acid deposition model chemical mechanism for regional air quality modelling. *Journal of Geophysical Research*, **95**, 16343–16367.

Storelli, M., Stuffler, R., and Marcotrigiano, G. (2002). Total and methylmercury residues in tuna-fish from the mediterranean sea. *Food Additives & Contaminants*, **19**(8), 715–720.

Storelli, M., Giacominelli-Stuffler, R., Storelli, A., and Marcotrigiano, G. (2005). Accumulation of mercury, cadmium, lead and arsenic in swordfish and bluefin tuna from the mediterranean sea: A comparative study. *Marine pollution bulletin*, **50**(9), 1004–1007.

Storelli, M. M., Barone, G., Cuttone, G., Giungato, D., and Garofalo, R. (2010). Occurrence of toxic metals (hg, cd and pb) in fresh and canned tuna: Public health implications. *Food and Chemical Toxicology*, **48**(11), 3167 – 3170.

Streets, D. G., Devane, M. K., Lu, Z., Bond, T. C., Sunderland, E. M., and Jacob, D. J. (2011). All-time releases of mercury to the atmosphere from human activities. *Environmental Science & Technology*, **45**(24), 10485 – 10491.

Strode, S. A., Jaeglé, L., Jaffe, D. A., Swartzendruber, P. C., Selin, N. E., Holmes, C., and Yantosca, R. M. (2008). Trans-pacific transport of mercury. *J. Geophys. Res.*, **113**(D15), D15305–.

Subir, M., Ariya, P. A., and Dastoor, A. P. (2011). A review of uncertainties in atmospheric modeling of mercury chemistry I. uncertainties in existing kinetic parameters fundamental limitations and the importance of heterogeneous chemistry. *Atmospheric Environment*, **45**(32), 5664 – 5676.

Subir, M., Ariya, P. A., and Dastoor, A. P. (2012). A review of the sources of uncertainties in atmospheric mercury modeling II. mercury surface and heterogeneous chemistry a missing link. *Atmospheric Environment*, **46**, 1 – 10.

Sunderland, E. M., Krabbenhoft, D. P., Moreau, J. W., Strode, S. A., and Landing, W. M. (2009). Mercury sources, distribution, and bioavailability in the north pacific ocean: Insights from data and models. *Global Biogeochem. Cycles*, **23**(2), GB2010–.

Tan, S. W. andMeiller, J. C. and Mahaffey, K. R. (2009). The endocrine effects of mercury in humans and wildlife. *Critical Reviews in Toxicology*, **39**, 228–269.

Tas, E., Obrist, D., Peleg, M., Matveev, V., Faïn, X., Asaf, D., and Luria, M. (2012). Measurement-based modelling of bromine-induced oxidation of mercury above the dead sea. *Atmospheric Chemistry and Physics*, **12**(5), 2429–2440.

Tie, X., Madronich, S., Li, G. H., Ying, Z., Zhang, R., Garcia, A. R., Lee-Taylor, J., and Liu, Y. (2007). Characterizations of chemical oxidants in Mexico City: A regional chemical dynamical model (WRF-Chem) study. *Atmospheric Environment*, **41**(9), 1989 – 2008.

Tuccella, P., Curci, G., Visconti, G., Bessagnet, B., Menut, L., and Park, R. J. (2012). Modeling of gas and aerosol with wrf/chem over europe: Evaluation and sensitivity study. *J. Geophys. Res.*, **117**(D3), D03303–.

UNEP (2013a). Global mercury assessment: Sources, emissions, releases and environmental transport. Technical report, Chemicals Branch, Division of Technology, Industry and Economics, United Nations Environment Programme (UNEP).

UNEP (2013b). Mercury: Time to act. Technical report, Chemicals Branch, Division of Technology, Industry and Economics, United Nations Environment Programme (UNEP).

Velchev, K., Cavalli, F., Hjorth, J., Marmer, E., Vignati, E., Dentener, F., and Raes, F. (2010). Ozone over the western mediterranean sea results from two years of shipborne measurements. *Atmospheric Chemistry and Physics Discussions*, **10**(3), 6129–6165.

Vestreng, V., Mareckova, K., Kakareka, S., Malchykhina, A., and Kukharchyk, T. (2007). Inventory review 2007; emission data reported to lrtap convention and nec directive, msc-w technical report 1/07,. Technical report, The Norwegian Meteorological Institute, Oslo, Norway.

Vingarzan, R. (2004). A review of surface ozone background levels and trends. *Atmospheric Environment*, **38**(21), 3431 – 3442.

Vinken, G. C. M., Boersma, K. F., Jacob, D. J., and Meijer, E. W. (2011). Accounting for non-linear chemistry of ship plumes in the geos-chem global chemistry transport model. *Atmospheric Chemistry and Physics Discussions*, **11**(6), 17789–17823.

Vutukuru, S. and Dabdub, D. (2008). Modeling the effects of ship emissions on coastal air quality: A case study of southern california. *Atmospheric Environment*, **42**(16), 3751 – 3764.

Žagar, D., Petkovšek, G., Rajar, R., Sirnik, N., Horvat, M., Voudouri, A., Kallos, G., and Četina, M. (2007). Modelling of mercury transport and transformations in the water compartment of the mediterranean sea. *Marine Chemistry*, **107**(1), 64–88.

Žagar, D., Sirnik, N., Četina, M., Horvat, M., Kotnik, J., Ogrinc, N., Hedgecock, I. M., Cinnirella, S., De Simone, F., Gencarelli, C. N., and Pirrone, N. (2013). Mercury in the mediterranean. part 2: processes and mass balance. *Environmental Science and Pollution Research*, pages 1–14.

Wallace, J. M. and Hobbs, P. V. (1977). *Atmospheric Science: An Introductory Survey*. Academic Press.

Wängberg, I., Munthe, J., Pirrone, N., Iverfeldt, A., Bahlman, E., Costa, P., Ebinghaus, R., Feng, X., Ferrara, R., Gårdfeldt, K., Kock, H., Lanzillotta, E., Mamane, Y., Mas, F., Melamed, E., Osnat, Y., Prestbo, E., Sommar, J., Schmolke, S., Spain, G., Sprovieri, F., and Tuncel, G. (2001a). Atmospheric mercury distribution in northern europe and in the mediterranean region. *Atmospheric Environment*, **35**(17), 3019 – 3025.

Wängberg, I., Munthe, J., Pirrone, N., Iverfeldt, ., E., B., Costa, P., Ebinghaus, R., Feng, X., Ferrara, R., Grdfeldt, K., Kock, H., Lanzillotta, E., Mamane, Y., Mas, F., Melamed, E., Osnat, Y., E., P., Sommar, J., Spain, G., Sprovieri, F., and Tuncel, G. (2001b). Atmospheric mercury measurements in europe during mamcs and moe. *Atmosperic Environment*, **35**, 3019–3025.

Wängberg, I., Munthe, J., Amouroux, D., Andersson, M., Fajon, V., Ferrara, R., Gårdfeldt, K., Horvat, M., Mamane, Y., Melamed, E., Monperrus, M., Ogrinc, N., Yossef, O., Pirrone, N., Sommar, J., and Sprovieri, F. (2008). Atmospheric mercury at mediterranean coastal stations. *Environmental Fluid Mechanics*, **8**(2), 101–116.

Wanninkhof, R. (1992). Relationship between wind speed and gas exchange over the ocean. *Journal Of Geophysical Research - Atmospheres*, **97**, –.

Wesely, M. (1989). Parameterization of surface resistances to gaseous dry deposition in regional-scale numerical models. *Atmospheric Environment*, **23**(6), 1293 – 1304.

Wiedinmyer, C., Akagi, S. K., Yokelson, R. J., Emmons, L. K., Al-Saadi, J. A., Orlando, J. J., and Soja, A. J. (2011). The fire inventory from ncar (finn): a high resolution global model to estimate the emissions from open burning. *Geoscientific Model Development*, **4**(3), 625–641.

Wild, O., Zhu, X., and Prather, M. J. (2000). Fast-j: Accurate simulation of in- and below-cloud photolysis in tropospheric chemical models. *Journal of Atmospheric Chemistry*, **37**(3), 245–282.

Willmott, C. J., Davis, R. E., Feddema, J. J., Klink, K. M., Legates, D. R., Rowe, C. M., Ackleson, S. G., and O'Donnell, J. (1985). Statistics for the evaluation and comparison of models. *J. Geophys. Res*, **90**, 8995–9005.

Worden, H. M., Bowman, K. W., Kulawik, S. S., and Aghedo, A. M. (2011). Sensitivity of outgoing longwave radiative flux to the global vertical distribution of ozone characterized by instantaneous radiative kernels from aura-tes. *J. Geophys. Res.*, **116**(D14), D14115–.

Zhang, W., Tong, Y., Hu, D., Ou, L., and Wang, X. (2012a). Characterization of atmospheric mercury concentrations along an urbanrural gradient using a newly developed passive sampler. *Atmospheric Environment*, **47**(0), 26 – 32.

Zhang, Y. (2008). Online-coupled meteorology and chemistry models: history, current status, and outlook. *Atmospheric Chemistry and Physics*, **8**(11), 2895–2932.

Zhang, Y. and Dubey, M. K. (2009). Comparisons of wrf/chem simulated o3 concentrations in mexico city with ground-based rama measurements during the milagro period. *Atmospheric Environment*, **43**(30), 4622 – 4631.

Zhang, Y., Jaeglé, L., van Donkelaar, A., Martin, R. V., Holmes, C. D., Amos, H. M., Wang, Q., Talbot, R., Artz, R., Brooks, S., Luke, W., Holsen, T. M., Felton, D., Miller, E. K., Perry, K. D., Schmeltz, D., Steffen, A., Tordon, R., Weiss-Penzias, P., and Zsolway, R. (2012b). Nested-grid simulation of mercury over north america. *Atmospheric Chemistry and Physics*, **12**(14), 6095 – 6111.